In presenting the dissertation as a partial fulfillment of the requirements for an advanced degree from the Georgia Institute of Technology, I agree that the Library of the Institute shall make it available for inspection and circulation in accordance with its regulations governing materials of this type. I agree that permission to copy from, or to publish from, this dissertation may be granted by the professor under whose direction it was written, or, in his absence, by the Dean of the Graduate Division when such copying or publication is solely for scholarly purposes and does not involve potential financial gain. It is understood that any copying from, or publication of, this dissertation which involves potential financial gain will not be allowed without written permission.

7/25/68

STATISTICAL MODEL FOR ION-MOLECULE REACTIONS

A THESIS

Presented to

The Faculty of the Division of Graduate

Studies and Research

By

David Cleo Fullerton

In Partial Fulfillment

of the Requirements for the Degree

Doctor of Philosophy

in the

School of Chemistry

Georgia Institute of Technology

May, 1971

STATISTICAL MODEL FOR ION-MOLECULE REACTIONS

Approved:

Chairman

Date approved by Chairman: May 29, 1971

ACKNOWLEDGMENTS

First, I give my deepest appreciation to Dr. Tom Moran, thesis director, researcher, counselor, protagonist, and friend, for his leading and pushing in the pursuit of my degree.

I sincerely appreciate the instructorship I had for the five years spent at Georgia Tech. I thank Dr. Wm. M. Spicer for the opportunity to gain teaching experience.

I thank Dr. Ray Borkman and Dr. Ron Felton for serving on my reading committee, and Dr. Earl McDaniel and Dr. Ed Thomas for reading my thesis and serving on my examining committee.

I appreciate the encouragement and friendship of my compatriots in atomic collisions, Frederick Petty and Fred Hedrick, and my many other friends both at Georgia Tech and in Atlanta.

I thank those who made the computing facilities at RECC available for this research.

Finally, I thank Juana Mae. She has provided encouragement and understanding when needed. Also, I thank her for typing my thesis.

TABLE OF CONTENTS

TABLE OF CONTENTS (Continued)

LIST OF TABLES

LIST OF ILLUSTRATIONS

LIST OF ILLUSTRATIONS (Continued)

LIST OF ILLUSTRATIONS (Continued)

LIST OF ILLUSTRATIONS (Continued)

SUMMARY

Ion-molecule reactions are studied using a statistical phase space model, and the theoretical predictions compared with experimental results. The phase space model assumes that a collision complex is formed between the interacting species, and the probability for a given process occurring is given as the phase space available to that process divided by the total phase space available for decomposition of the collision complex. In the basic form of the theory decomposition of the complex is governed only by conservation of total energy and total angular momentum. These conservation principles determine the phase space available to a given product channel.

Charge transfer and dissociative charge transfer reactions of rare gas ions with nitrogen are studied in the 0.05 to 200 eV energy range. Comparison between calculated and experimental cross sections for the charge transfer processes indicate an incomplete mixing of statistically available N_2^+ product states. If experimental observation is used to select the dominant charge transfer product state, qualitative agreement between calculated and experimental cross sections is obtained. Cross sections computed for endoergic dissociative channels of reaction are in good

agreement with experiment.

Cross sections for the collision induced dissociation of O_2^+ and NO^+ ions have been calculated as a function of reactant ion kinetic energy. The reactant ion cross sections were weighted to account for the internal state distributions of reactant ions produced in electron impact processes. Given the preparation conditions, which *a priori* determine the reactant ion vibronic distribution, the phase space model reproduces observed thresholds and kinetic energy dependences for the collision induced dissociation processes.

The mass transfer reactions between C^+ and N_2 and O_2 to form CN^+ and CO^+, respectively, show that it is necessary to consider spin conservation in addition to conservation of energy and angular momentum in considering the products of ion-molecule reactions. Consideration of spin conservation for the above processes gives calculated cross sections that are in qualitative agreement with experimentally observed cross sections. Phase space predictions for dissociative charge transfer and charge transfer processes are in agreement with experimental measurements at low ion kinetic energies. At high ion kinetic energies charge transfer channels of reaction are more adequately described using a nearest resonance method.

The phase space model is shown to give product ion internal energy distributions that are consistent with experimental observations. The vibrational and rotational

distributions of N_2^+ produced in charge transfer reactions calculated using the phase space model compare favorably with experimentally determined relative radiative intensities from product ions. In addition, kinetic energy distributions of the charge transfer and dissociative charge transfer show a good correlation with observed diatomic product ion vibrational distributions.

CHAPTER I

INTRODUCTION

It has been known since early in this century that gas phase ion-molecule reactions occur in mass spectrometric ion sources. The first important theoretical work of relevance was Langevin's (1) work on mobilities in which he considered clustering of molecules about gaseous ions and orbiting collisions between ions and molecules. The collision of an ion with a molecule can result in many different things: elastic scattering, inelastic scattering (involving exchange of translational, vibrational, or electronic energy), charge transfer, dissociative charge transfer, or collision induced dissociation. In order to calculate the probability that any of these events occur, it would be necessary to follow the dynamics of the nuclei and electrons. However, even in the Born-Oppenheimer approximation the problem is incalculable quantum mechanically or classically.

Light (2) has suggested a relatively simple method of calculating the cross section for a given process, avoiding the intermediate steps of calculating the potential and the dynamics by postulating the reactions proceeding without activation energy:

> The probability of formation of any given product in a strong coupling collision is proportional to the ratio of the phase space available to that product divided by the total phase space available with conservation of energy and angular momentum.

He reasoned that everything except elastic scattering occurs via formation of a collision complex. The total cross section for formation of the complex is then statistically distributed among the possible products of the reaction, the distribution depending only on the energetics of the reaction. Strong coupling is necessary to ensure that the complex loses all memory so that decomposition of the complex is governed only by the available phase space. By strong coupling we mean that the particles are brought to a point where chemical bonding forces are felt; that is, to a region of large forces and small separations between the particles.

Application of this hypothesis requires that the collision complex exist for a time long enough that the available energy be distributed randomly among all degrees of freedom; that is, all possible quantum states are taken to be equally probable, given conservation of energy and angular momentum. On the other hand, if collision times are short, the relative positions of the nuclei do not vary appreciably, and averages over small variations in the phases may give cross sections correlating with the available phase space.

The criteria for formation of a collision complex are: (a) There must be strong coupling. (b) When the particles

come to the complex configuration, the kinetic energy of the particles is large compared to the energy level separation of the complex so that decomposition of the complex is statistical. (c) The initial state of the reactants is unknown in the complex. However, all of these conditions may not be necessary for the phase space model to be applicable.

The phase space model is expected to fail when quantities other than energy and angular momenta are conserved; or, in general, when there is an incomplete mixing of product states. The problem of spin conservation will be explored in our application of this model. The three-body phase space theory (2,3) applied to neutral-neutral reactions (4-6) has been moderately successful in predicting total cross sections, isotope ratios, and product excitation (electronic, vibrational, and rotational). Application to ion-neutral processes are quite limited (7-10) and thus far there has been little comparison between theory and experiment. Limited success has been achieved only in application to certain channels such as dissociative charge transfer reactions of inert gas ions with CO (7). Since these early applications, experimental measurements with which to make a comparison have become more abundant. More recently the phase space treatment has been extended to four-body processes (11) with the inclusion of a resonance potential (12) to describe the $H_2 + H_2^+$ reaction. In most cases ion-molecule

reactions are represented by the ion-induced dipole potential based on Langevin's (1) original work as carried out by Gioumousis and Stevenson (13). Whenever there is complete mixing of product states, the phase space model has proven adequate (14) whereas quantum mechanical or classical dynamical calculations have proven cumbersome or difficult. However, the statistical model is not expected to be applicable when certain product states are especially favored, such as resonant charge transfer processes (15). Another example of a statistical calculation applied to energy conversion has been the computation of vibrational-rotational distributions for decomposition products of excited molecules (16-18) formed in electron collision processes.

The object of this thesis is to give a thorough test of the phase space model and its limits of applicability in predicting product distributions in ion-molecule reactions. After giving a brief quantum mechanical basis to the statistical theory, in Chapter II we give the mathematical formulation for a semiclassical treatment following Light et al. (2,3,7). To test thoroughly the model we have selected systems which give the widest range of product channels and for which there is sufficient experimental data with which to make comparisons.

We first examine the mixing of product electronic states in the reactions of rare gas ions with nitrogen. These reactions show that the most energetically allowed

product is not always the most abundant product produced in charge transfer processes. However, by *a priori* selecting a certain product state for the charge transfer we find that we can obtain good agreement with experimental observations. One important feature of the phase space model is that within a given product electronic state the predicted relative population of internal states is in agreement with experimental observations. Also, excellent agreement for dissociative charge transfer processes is obtained.

In Chapter IV we examine the collision induced dissociation of excited O_2^+ and NO^+. These reactions afford the opportunity to test the phase space model as a function of incident internal energy. As above, the dissociative processes are well described by phase space methodology and the dependence on internal energy of reactant ions is in agreement with experimental observations. The ion-molecule reactions of C^+ with N_2 and O_2 considered in Chapter V have mass transfer reaction channels available in addition to the charge transfer and dissociative charge transfer processes. Here we observe a very strong dependence on spin conservation in all processes. Agreement between phase space predictions and observed energy dependence of cross sections for charge transfer reactions between C^+ and N_2 or O_2 to give N_2^+ and O_2^+ respectively is not attained except at low ion kinetic energies. Many cases of long distance charge transfer processes are known (19), and to represent these processes we have used

a near-resonance formalism in which the cross section is a function of the exothermicity of the reaction (20,21).

To further examine internal product energy distribution we consider the rotational distribution in a given product vibronic state resulting from charge transfer processes. Application of the phase space model to neutral-neutral processes has shown reasonable accord with experimental observation (4-6), but comparison of calculated rotational distributions with those observed in ion-molecule reactions has not been made previously.

In Chapter VII we consider the $He^+ + N_2 \rightarrow N_2^+$ reaction further. Using electron correlation arguments we show that $N_2^+(C^2\Sigma_u)$ is the dominant product state. In addition we incorporate a more suitable potential in the phase space model.

CHAPTER II

MATHEMATICAL FORMULATION OF PHASE SPACE THEORY

Quantum Mechanical Formalism

To give a basis for the classical formalism we will use for the model, we first give a brief quantum mechanical description of inelastic and reactive scattering developed in terms of the scattering matrix (22-25). A given state (or channel) can be specified by a set of quantum numbers which define a wave function that satisfies the Schrödinger equation and is defined as a region of configuration space in which the particles have a definite internal state at large separation. In this region of space the interaction between particles is negligible. The quantum numbers [α], [β], ..., denoting a channel represented by α, β, ..., and wave numbers $k_\alpha = |p_\alpha|/\hbar = \mu v_\alpha/\hbar$ will specify a scattering channel. If we consider a channel specified further by orbital angular momentum quantum number ℓ and its projection m_ℓ, the wave function for channel α can be written (24)

$$\Psi_\alpha = r^{-1} G_\alpha(r) \psi(\alpha|\vec{r}_i\vec{r}_j)\ Y_{\ell m_\ell}(\hat{r}), \qquad (1)$$

where $\psi(\alpha|\vec{r}_i\vec{r}_j)$ is constructed from the eigenfunctions of particles i and j and defines state α for a given separation of the particles given by the position vectors $\vec{r}_i$ and $\vec{r}_j$.

Y is a spherical harmonic. If we specify that the radial function, $G_\alpha(r)$, behave asymptotically as

$$G_\alpha(r) \sim v^{1/2} \left[A_\alpha exp\{-i(k_\alpha r - \ell\pi/2)\} - B_\beta exp\{+i(k_\beta r - \ell\pi/2)\}\right], \quad (2)$$

the S matrix is defined by

$$B_\beta = \sum_\alpha S_{\beta\alpha} A_\alpha. \quad (3)$$

The S matrix connects the amplitude of the outgoing wave in channel β, given by B_β, with the amplitude of the incoming wave in channel α. The outgoing flux in channel β is given by

$$\frac{4\pi}{(2\ell+1)} r^2 |G_\alpha(r)|^2 v_\beta = \frac{4\pi}{(2\ell+1)} |S_{\alpha\beta}|^2 |A_\alpha|^2. \quad (4)$$

The incoming flux in channel α is $4\pi|A_\alpha|^2/(2\ell+1)$, and the outgoing flux is $4\pi|S_{\alpha\beta}|^2|A_\alpha|^2/(2\ell+1)$. Conservation of flux requires that

$$\sum_\beta |S_{\alpha\beta}|^2 = 1; \quad (5)$$

the S matrix is unitary.

Writing $|A_\alpha|^2 = (2\ell+1)/4k_\alpha^2$ gives for the partial cross section for scattering into channel β

$$\sigma(\alpha,\beta) = \pi(2\ell+1)|S_{\alpha\beta}|^2/k_\alpha^2, \quad \alpha \neq \beta. \quad (6)$$

In addition, if we denote a channel by total angular momentum K coupled to orbital angular momentum ℓ and rotational angular momentum m, the cross section for scattering from state α to state β is given as (25)

$$\sigma(\alpha,\beta) = \frac{\pi}{(2m+1)k_\alpha^2} \sum_K (2K+1) \left| S_K(\alpha \ell_\alpha ; \beta \ell_\beta) - (-1)^{\ell} \delta_{\alpha \ell_\alpha, \beta \ell_\beta} \right|^2 . \quad (7)$$

If we define $\Gamma(\beta) = |S_{\alpha\beta}|^2$ as the amplitude for production of state β, then

$$\Gamma_t = \sum_{[\beta]} \Gamma(\beta) \quad (8)$$

is the total amplitude for decay of the complex in the mode defined by $[\beta]$. The sum is over all quantities defining state β.

If Γ_t is small compared to the level spacing of the complex, D_K, for a given K and if $\Gamma(\beta)$ is independent of ℓ for all ℓ satisfying conservation of angular momentum, the cross section for forming state β from α becomes (24)

$$\sigma(\alpha,\beta) = \frac{2\pi^2}{(2m+1)k_\alpha^2} \sum_{K \ell_\alpha \ell_\beta} (2K+1) \langle \Gamma(\alpha)\Gamma(\beta)/\Gamma_t D \rangle_{av}. \quad (9)$$

If we assume that events in different channels are statistically independent,

$$\langle \Gamma(\alpha)\ \Gamma(\beta)/\Gamma_t D_K \rangle_{av} = \langle \Gamma(\alpha)/D_K \rangle_{av} \langle \Gamma(\beta)/\Gamma_t \rangle_{av}, \quad (10)$$

we have for the partial cross section for the production of state β from state α given as

$$\sigma(\alpha,\beta) = \sigma(\alpha) \sum_K \sum_{\ell_\beta} \langle \Gamma(\beta)/\Gamma_t \rangle_{av} \quad (11)$$

where $\sigma(\alpha)$ is the cross section for forming the complex.

A decay probability can be defined as

$$P_K(\beta) = \sum_{\ell_\beta} \langle \Gamma(\beta)/\Gamma_t \rangle_{av}. \tag{12}$$

This specifies that the probability of decomposition of the complex of angular momentum K is independent of the mode of formation. In application we must also assume that the probability of formation of the complex, $2\pi\sum_{\ell} \langle \Gamma(\alpha)/D_K \rangle_{av}$, is unity for ℓ less than some ℓ_{max} and zero otherwise (14).

The cross section for formation of the complex is given by (14)

$$\sigma(\alpha) = \frac{\pi}{k_\alpha^2} \sum_{\ell=0}^{\ell_{max}} (2\ell+1) \quad [\frac{(2K+1)}{(2\ell+1)(2m+1)}]. \tag{13}$$

The summation over ℓ is restricted by the stronger of the two conditions: (a) there must be conservation of angular momentum: $|\ell - m| \leq K \leq |\ell + m|$, and (b) that $\ell \leq \ell_{max}$.

If there is no initial rotational angular momentum, Eq. (13) becomes (3)

$$\sigma(\alpha) = \frac{\pi}{k_\alpha^2} \sum_{\ell=0}^{\ell_{max}} (2\ell+1) \tag{14}$$

$$= \frac{\pi}{k_\alpha^2} (\ell_{max}+1)^2. \tag{15}$$

For large ℓ, writing $\ell = \mu v b = k_\alpha b$, we obtain for the cross section for complex formation

$$\sigma(\alpha) = \pi b_{max}^2 \tag{16}$$

where b_{max} is the maximum impact parameter expected from classical considerations (13).

Since we require that the mode of decomposition of the complex is uncorrelated with the mode of formation, except through conservation principles and detailed balancing, the cross section for forming state β from state α is

$$\sigma(\alpha,\beta) = \sum_K \sigma(\alpha,K)\ P_K(\beta) \tag{17}$$

where $\sigma(\alpha,K)$ is the cross section for forming a complex of angular momentum K from reactant state α. $P_K(\beta)$ is the probability for forming state β from the complex. The requirement of detailed balancing (3), namely that

$$(2m_\alpha+1)\ k_\alpha\ \sigma(\alpha,\beta) = (2m_\beta+1)\ k_\beta\ \sigma(\beta,\alpha), \tag{18}$$

places severe restrictions on the relative probabilities for decay into the available modes.

From Eqs. (13), (17), and (18) we obtain (14)

$$\pi \sum_K (2K+1) \sum_{\ell_\alpha} P_K(\beta) = \pi \sum_K (2K+1) \sum_{\ell_\beta} P_K(\alpha). \tag{19}$$

Since we have assumed that $P_K(\beta)$ is independent of state α, we can write Eq. (19) as

$$\pi \sum_K (2K+1)\ P_K(\beta) \sum 1 = \pi \sum_K (2K+1)\ P_K(\alpha) \sum 1. \tag{20}$$

The last sums must be equal to the numbers of states available to a given channel which can be formed from a complex

of specified energy and angular momentum:

$$\sum_{\ell_\alpha} 1 = n(\alpha). \tag{21}$$

Therefore,

$$P_K(\beta)/n(\beta) = P_K(\alpha)/n(\alpha) = N_t, \tag{22}$$

where N_t is the total number of states available from a given complex (14) and must be a constant. Therefore, the probability of forming a given product state β is

$$P_K(\beta) = n(\beta) \; / \; N_t. \tag{23}$$

Eq. (23) is analogous to Eq. (12) if we assume the probability of formation of a given product state is unity or zero contingent upon the conservation principles.

Classical Mechanical Formulation

If we replace the summation over angular momentum in Eq. (14) by an integration over impact parameter and assume that the amplitude is proportional to the phase space available to a given channel, we obtain the corresponding classical formulation. Following is a derivation of the classical version of the phase space theory for a three-body process emphasizing the conservation principles involved based primarily on the derivation of Light et al. (2,3,7,8). The phase space theory of chemical kinetics is based on the assumption that a strong coupling collision complex is formed between the reactant ion and neutral target. A strong cou-

pling complex is defined by the property (14) that the mode of decomposition of the complex is uncorrelated with the mode of formation except through conservation laws and detailed balancing (3). The quantities conserved are energy and total angular momentum and its projection on one axis. A further assumption which greatly simplifies (and allows) calculation is that the probability of formation of a strong coupling complex from a given incident channel is either unity or zero. If b_m is the maximum impact parameter in the incident channel; defined by the potential of interaction and the energetics of interaction, then the probability of formation of the complex is unity for all impact parameters less than b_m and zero otherwise. While this is not absolutely true in the quantum mechanical picture, the error introduced when considering heavy particles such as atoms is negligible. To a first approximation ion-molecule interactions leading to formation of the complex can be described by a long range polarization potential and a centrifugual repulsion barrier;

$$V(r) = -e^2\alpha/2r^4 + \hbar^2\ell(\ell+1)/2\mu r^2, \qquad (24)$$

where e is the electronic charge, α the polarizability of the neutral, ℓ the angular momentum quantum number, and μ the reduced mass of the system. Under the influence of this potential, the maximum impact parameter for formation of the complex is (13)

$$b_m = (2e^2\alpha/E)^{1/4} \tag{25}$$

where E is the relative translational energy, and the cross section for formation of the complex is

$$\sigma_m = \pi b_m^2 = \pi(2e^2\alpha/E)^{1/2}. \tag{26}$$

From the fundamental hypothesis (2) the probability of formation of a given product state i with conservation of total energy E_t and total angular momentum K is

$$P_i(E_t,K) = \Gamma_i/\Gamma(E_t,K), \tag{27}$$

where Γ_i is the phase space available to that product state, and $\Gamma(E_t,K)$ is the total phase space available given by

$$\Gamma(E_t,K) = \sum_{i=1}^{n} \Gamma_i \tag{28}$$

where the sum is over all product channels. The cross section for formation of a given product state is thus

$$\sigma(E_t,i) = 2\pi\int_0^{b_m} P_i(E_t,K)\, b\,db, \tag{29}$$

where the integration is over reactant impact parameter.

Our first task is to evaluate the phase space elements for Eq. (28). The classical three-particle phase space element is given by

$$d\Gamma = \prod_{i=1}^{3} d^3\vec{r}_i \; d^3\vec{p}_i$$

$$= d^3\vec{R} \; d^3\vec{P} \; d^3\vec{r} \; d^3\vec{p} \; d^3\vec{r}' \; d^3\vec{p}', \qquad (30)$$

where $\vec{r}_i$ and $\vec{p}_i$ are the vector coordinates and momenta of particle i; $\vec{R}$ and $\vec{P}$ are the vector coordinates and momenta of the center of mass; $\vec{r}$ and $\vec{p}$ are the relative coordinates of the third particle with respect to the center of mass of the diatomic specie; and $\vec{r}'$ and $\vec{p}'$ are the relative coordinates of the diatomic specie. Since the center of mass coordinates are cyclic, the center of mass is either at rest or moving uniformly (26). Thus, we can drop the center of mass coordinates, and the remaining twelve coordinates will define the phase space of interest. Rewriting the phase space volume element in terms of the total rotational, M, and orbital, L, angular momentum, the angular momentum in the z-direction, and the corresponding angular and radial coordinates gives for the volume element

$$d\Gamma = (dr \; dp_r \; dL \; dL_z \; d\alpha_L \; d\beta_L) \; (dr' \; dp') \times$$

$$(dM \; dM_z \; d\alpha_M \; d\beta_M). \qquad (31)$$

The first set of elements correspond to the radial coordinate, momentum coordinate, orbital angular momenta, and corresponding angular coordinates of the third body with respect to the center of mass of the diatomic specie; and the other elements

correspond to motion of the diatomic specie. It is desirable to reduce the volume element to an expression in terms of total energy, E_t, vibrational energy E_v, and total angular momentum, K, by taking the Jacobian transformation of $dr\ dp_r\ dL\ dL_z\ d\beta_L\ dr'\ dp' \rightarrow dE_t\ d\tau_t\ dK\ dK_z\ d\beta_K\ dE_v\ d\tau_v$.

For the transformation we need to consider the conservation principles:

(a) The total energy must be conserved,

$$E_t = E_{tr}^{\circ} + E_v^{\circ} + E_r^{\circ} = E_{tr}^{f} + E_v^{f} + E_r^{f} - Q_{of}, \quad (32)$$

where superscripts $^{\circ}$ and f refer to the incident and product states respectively and Q_{of} is the exothermicity of reaction. Writing $E_{tr}^{\circ} = p_r^2/2\mu$, the transformation $drdp \rightarrow dEd\tau$ is

$$\frac{\partial(r,p)}{\partial(E,\tau)} = \begin{vmatrix} 0 & p/\mu \\ -\mu/p & \partial p/\partial\tau \end{vmatrix}$$

$$= 1. \quad (33)$$

(b) Conservation of angular momentum $\vec{K} = \vec{L} + \vec{M}$. For the transformation $dLdL_z d\beta_L \rightarrow dKdK_z d\beta_K$, it is easier to transform an arbitrary angular momentum vector to Cartesian coordinates. Then, since the Cartesian components of L and K are linearly related with a Jacobian of unity, we obtain the desired transformation.

For an arbitrary angular momentum vector $\vec{J}$:

$$J^2 = J_x^2 + J_y^2 + J_z^2$$

$$\tan \beta = J_y/J_x$$

$$\frac{\partial(J, J_z, \beta)}{\partial(J_x, J_y, J_z)} = \begin{vmatrix} J_x/J & 0 & -J_y/(J_x^2 + J_y^2) \\ J_y/J & 0 & J_x/(J_x^2 + J_y^2) \\ J_z/J & 1 & 0 \end{vmatrix}$$

$$= 1/J. \qquad (34)$$

Therefore,

$$\begin{aligned} L dL dL_z d\beta_L &= dL_x dL_y dL_z \\ &= dK_x dK_y dK_z \\ &= K dK dK_z d\beta_k. \end{aligned} \qquad (35)$$

The phase space element thus becomes

$$\begin{aligned} d\Gamma = (K/L)\ & dE_t\ d\tau_t\ dE_v\ d\tau_v\ d\alpha_L\ d\alpha_M \times \\ & d\beta_K\ d\beta_M\ dK\ dK_z\ dM\ dM_z. \end{aligned} \qquad (36)$$

The integrals over α_L, α_M, β_M, β_K, τ_t, and τ_v are constants that are independent of channel and vibrational energy; thus, we can neglect them without affecting our results. Also, the integration over vibrational energy will be neglected for now, and later we will sum over vibrational states.

Taking K to lie along the z-axis, conservation of angular momentum yields

$$L^2 = K^2 + M^2 - 2KM_z, \qquad (37)$$

and the phase space for forming a given product state i consisting of a diatomic in vibrational state v_i with conservation of total energy and total angular momentum is given by

$$\Gamma_i(E_t, K, v_i) = \iint [1 + (M/K)^2 - 2M_z/K)]^{-1/2} dM dM_z. \quad (38)$$

The limits of integration of Eq. (38) are found from the physical constraints on the system as defined by the limits of a strong coupling collision and a definition of what constitutes a stable product state:

(a) The final translational energy must be positive. Writing $E_r = M^2/2I$ where I is the moment of inertia of the diatomic, gives the upper bound on the final rotational angular momentum

$$M^2/2I \leq E_t - E_v{}^f + Q_{of} = \varepsilon. \quad (39)$$

(b) The limit imposed on the rotational energy to prevent the product diatomic from dissociating is

$$M^2/2I < D_v{}^f, \quad (40)$$

where $D_v{}^f$ is the dissociation energy of the diatomic molecule from vibrational state v.

(c) The final requirement is product separation; that is, the products must have sufficient energy to pass over the angular momentum barrier. The actual limitations depend on the attractive forces between the products given by Eq. (24). The maximum in the potential occurs when

$(dV/dr)_{r=r^*} = 0$. Evaluating Eq. (24) at r^* gives for the potential evaluated at r^*

$$V(r^*) = [\hbar^2 \ell(\ell+1)]^2/(8\mu^2 e^2 \alpha). \tag{41}$$

From Eqs. (32) and (39) the final translational energy is given by

$$E_f = E_{tr}^f = \varepsilon(1 - M^2/2I\varepsilon). \tag{42}$$

In order that the products separate, we must have $E_f \geq V(r^*)$. Writing $L^2 = \hbar^2 \ell(\ell+1)$ and taking L_f to be equal to $\mu v_f b_f$, where v_f and b_f are the product velocity and impact parameter respectively, we have as a limitation on the final orbital angular momentum

$$L_f \leq (8e^2 \alpha \mu^2 E_f)^{1/4}. \tag{43}$$

From Eqs. (39) and (43) the constraint on the z-component of rotational angular momentum is given by

$$M_z \geq [K^2 + M^2 - (8e^2 \alpha \mu^2 \varepsilon)^{1/2}(1 - M^2/2I\varepsilon)^{1/2}]/2K. \tag{44}$$

Normally the integration over M_z will be from $-M$ to $+M$, but if $-M$ is less than the right hand side of Eq. (44), the integration will be from Eq. (44) to $+M$.

To find the limits of integration over M we need to find the roots of the equation

$$(K - M)^2 - (8e^2 \alpha \mu^2 \varepsilon)^{1/2} (1 - M^2/2I\varepsilon)^{1/2} = 0. \tag{45}$$

If M_1 and M_2 are the roots of Eq. (45) such that $M_2 \geq |M_1|$, the limits of integration of the phase space integral, Eq. (38), are

(a) over M_z: Upper limit = $+M$,

$$\text{Lower limit} = \begin{cases} -M, & M < |M_1|; \\ Eq.\ (44), & M > |M_1|; \end{cases}$$

(b) over M: Upper limit = M_2,

Lower limit = $|M_1|\ H(M_1)$.

Integrating Eq. (38) over M_z gives

$$\Gamma_r dM = 2M, \qquad M<|M_1| \qquad (46a)$$

$$= M - K + (8e^2\alpha\mu^2\varepsilon)^{1/4}\ (1-M^2/2I\varepsilon)^{1/4}, \quad M>|M_1|. \qquad (46b)$$

Eq. (46) will give the phase space for forming a diatomic with a given rotational angular momentum M. Integrating over M then gives the phase space for a given product state containing a diatomic molecule and a free particle

$$\Gamma_i(M_1,M_2,K,\varepsilon) = (8e^2\alpha\mu^2\varepsilon)^{1/4} \int_{|M_1|}^{M_2} (1-M^2/2I\varepsilon)^{1/4} dM +$$

$$[K|M_1| + \tfrac{1}{2} M_1^2]\ H(-M_1) - [KM_2^2 - \tfrac{1}{2} M_2^2]S(K-M_2) +$$

$$[K|M_1| - \tfrac{1}{2} M_1^2]\ H(M_1)S(K-M_1) - K^2H(M_2-K)H(K-M_1), \qquad (47)$$

where

$$H(f) = \begin{cases} 0, & f<0, \\ 1, & f>0, \end{cases}$$

and

$$S(f) = \begin{cases} -1, & f<0, \\ +1, & f>0. \end{cases}$$

The total phase space is obtained by summing Γ_i over all product states, electronic and vibrational. However, Eq. (47) includes the phase space available for rotational dissociation, Eq. (40). Writing $M_3 = (2ID_v{}^i)^{1/2}$, we have for the phase space containing a stable diatomic in channel i and vibrational state v_i

$$\begin{aligned} \Gamma_i(E_t,K,v_i) = {} & \Gamma_i(M_1,M_2,K,\varepsilon)H(M_3-M_2) + \\ & \Gamma_i(M_1,M_3,K,\varepsilon)H(M_3-|M_1|)H(M_2-M_3) + \\ & [2(KM_3-K^2)H(M_3-K) + M_3{}^2H(K-M_3)] \times \\ & H(-M_1)H(|M_1|-M_3); \end{aligned} \tag{48}$$

and the phase space for three-body breakup from vibrational state v_i is

$$\Gamma_i{}^d = \Gamma_i(M_1,M_2,K,\varepsilon) - \Gamma_i(E_t,K,v_i). \tag{49}$$

Eq. (48) gives the phase space for a product channel containing a diatomic and a free particle, and by summing Eq. (49) over all product vibrational states we obtain the phase space for dissociation of a particular diatomic specie. Thus, using Eqs. (27) and (29) we are able to obtain the

cross sections for production of a given product state, given the total energy and angular momentum. To simplify the calculation, we assume that the initial rotational energy and rotational angular momentum are negligible compared to the total energy and total angular momentum. This assumption allows us to take $K^2 = L_o^2 = 2\mu E_{tr} {}^{o}b^2$, where b is reactant impact parameter, and μ is the reduced mass in the incoming channel. The total cross section for a given channel requires summation over initial and final vibrational states;

$$\sigma_{tot}(i) = \sum_{v_o} W(v_o) \sum_{v_i} \sigma(E_{tr}, i, v_i), \tag{50}$$

where $W(v_o)$ is the probability that the initial vibrational state was v_o.

Our calculations make use of spectroscopic data available in the literature on the atomic and molecular properties. Relevant data for the systems investigated in this work are given in Appendix A. The vibrational energies of the diatomic species in channel i are given by (27)

$$E_v{}^{i} = (v+\tfrac{1}{2})\ \omega_e(i) - (v+\tfrac{1}{2})^2\ \omega_e x_e(i), \tag{51}$$

and dissociation energies are given as

$$D_v{}^{i} = D_o - E_v{}^{i}. \tag{52}$$

The moment of inertia of the diatomic, $I = \mu r_{eq}{}^2$, in a given vibrational level is approximated by taking

$$r_{eq} = \tfrac{1}{2}(r_+ + r_-). \tag{53}$$

r_+ and r_- are obtained from a Morse potential function (27)

$$U(r-r_e) = D_e(1 - exp\ [-\beta(r-r_e)]) \tag{54}$$

where β is given by $\omega_e(2\pi\mu c/D_e h)^{1/2}$ (27). Solving Eq. (54) for r gives

$$r_{\pm} = r_e - \beta^{-1} ln\ [\bar{+}(E_v{}^i/D_e)^{1/2} - 1]. \tag{55}$$

The values of internuclear separation from Eq. (53) are in approximate agreement with those obtained from more accurate RKR curves.

The calculations were performed on a UNIVAC 1108 computer. Appendix B gives an outline of the computer calculation used in the following sections. We have selected systems to allow a thorough testing of the phase space model as a viable model for predicting the outcome of gas-phase reactions. The possibilities included are charge transfer, dissociative charge transfer, collision induced dissociation, rearrangement, and distribution of internal vibrational and rotational energy. Also, calculations were performed for those systems for which experimental data were available with which to compare results of the calculations.

CHAPTER III

CHARGE TRANSFER AND DISSOCIATIVE CHARGE TRANSFER REACTIONS OF RARE GAS IONS WITH NITROGEN

In this chapter we compare experimental reaction cross sections for reactions of rare gas ions with nitrogen with those predicted using phase space arguments. Since recombination energies of reactant rare gas ions vary from 13.99 to 24.58 eV, one might hope to examine the "mixing" of energetically accessible N_2^+ electronic states at low relative velocities and the effect of increasing translational energy on various reaction channels. We observe that those product states which are most energetically favorable may not be the experimentally preferred product. In these cases it is necessary to make some *a priori* assumptions as to allowed products. Calculated product energy distributions are compared with those obtained from experimental product kinetic energies measured at specified scattering angles and with the internal energy distributions estimated from measurements of radiation intensity from spontaneous decay of electronically excited reaction products. Table 1 shows the exothermicities for the various reaction channels calculated from the data in Appendix A.

Table 1: Energetics of Rare Gas Ion-Nitrogen Reaction (in eV)

Reactant Ion	Product Ion				
	$N_2^+(X^2\Sigma_g)$	$N_2^+(A^2\pi_u)$	$N_2^+(B^2\Sigma_u)$	$N_2^+(C^2\Sigma_u)$	$N^+(^3P)$
$He^+(^2S)$	9.004	7.887	5.887	1.005	0.280
$Ne^+(^2P_{3/2})$	5.983	4.866	2.814	-2.016	-2.741
$Ne^+(^2P_{1/2})$	6.080	4.963	2.911	-1.919	-2.644
$Ar^+(^2P_{3/2})$	0.179	-0.938	-2.990	-7.820	-8.545
$Ar^+(^2P_{1/2})$	0.357	-0.760	-2.812	-7.642	-8.367
$Kr^+(^2P_{3/2})$	-1.580	-2.697	-4.749	-9.579	-10.304
$Kr^+(^2P_{1/2})$	-0.914	-2.031	-4.083	-8.913	-9.638

$He^+ + N_2$

N_2^+ and N^+ are formed by charge transfer and dissociative charge transfer processes respectively. For the $He^+ + N_2$ reaction the various channels of reaction are

$$He^+(^2S) + N_2(X^1\Sigma_g, v = 0) \rightarrow \begin{cases} He(^1S) + N_2^+(X^2\Sigma_g, v') & (56a) \\ He(^1S) + N_2^+(A^2\pi_u, v') & (56b) \\ He(^1S) + N_2^+(B^2\Sigma_u, v') & (56c) \\ He(^1S) + N_2^+(C^2\Sigma_u, v') & (56d) \\ He(^1S) + N(^4S) + N^+(^3P) & (56e) \\ He^+(^2S) + N_2(X^1\Sigma_g, v') & (56f) \end{cases}$$

and cross sections obtained are given in Fig. 1. The dashed line is the Langevin total cross section calculated from the ion-induced dipole potential and the dot-dash curve is that calculated for dissociative N^+ reactions. Individual molecular charge transfer channels are given by solid curves. Results in Fig. 1 have been obtained under the assumption that mixing of various states occurs in the collision with the consequence that all final states are statistically available. However, it is possible that certain electronic states do not mix and are preferentially formed due to conditions such as spin conservation not strictly included in the simple phase space treatment. If one N_2^+ product state

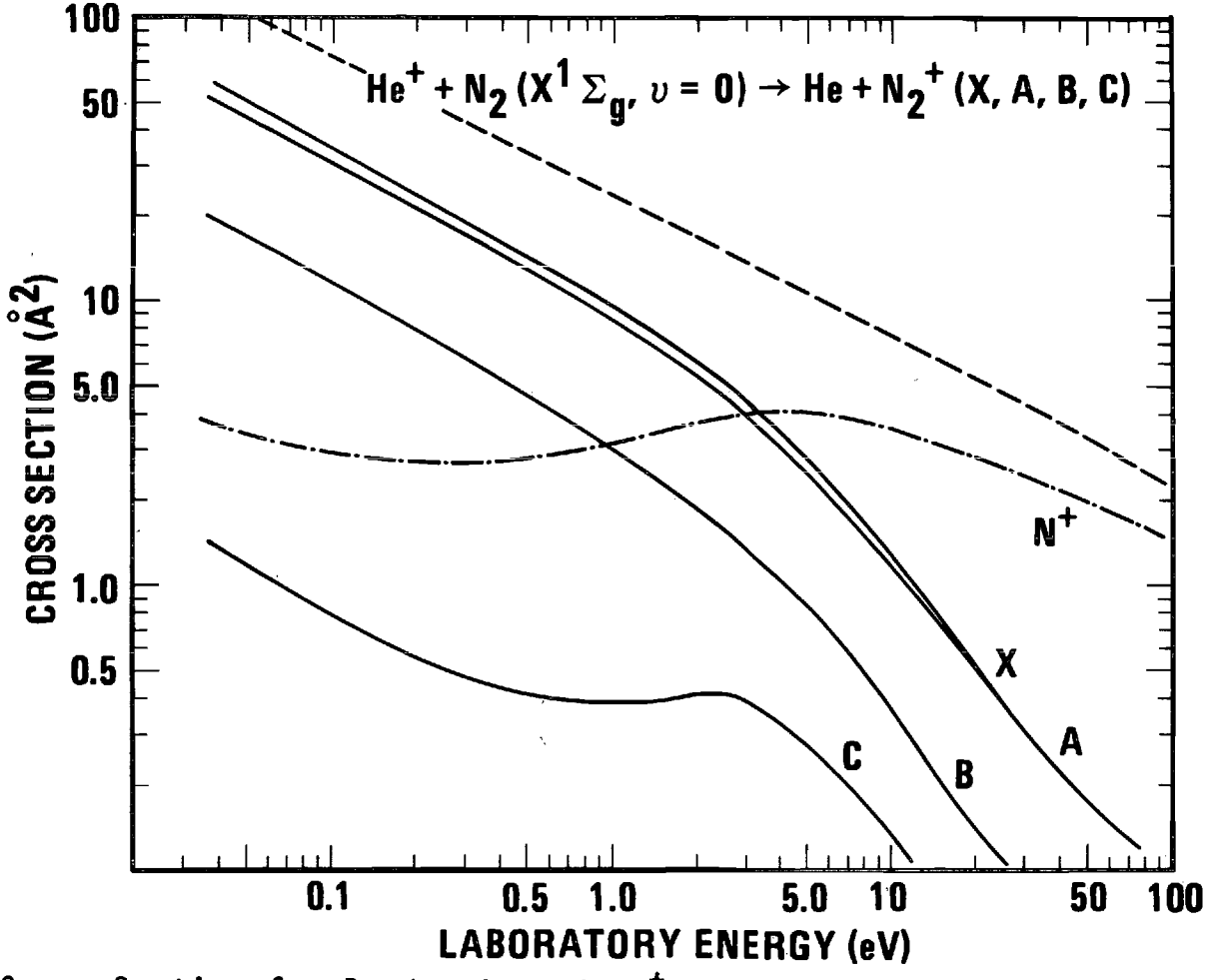

Figure 1. Cross Section for Production of N_2^+ Assuming Complete Mixing of Product States. (The dashed curve is the cross section for formation of the complex, and the solid lines are the calculated cross sections for the indicated electronic state.)

is considered dominant in the interaction, the curves in Fig. 2 are obtained from the phase space calculations. For example, the curve labeled C is obtained when the $N_2^+(C^2\Sigma_u, v')$ state is considered to predominate over transitions forming ions in the X, A, and B states. When only one N_2^+ electronic state is preferentially formed, the cross sections are similar which renders determination of the dominant state difficult when comparing theory and experiment. For clarity the cross sections presented in Figs. 1 and 2 are summed over all vibrational levels in each electronic state. Typical cross sections for individual vibrational channels of reaction are given for the C state in Fig. 3. The phase space model applied to this reaction predicts N_2^+ ions formed with high vibrational excitation; however, the $v = 0$ cross section predominates at all energies. A summary of experimental cross sections (28-40) for N_2^+ formation as a function of He^+ LAB kinetic energy is given in Fig. 4. The lowest energy point was obtained from total rate constants (29-31,33-38) with the assumption that the N^+ to N_2^+ abundance at thermal energies is 58 per cent to 42 per cent respectively (32,36,37). The solid curve is the total N_2^+ cross section calculated by assuming the $C^2\Sigma_u$ product state dominant.

Experimental data (28,40-42) for the competitive N^+ reaction channel are presented in Fig. 5. The data of Ref.

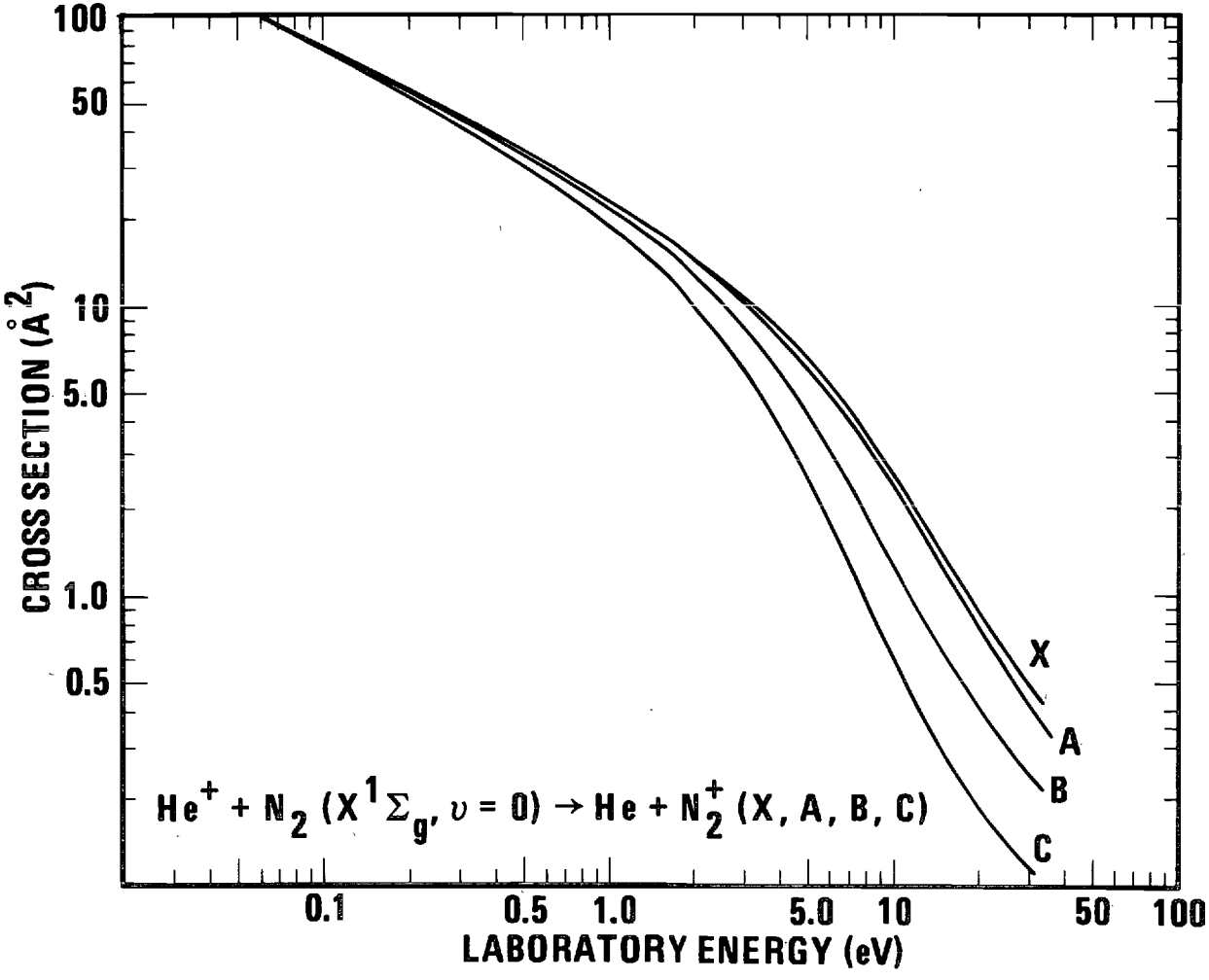

Figure 2. Cross Section for the Production of N_2^+ Calculated as a Function of He^+ Kinetic Energy with no Mixing of Product States.

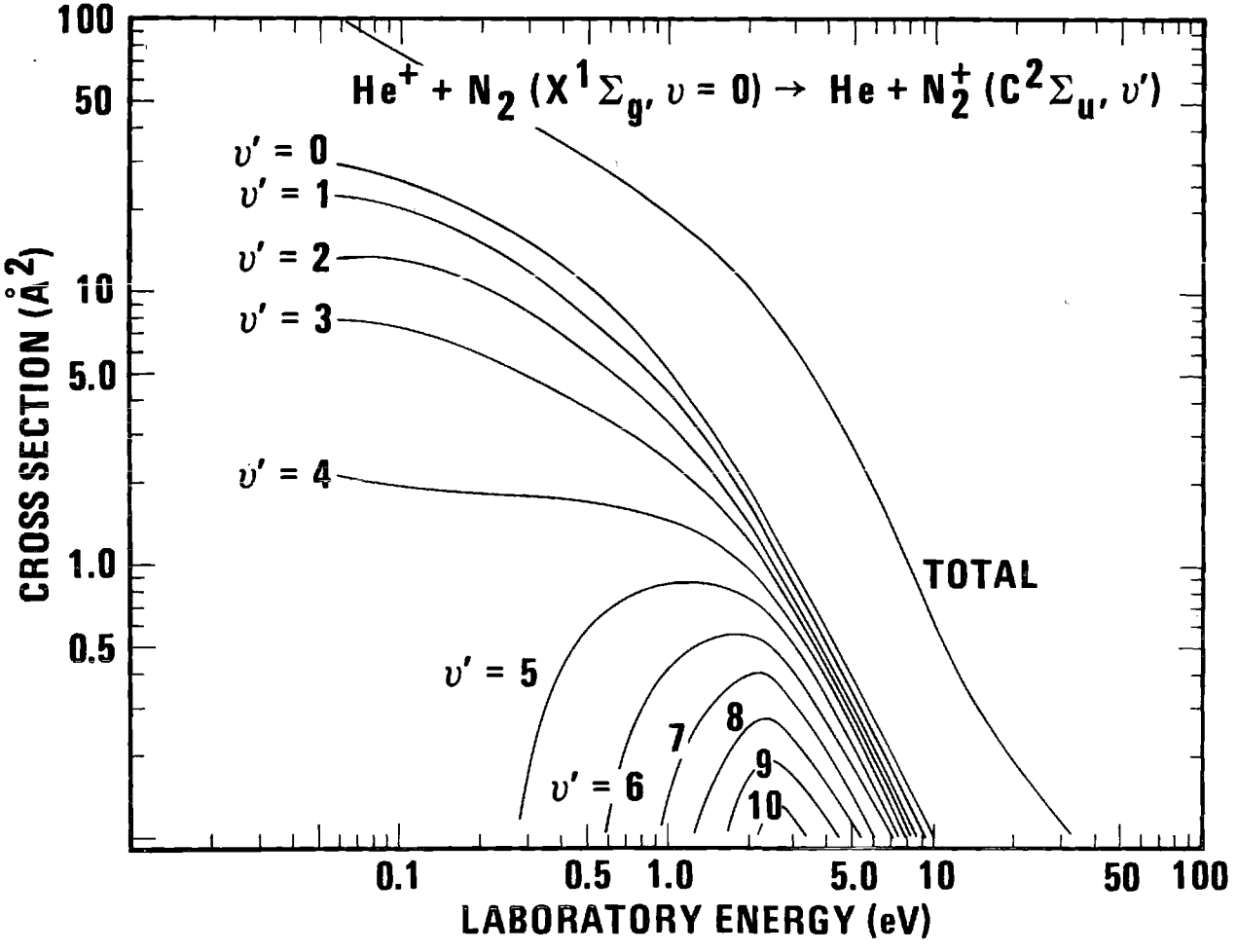

Figure 3. Vibration Distribution of $N_2^+(C^2\Sigma_u)$ Calculated as a Function of He^+ Kinetic Energy.

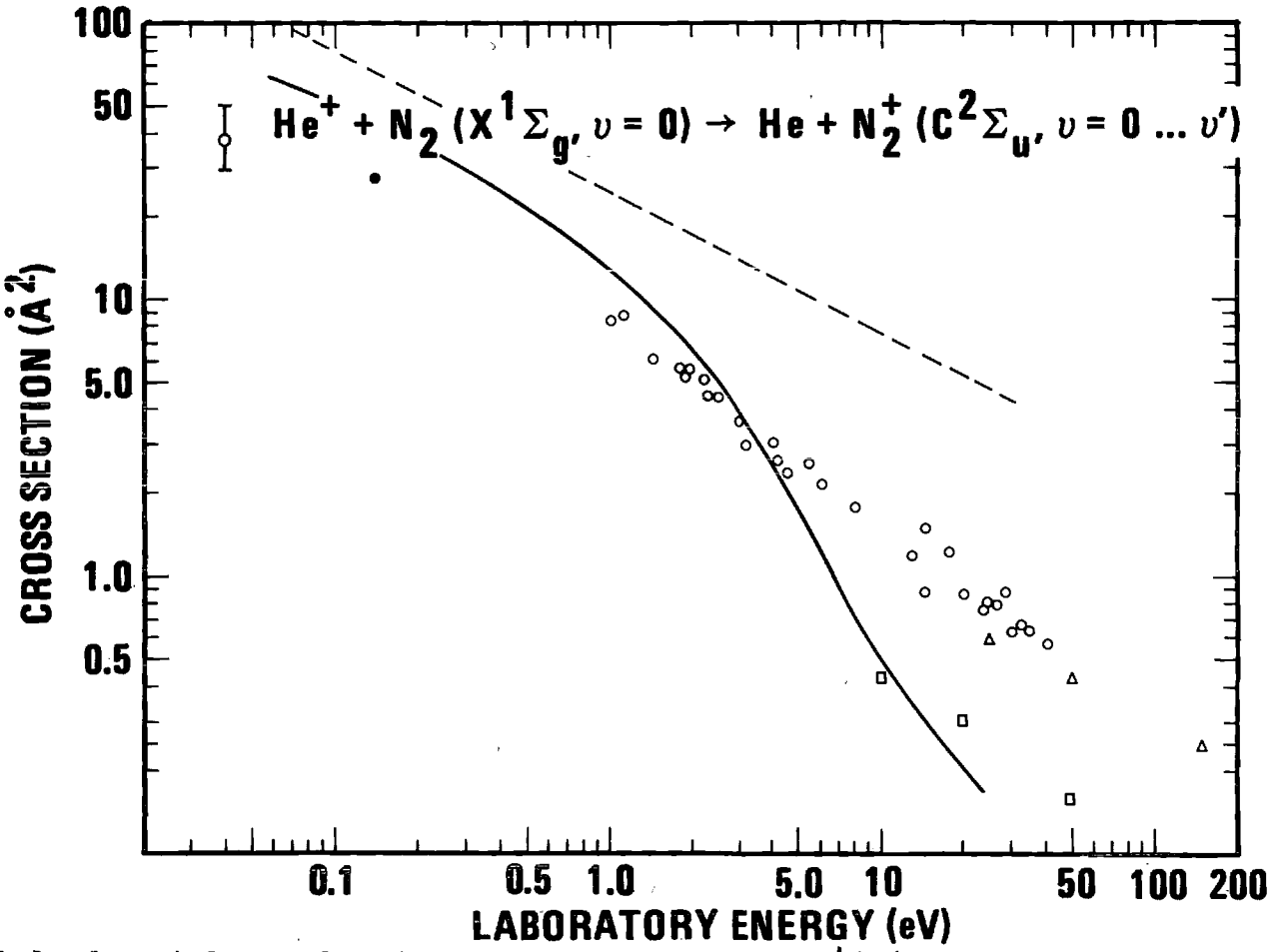

Figure 4. Calculated Cross Section for Formation of $N_2^+(C^2\Sigma_u)$ as a Function of He^+ Kinetic Energy. (The dashed curve is the total cross section for formation of the complex, the data points are from Ref. (28) O; Ref. (40) □; Ref. (39) △; Ref. (32) ●; Ref. (29-36) ⊖ represents the average of the thermal data.)

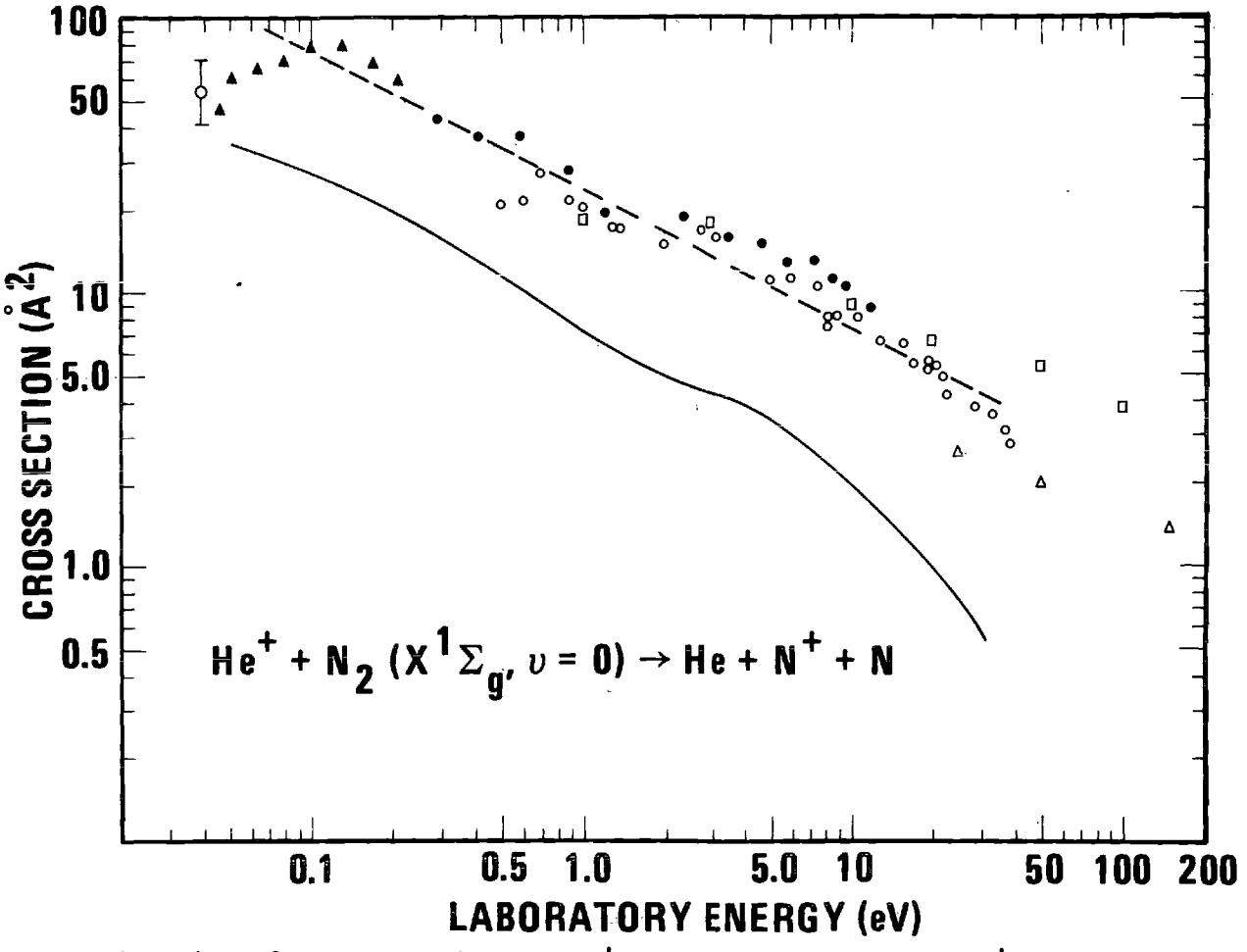

Figure 5. Cross Section for Formation of N^+ as a Function of He^+ Kinetic Energy. (The data points are: Ref. (28) ○; Ref. (41) ●; Ref. (40) □; Ref. (39) △; Ref. (42) ▲; Ref. (29-36) ⊖ represents the average of the thermal data.

(40) has been normalized to the N^+ data of Maier (28) and Moran and Friedman (41) to obtain absolute cross sections. Spectroscopic investigation (31,43,44) of the products of $He^+ - N_2$ charge transfer reactions have shown that the second negative band system corresponding to the transitions

$$N_2^+(C^2\Sigma_u v = v') \rightarrow N_2^+(X^2\Sigma_g v = v'') + h\nu \qquad (57)$$

are particularly intense indicating that $N_2^+(C^2\Sigma_u)$ is the primary charge transfer product state. Additional evidence that Eq. (56d) is the main reaction channel has been obtained by Champion and Doverspike (45) using ion beam techniques. They find that N_2^+ product ion kinetic energies are consistent with the formation of C state ions which are energetically close to the recombination energy of He^+. Carroll (43) has shown that a predissociation process occurs to form N^+ and N via the reactions

$$N_2^+(C^2\Sigma_u) \rightarrow N(^4S) + N^+(^3P). \qquad (58)$$

Due to the facts that Inn (31) has shown that the molecular charge transfer favors high rotational states, and high rotational states of the $v=2$ level in the C state are slightly above the X state dissociation limit (46), and spontaneous radiative transitions from the $v=2$ level are not observed (43); we have considered all the $N_2^+(C^2\Sigma_u, v=2)$ ions to predissociate, forming N^+. It is estimated that spontaneous

radiative transitions and predissociation processes, Eqs. (57) and (58) respectively, occur with equal probability for the $v=3$ to 6 levels (31,37,43,44); and we have accordingly assumed that one half of the N_2^+ ions in these levels predissociate, Eq. (58). At approximately 4eV He^+ kinetic energy the phase space model predicts the appearance of $N^+(^3P)$ and $N(^2D)$ from dissociation of $N_2^+(C^2\Sigma_u)$ ions formed with internal energies in excess of the dissociation limit. The N^+ cross section calculated from phase space theory assuming both predissociation and direct dissociation of $N_2^+(C^2\Sigma_u)$ ions is presented in Fig. 5 for comparison with experimental data. Although there is only approximate accord between the magnitude of the calculated and experimental cross sections, the energy dependences of the cross sections predicted by the phase space model are in reasonable agreement with experiment. It should be remembered that the ion-induced dipole potential has been considered rather than a more accurate quantum mechanical potential (24).

Schmeltekopf et al. (37) have examined the role of reactant internal state preparation on the reaction mechanism by changing the $N_2(X^1\Sigma_g, v)$ vibrational temperature. Increasing the internal vibrational energy of N_2 has been shown to enhance the production of N^+. Fig. 6 displays their experimental $N^+/(N_2^+ + N^+)$ product ion ratios as a function of reactant molecule vibrational temperature. In order to com-

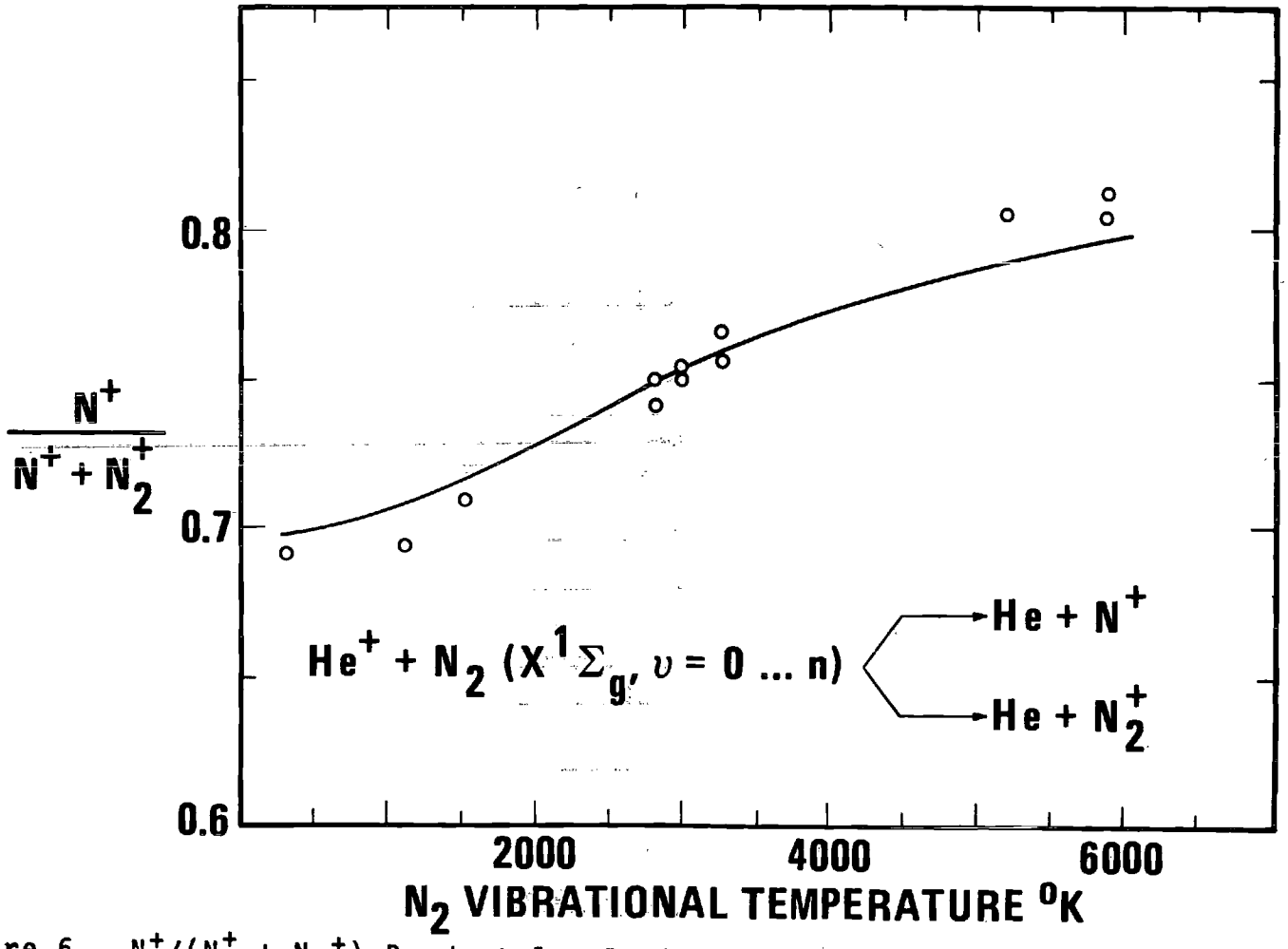

Figure 6. $N^+/(N^+ + N_2^+)$ Product Ion Ratios Given as a Function of Reactant N_2 Vibrational Temperature. (The data are from Ref. (37) and the solid line is the calculated ratio.)

pare the phase space results with their experiments, we have estimated the vibrational population distribution of the $N_2(X^1\Sigma_g, v)$ molecules at the various temperatures from the relation (27)

$$N_v/N_o = exp\ \{-G_o(v)hc/kT\} \qquad (59)$$

using vibrational term values given by Wallace (48). These initial N_2 distributions were then used in the phase space model. The results of this calculation were normalized to the data of Ref. (37) and are shown as the solid line in Fig. 6. The agreement between the two tends to support the application of the theoretical model to these ion-molecule reactions but does not unambiguously identify the C state as the important product ion state in $He^+ - N_2$ interactions. Champion and Doverspike (45) have measured product ion kinetic energy distributions at specified scattering angles for this reaction. They have shown that the kinetic energy of a product ion, M_3, appearing at a given LAB scattering angle θ for a given LAB collision energy, E_1, is given by

$$E_3 = [M_1M_3/(M_1+M_2)^2]\ \{cos\ \theta \pm [(1/\gamma^2) - sin^2\theta]^{1/2}\}^2 E_1, \qquad (60)$$

where M_1 is the mass of the incident ion and M_2 that of the incident neutral. γ is given by the relation

$$\gamma = \{(M_1M_3/M_2M_4)\ [E/(E+\Delta E)]\}^{1/2} \qquad (61)$$

where E is the center-of-mass energy and ΔE is the energy

defect of the reaction. Their experimental data (44) obtained at $\theta = 0^o$ for 6.24eV He^+ ions are given in Fig. 7. Relative vibrational level populations of ions in the $N_2^+(C^2\Sigma_u)$ state, (Fig. 3), have been taken to be representative of vibrational population in the center of mass frame; and product ion kinetic energy distributions in the LAB system were constructed using Eqs. (60) and (61). The correlation between the experimental and theoretical N_2^+ kinetic energy distributions, which have been corrected for the incident He^+ kinetic energy distribution, provide rather clear cut evidence that the $C^2\Sigma_u$ state is the important N_2^+ final state. The N^+ product ion kinetic energy distribution from the breakup process has been estimated using the aforementioned two-step predissociation mechanism in which $N_2^+(C^2\Sigma_u, v' = 2\text{-}6)$ ions are first formed, and then a fraction dissociate in a two body process. The agreement observed in Fig. 7 gives credibility to the model and the use of the phase space treatment to predict product vibrational distributions.

It has been estimated (37) that the fraction of molecular charge transfer processes that populate the $N_2^+(B^2\Sigma_u)$ state is less than 5 per cent. The lifetime of the B state with respect to spontaneous radiative transitions is 6×10^{-8} seconds, a time period short with respect to collisional deactivation. Thus, emitted light can be used to examine

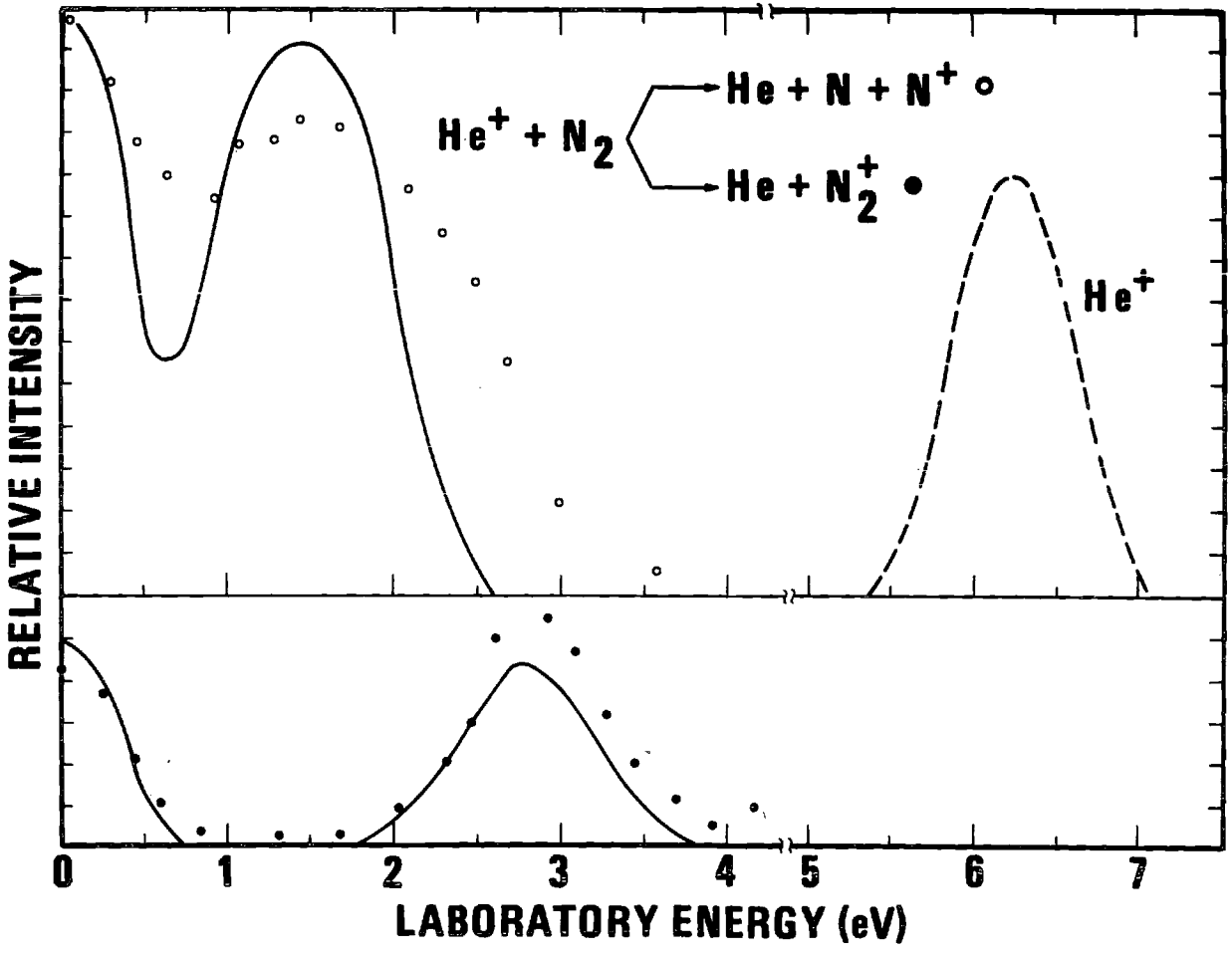

Figure 7. Kinetic Energy Distribution for the $He^+ + N_2$ Reactions Involving 6.24 eV He^+. (The data are from Ref. (45) and the solid curves are the calculated product ion relative intensities.)

vibrational energy content of N_2^+ product ions in this state. The intensity of radiation from $N_2^+(B^2\Sigma_u, v') \rightarrow N_2^+(X^2\Sigma_g, v'')$ transitions measured by Schmeltekopf et al. (37) is given in Table 2 along with the normalized calculated intensities. The latter have been obtained from cross sections computed from phase space theory and weighted by the respective Franck-Condon factors (49,50) for the $B \rightarrow X$ transitions. As the reactant N_2 vibrational temperature is altered from 300° to 4000°, no appreciable change in relative transition intensity is observed (37); and the normalized calculated intensities remain constant over this temperature change. The competitive inelastic scattering channels corresponding to vibrational excitation of the target molecules are predicted to occur simultaneously with the charge transfer reaction and are presented on Fig. 8. As previously noted, the least endoergic channels of reaction are statistically favored over the range of ion kinetic energies.

$Ne^+ + N_2$

Cross sections for individual N_2^+ and N^+ product channels in the $Ne^+ - N_2$ interactions have been calculated for a series of reaction possibilities analogous to the He^+ reactions, Eq. (56). The computed cross sections are displayed in Fig. 9 where large X, A, B, and C letters refer to cross sections calculated for respective electronic states of the product N_2^+ ions. Curves in Fig. 9 were calculated by

Table 2: Relative Transition Probabilities for N_2^+ First Negative Transitions

$$N_2^+(B^2\Sigma_u, v') \rightarrow N_2^+(X^2\Sigma_g, v'') + h\nu$$

for B state ions formed in the ion molecule reaction

$$He^+ + N_2(X^1\Sigma_g, v) \rightarrow N_2^+(B^2\Sigma_u, v')$$

Transition $v' \rightarrow v''$	Cross Section for forming $N_2^+(B^2\Sigma_u, v')$ T_v = 300°	4000°	$\{\Psi_{v'}\|R_e(r)\|\Psi_{v''}\}^2$	Normalized Calculated Intensity 300°	4000°	Observed Relative Intensity
$0 \rightarrow 1$	4.64	6.04	.2821	29.0	28.7	18
$1 \rightarrow 2$	4.54	5.92	.3128	31.6	31.6	33
$2 \rightarrow 3$	4.43	5.80	.2448	24.1	24.1	28
$3 \rightarrow 4$	4.33	5.68	.1603	15.3	15.5	21

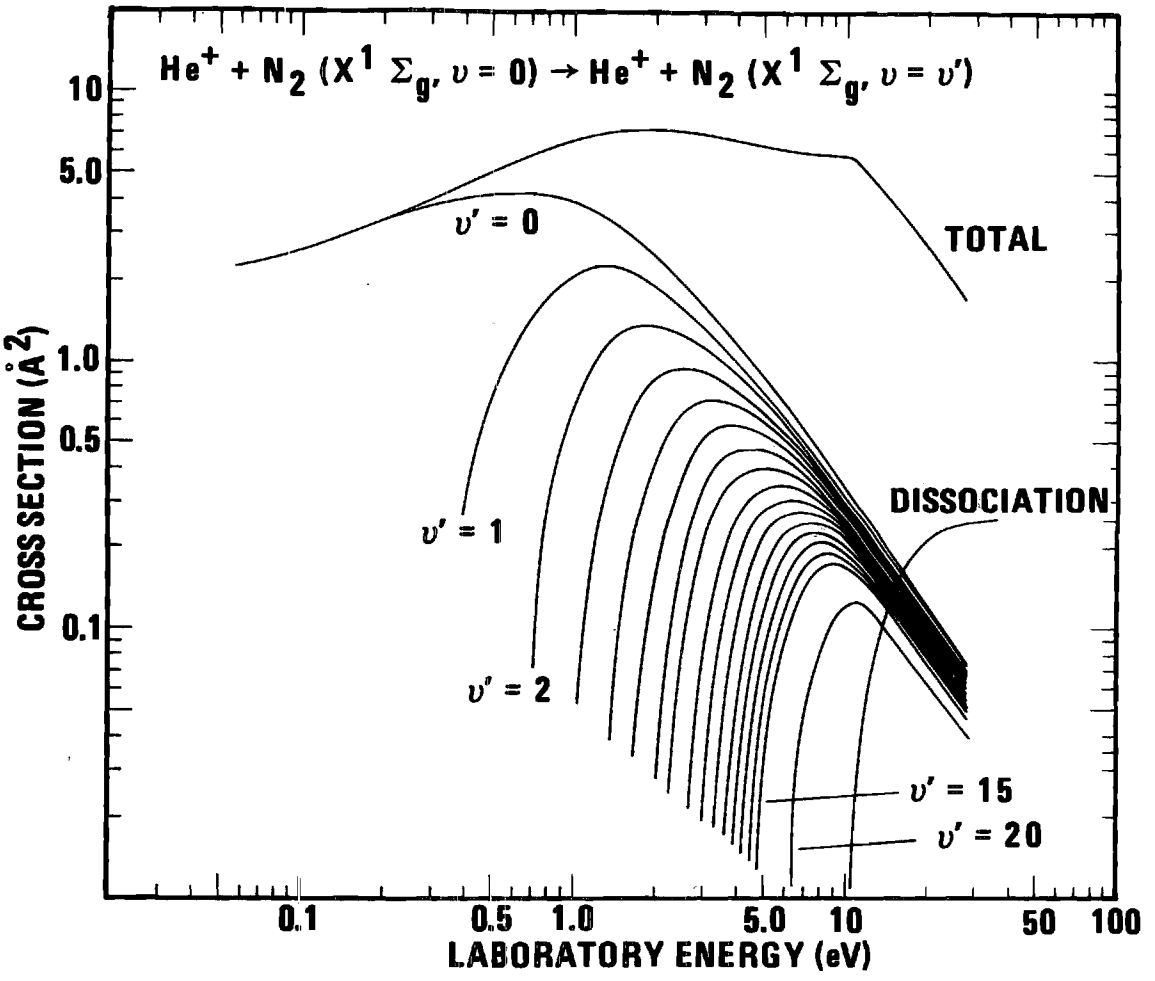

Figure 8. Vibration Distributions Calculated for the Inelastic Scattering Channels in $He^+ - N_2$ Interactions as a Function of He^+ Kinetic Energy.

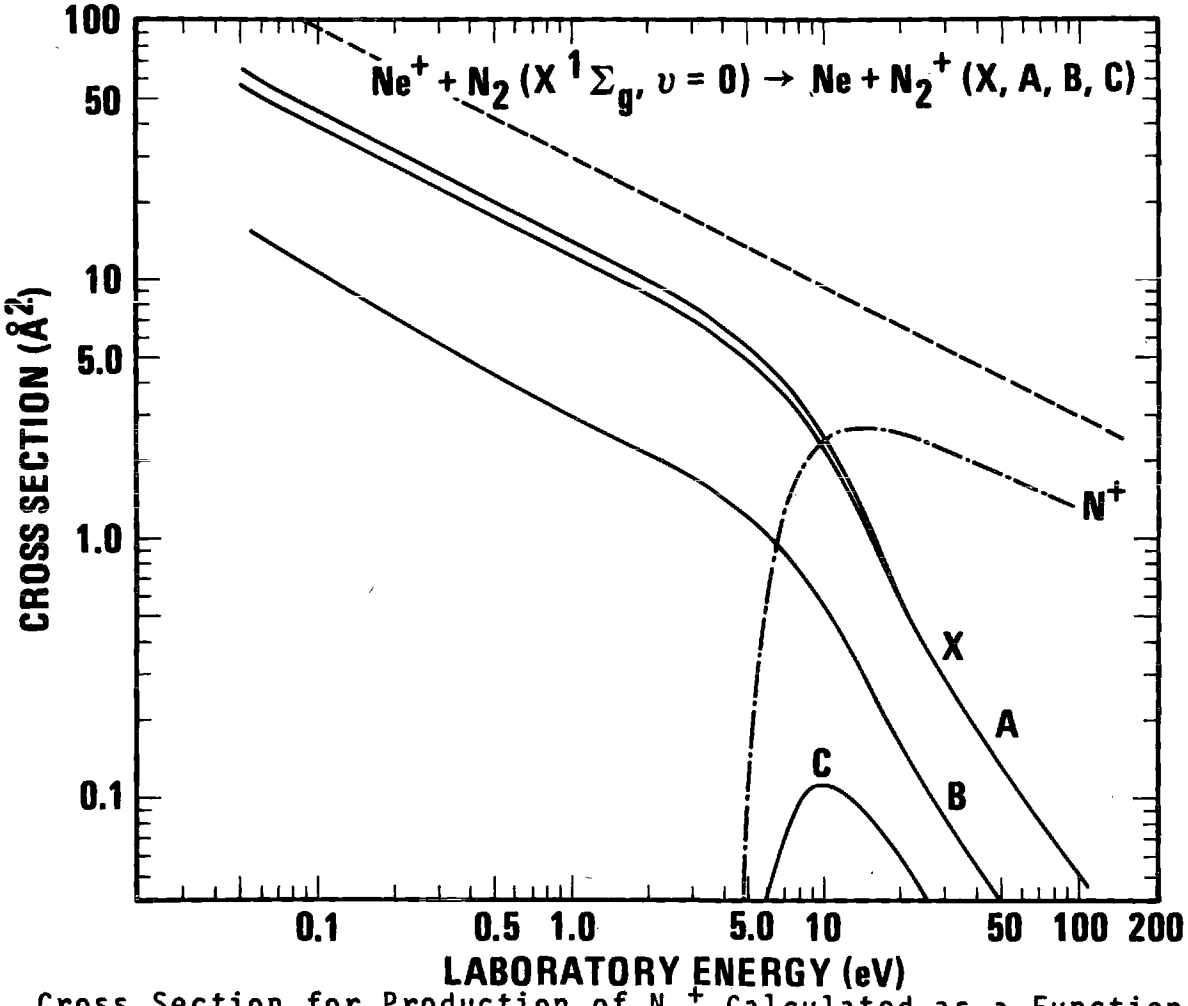

Figure 9. Cross Section for Production of N_2^+ Calculated as a Function of Ne^+ Kinetic Energy Assuming Complete Mixing of Product States. (The dashed line is the cross section for formation of the complex, and the solid lines are calculated cross sections for the indicated electronic state.)

assuming that all electronic states "mix" and the cross sections can be calculated statistically. The alternate point of view adopted in $He^+ - N_2$ interaction involves the assumption that only one product state is available. If a similar assumption is adopted for $Ne^+ - N_2$ reactions, then the cross sections for N_2^+ formation given in Fig. 10 result. For example, the curve labeled X is computed by considering the X electronic state the only accessible electronic state for product N_2^+. Also shown in this graph is the experimental upper limit reported by Hemsworth et al. (51). If one considers the X, A_u or B electronic states as statistically possible products, then the calculated cross section shown in Fig. 10 is in disagreement with experimental data. This small cross section at low kinetic energies is consistent with formation of $N_2^+(C^2\Sigma_u, v')$ ions as the only allowed product ion state. Evidence has been given in the $He^+ - N_2$ case that the $N_2^+(C^2\Sigma_u, v)$ state predissociates; and we have accordingly taken all the $v'=2$ and one half of the ions in the $v'=3$, 4, 5, and 6 levels to predissociate giving N^+ which results in the irregular structure of the C state curve given in Fig. 10.

Dissociative reactions producing N^+ are given in Fig. 11 where the experimental data of Maier (52) and Schlumbohm (53) are given as the open and closed circles respectively, and the curves are the cross sections calculated

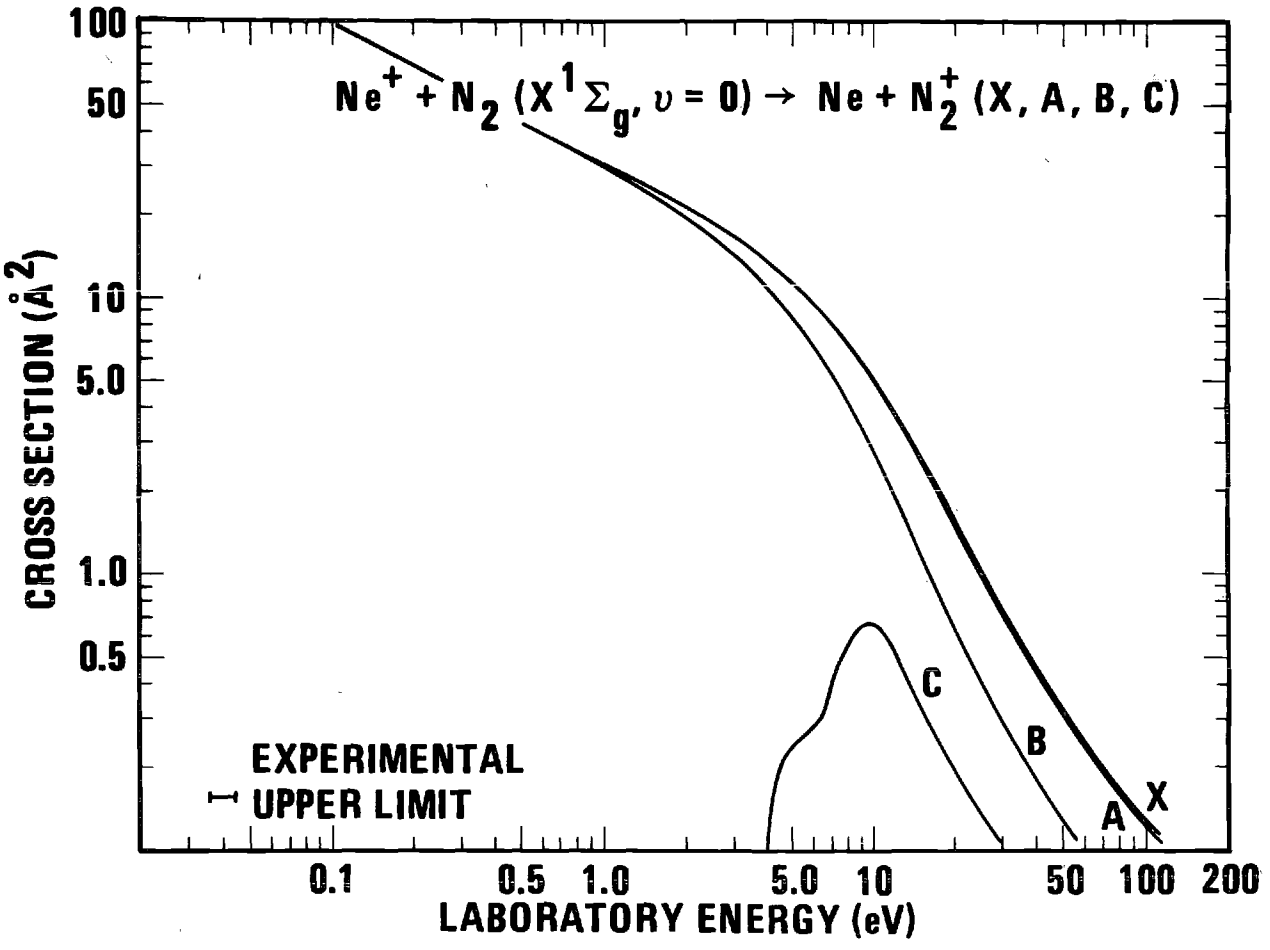

Figure 10. Cross Section for Production of N_2^+ Calculated as a Function of Ne^+ Kinetic Energy. (The experimental upper limit is given by Ref. (51).)

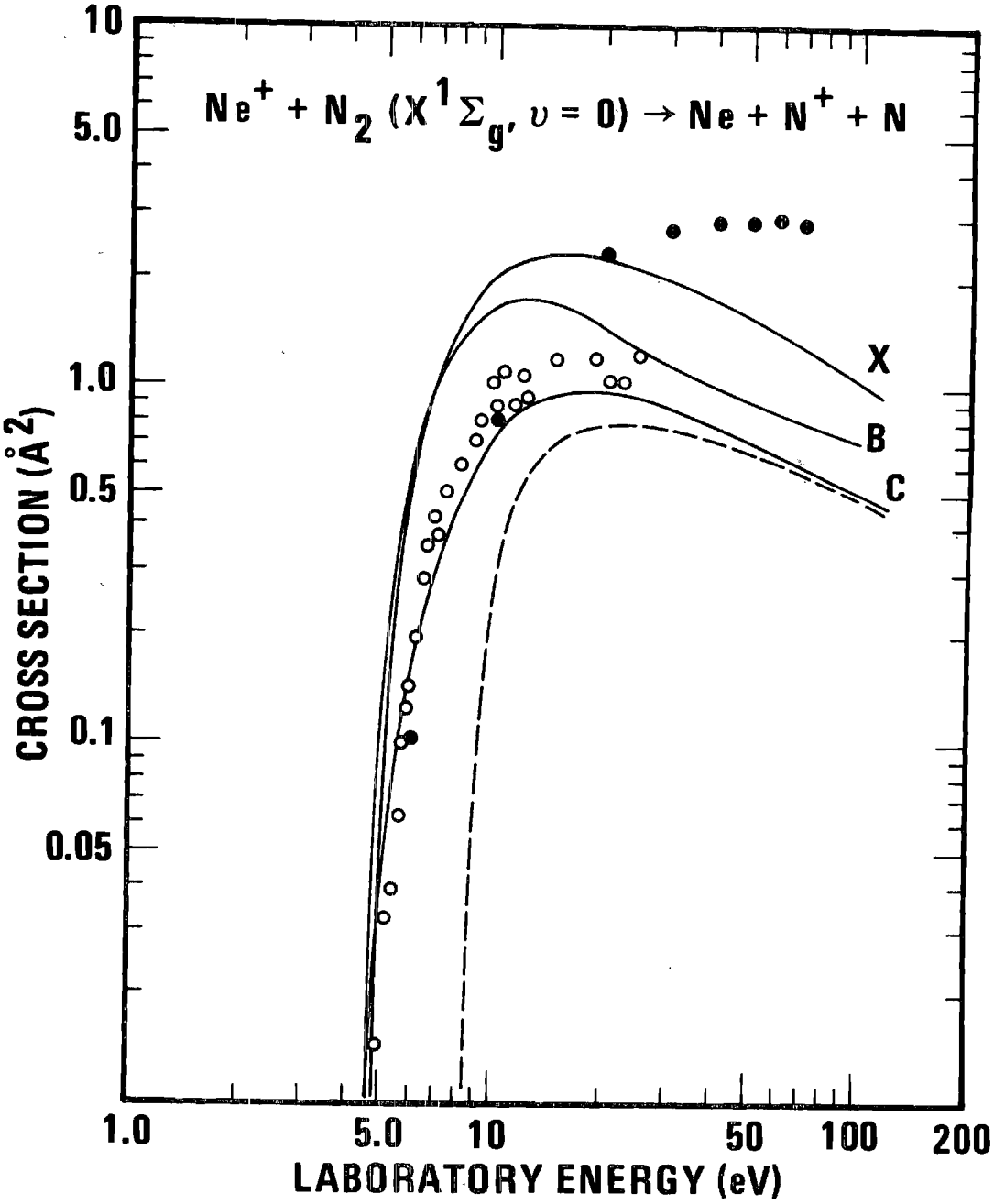

Figure 11. Cross Section for the Dissociative N^+ Reaction Channel as a Function of Ne^+ Kinetic Energy. (The data points are Ref. (52) O and Ref. (53) ●. The dashed line is that from direct dissociation of the C state, and the curve labeled C includes predissociation.)

statistically. The closed points (53) in Fig. 11 represent total ion production and, thus, are the upper limit to the dissociative cross sections since the N_2^+ channel of reaction is included. Curves labeled X and B are those calculated under the assumption that N^+ results from dissociation of $X^2\Sigma_g$ and $B^2\Sigma_u$ states respectively. The calculated result for dissociation from the $A^2\pi_u$ state is not presented in the figure since it is essentially the same as the X curve. The dashed line is that calculated for C state dissociation to its asymptotic limit giving rise to excited N atoms. The solid curve labeled C is that calculated by assuming the predissociation mechanism of the C state ions to form N^+ in addition to the N^+ ions formed from the direct dissociation of C state ions. This composite curve is in reasonable agreement with the experimental data. Additional evidence for C state formation is given in Fig. 12 where data of Champion and Doverspike (45) are presented. The dashed curve gives the distribution of reactant 5.5eV He^+ ions, and the closed and open circles are the kinetic energy distributions measured for N_2^+ and N^+ respectively. Solid curves are those calculated using Eqs. (60) and (61) along with vibrational distributions from phase space theory. The two peaked structure calculated for N_2^+ product ions is not as pronounced in the experimental data which would possibly indicate that not all the $N_2^+(C^2\Sigma_u, v'=2)$ ions predissociate giving N^+. The N^+

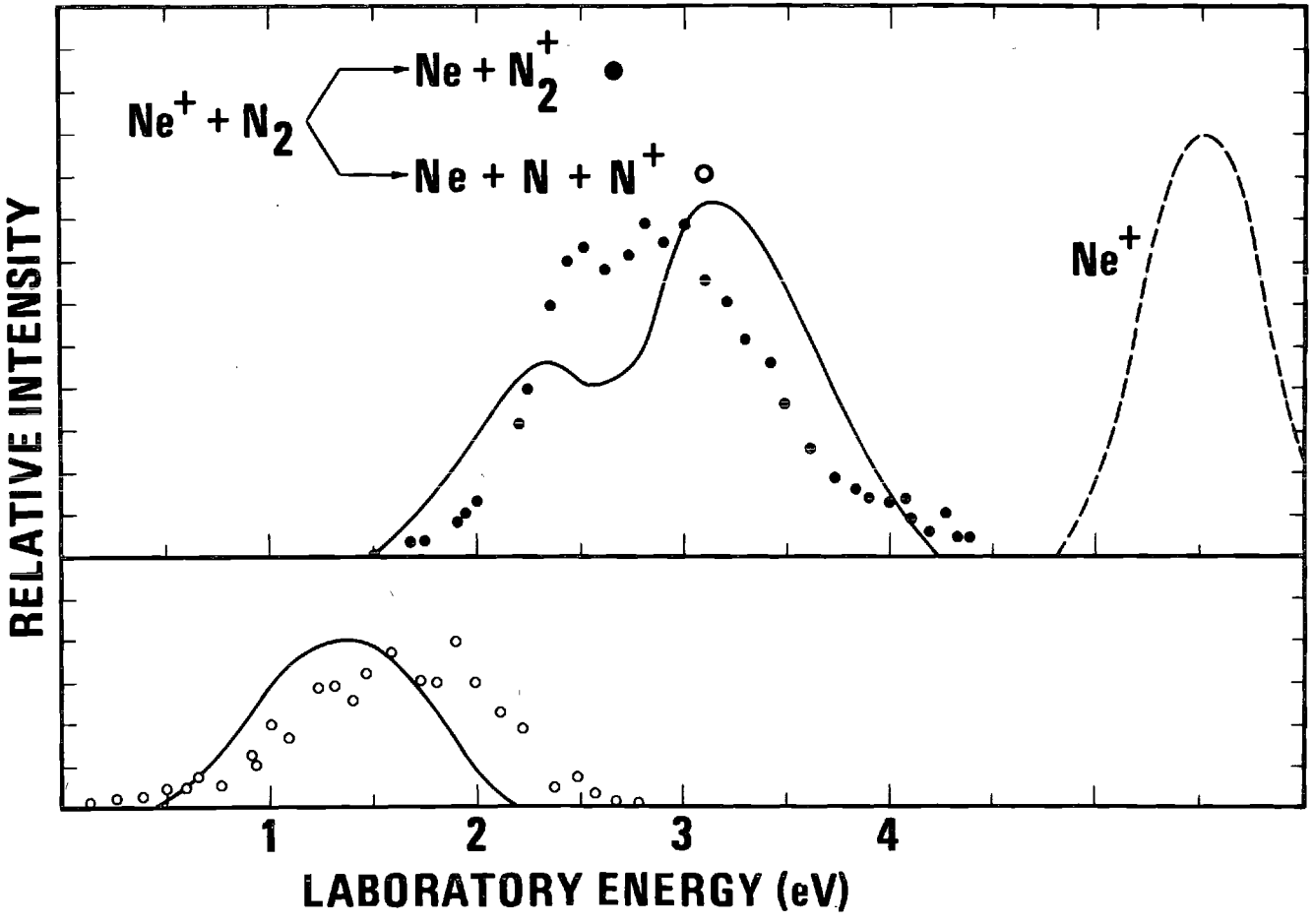

Figure 12. Kinetic Energy Distribution for the $Ne^+ - N_2$ Interaction Involving 5.5 eV Ne^+ Ions. (The data are from Ref. (45), and the solid lines are the calculated distributions.)

product ion distribution has been estimated from the previously proposed two-step mechanism in which atomic ions are considered to result from a two body breakup process of the molecular ion. The breakup process leads to N^+ from both the predissociation and direct dissociation of $N_2^+(C^2\Sigma_u)$ ions, and there is good agreement between calculated and experimental kinetic energy distributions.

However, the N_2^+ points in Fig. 12 between 4.0 - 4.5 eV are slightly above background and suggest the possibility that a small amount of $N_2^+(B^2\Sigma_u)$ ions are formed in the $Ne^+ - N_2$ interactions. Schlumbohm (54) has measured light emitted from $N_2^+(B^2\Sigma_u, v')$ ions which result from 200 eV $Ne^+ - N_2$ ion-molecule reactions. The spectral distribution of light emitted in spontaneous $B \rightarrow X$ transitions is given in Fig. 13 as the solid curve. Individual vibrational transitions cannot be completely resolved due to experimental resolution limitations; however, transitions corresponding to changes in vibrational quantum number of $|1|$, $|2|$, etc. can be clearly seen. Initial preparation of the $N_2^+(B^2\Sigma_u)$ in various vibrational levels has been calculated from the phase space model. The emitted light intensity has been computed from this phase space vibrational distribution and the Franck-Condon factors (50) for the respective transitions. The wavelengths for the individual vibrational transitions have been taken from the tabulation of Wallace (48), and

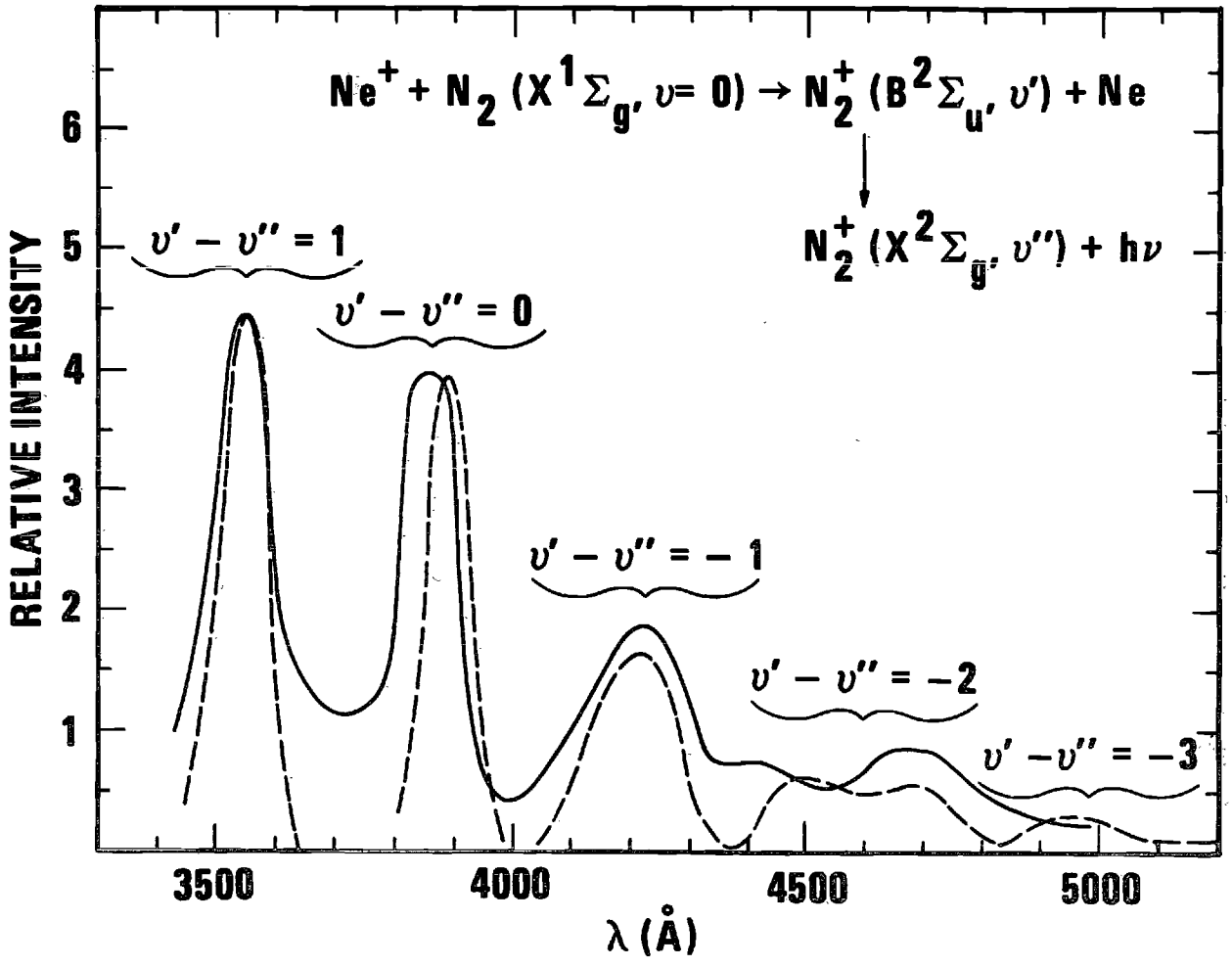

Figure 13. Spectral Distribution for the Transitions $N_2^+(B^2\Sigma_u, v') \rightarrow N_2^+(X^2\Sigma_g, v'')$. (The solid curve is taken from Ref. (54), and the dashed line is the calculated intensity.)

each of the calculated spectral lines has been broadened to match the resolution of the experimental apparatus so that a direct comparison can be made between theory and experiment. Again, the phase space model successfully predicts the internal energy distributions of product species once the electronic state of the product is established.

$Ar^+ + N_2$

Cross sections for molecular ion formation in $Ar^+ - N_2$ interactions are given in Fig. 14 where the solid curves are calculated using the phase space model. The X, A, B, and C designations refer to electronic states of the N_2^+ product ions. The dashed curve is the Langevin cross section while the dot-dot-dash and dot-dash curves are the experimental cross sections of Refs. (42) and (56) respectively. Agreement between different laboratories is not particularly good; however, it is apparent that the experimental cross sections are less than $10\ \mathring{A}^2$ at low kinetic energies. This reaction is different from those discussed previously in that the $N_2^+(X^2\Sigma_g, v')$ electronic state is the only energetically allowed product ion state at low kinetic energies. The separation between the $^2P_{3/2}$ and $^2P_{1/2}$ configuration of the reactant ions is sufficient to alter the energy defect of the respective reactions and the corresponding cross sections as calculated by the phase space methodology. The cross sections have been calculated separately and averaged by the

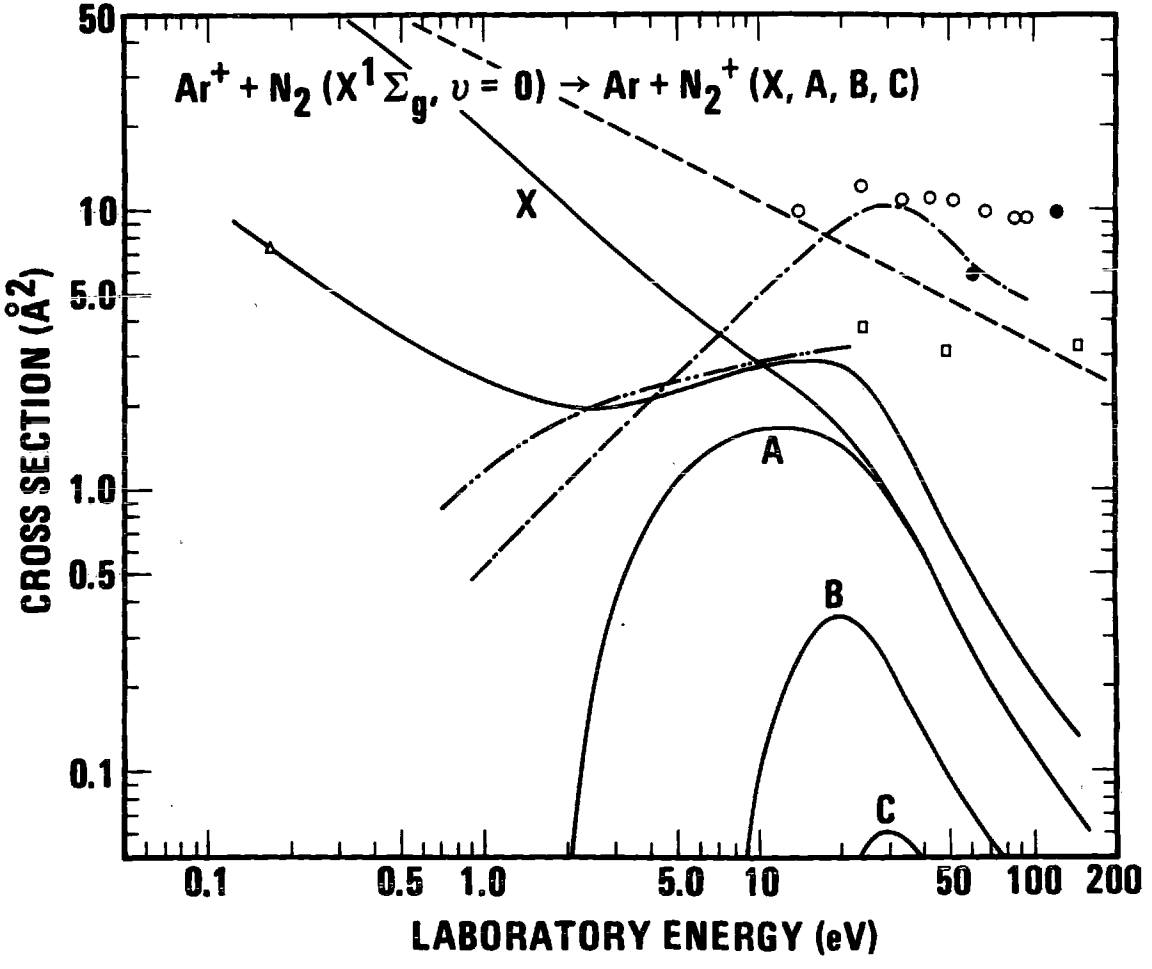

Figure 14. Cross Section for the Production of N_2^+ in the Various Electronic States as a Function of Ar^+ Kinetic Energy. (The data are from: Ref. (57) O; Ref. (58) ●; Ref. (39) □; Ref. (55) △; Ref. (56) the dash-dot-dash curve; and Ref. (42) the dash-dot-dot-dash curve.)

statistical weights of the Ar^+ spin states so that

$$\sigma = 1/3\ \sigma(Ar^+,\ J=1/2) + 2/3\ \sigma(Ar^+,\ J=3/2) \qquad (62)$$

In addition to the channels of reaction analagous to those in Eq. (56) it is necessary to also include de-excitation channels of the type

$$Ar^+(^2P_{1/2}) + N_2(X^1\Sigma_g, v) \rightarrow Ar^+(^2P_{3/2}) + N_2(X^1\Sigma_g, v') \qquad (63)$$

as well as the corresponding excitation channels in our overall set of reaction possibilities. The calculated curves have taken these interactions into account, but the measured cross section in Fig. 14 is significantly lower than that calculated for formation of $N_2^+(X^2\Sigma_g, v')$ state ions. It appears that only a fraction of collisions that are statistically calculated result in product $N_2^+(X^2\Sigma_g, v')$ ions. A crude estimate of the degree of state mixing is obtained by arbitrarily fixing the relative fraction of collisions that lead to a given electronic state. The solid curve passing through the Δ point is calculated by assuming that the fraction of collisions that lead to N_2^+ ions in the X, A, and B states is 0.10, 0.45, 0.45 respectively and independent of Ar^+ kinetic energy. The cross section calculated for the dissociative reaction using the above weighing factors for the X, A, and B electronic states is given as the solid curve in Fig. 15. Since they lead to the same dissociation asymptote, there is little difference in the cross sections

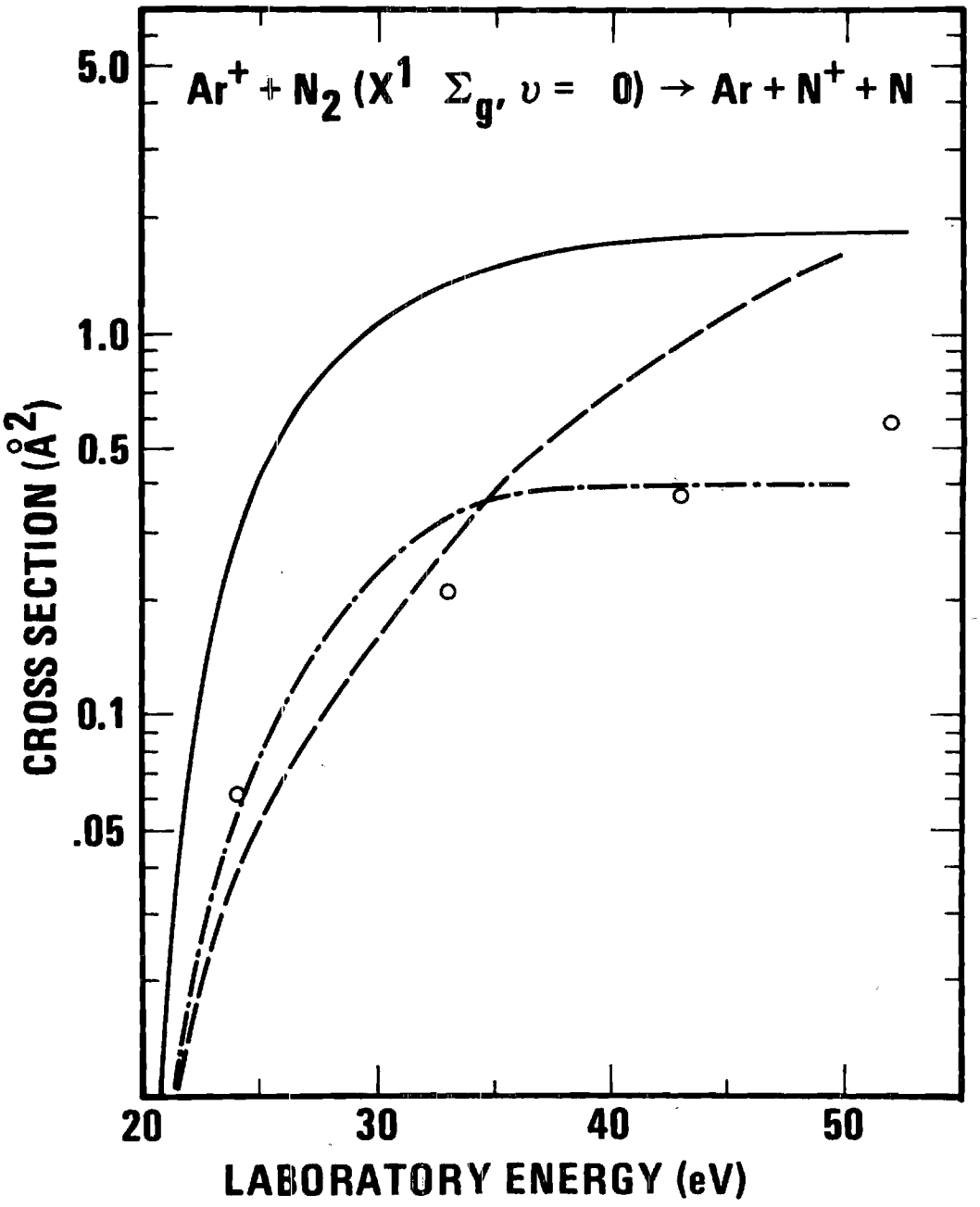

Figure 15. Cross Section for the Dissociative N^+ Reaction Channel as a Function of Ar^+ Kinetic Energy. (The data are from Ref. (57) O; Ref. (59), the dashed line; and Ref. (52), the dot-dash line.)

calculated from these states. Thus, the dissociative channel is not a particularly sensitive probe to determine the mixing of molecular ion states; however, it is this insensitivity that allows dissociative cross sections to be calculated rather accurately via phase space theory. N_2^+ product ion kinetic energy distributions, given in Fig. 16 for 0° scattering, provide additional information on this reaction. The open circles are data points of Ref. (45) and the solid curve is calculated using product state distributions calculated statistically. The kinetic energy spread of reactant Ar^+ ions has been folded into the calculated distributions resulting in a rather broad undefined spectrum in agreement with experimental data. This calculated curve is obtained by considering the $N_2^+(X^2\Sigma_g, v')$ and $N_2^+(A^2\pi_u, v')$ states mix statistically whereas the total cross sections indicate that the X state has a relatively minor contribution at low kinetic energy. This would be consistent with either completely different angular distributions for the X and A states, or mixing of the two states that is dependent on the reactant ion kinetic energy.

$Kr^+ + N_2$

The cross sections for formation of N_2^+ product ions are given in Fig. 17 as a function of kinetic energy. All reaction channels leading to N_2^+ and N^+ are endoergic except those corresponding to de-excitation $Kr^+(^2P_{1/2} \rightarrow {}^2P_{3/2})$

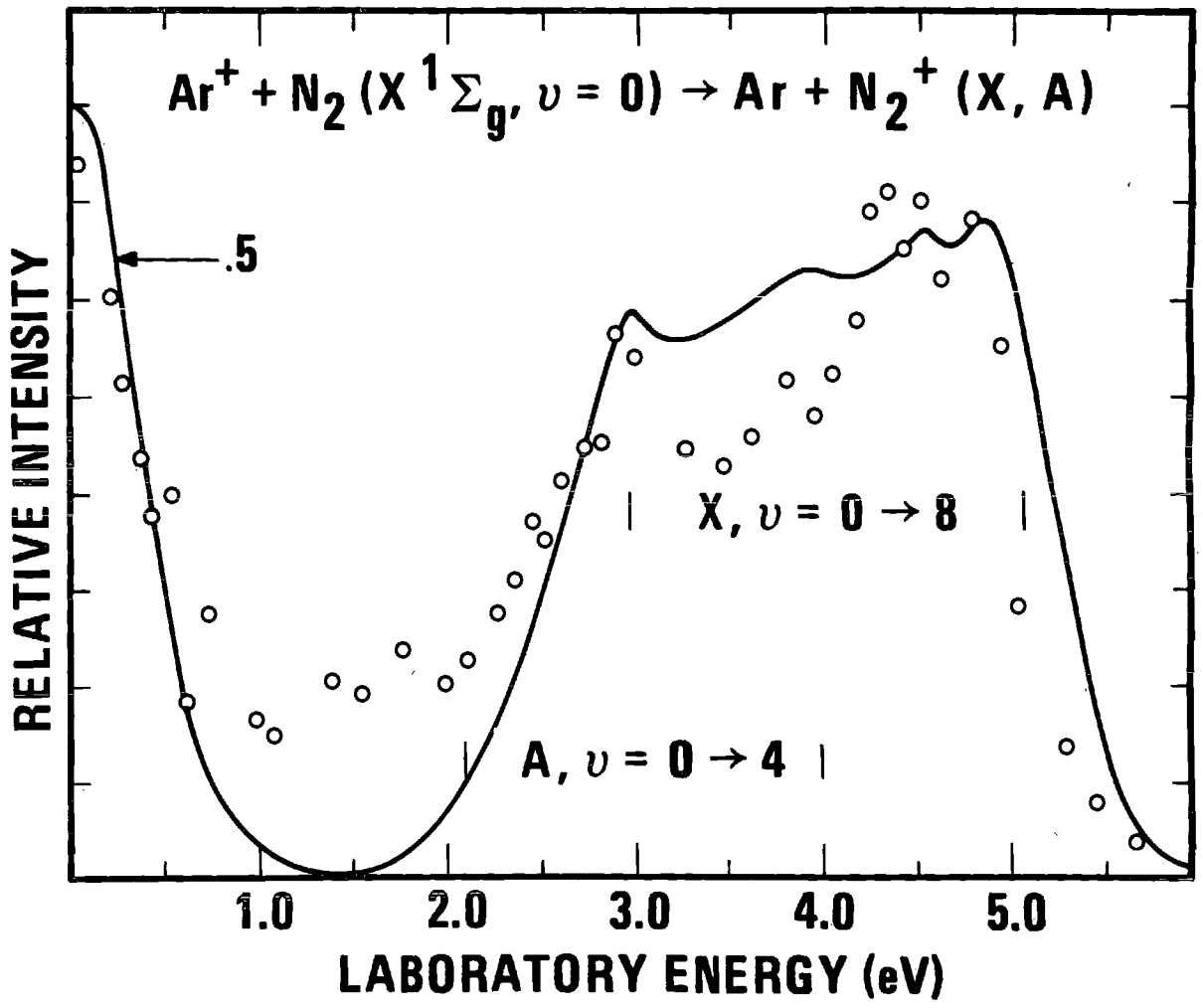

Figure 16. Kinetic Energy Distribution of N_2^+ Ions Formed in Ar^+-N_2 Interactions Involving 5.1 eV Ar^+ Reactant Ions. (The data points are from Ref. (45).)

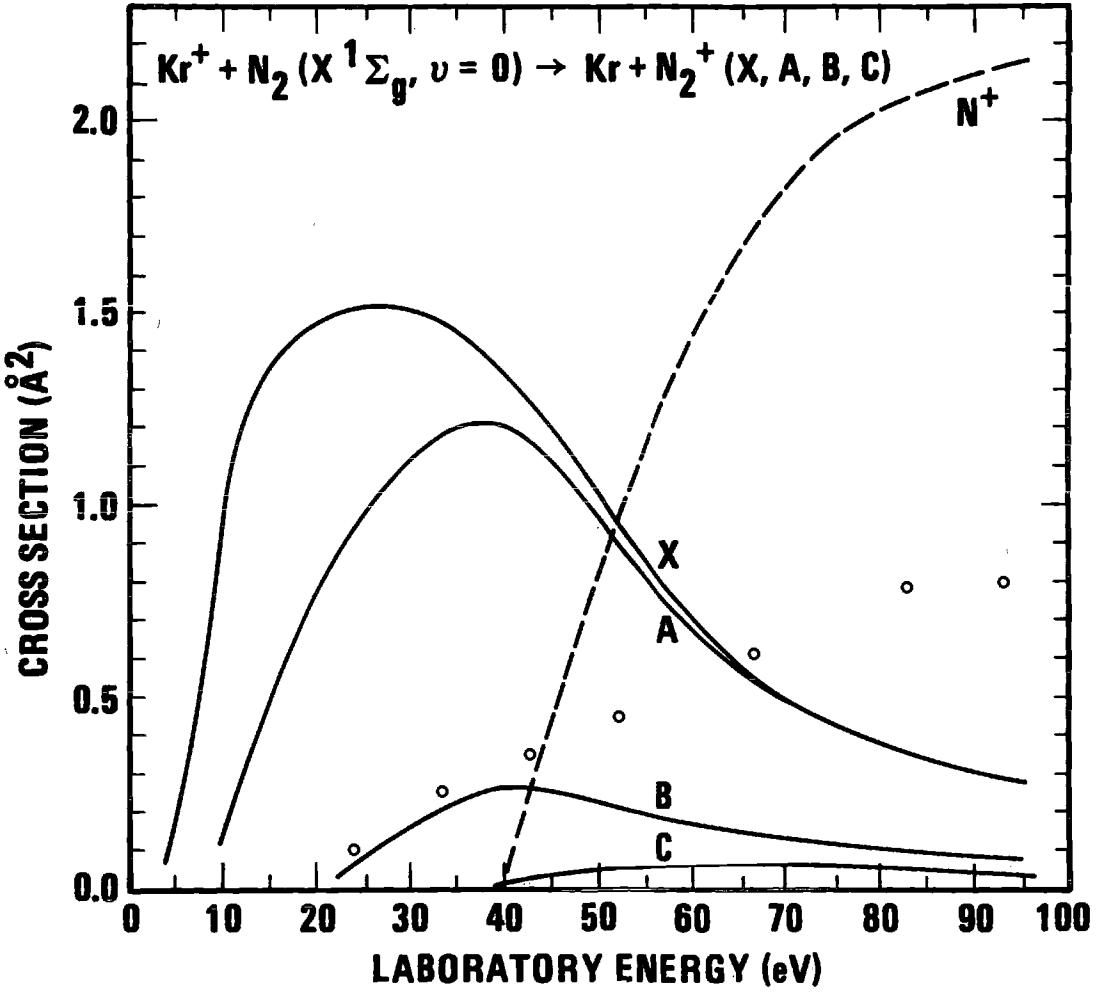

Figure 17. Cross Section for the Production of N_2^+ in the Various Electronic States as a Function of Kr^+ Kinetic Energy. (The data points are from Ref. (57).)

processes with the result that small cross sections are predicted by the phase space treatment. Calculated curves in Fig. 17 have been weighted to account for the respective Kr^+ spin states. The data points of Galli et al. (57) given in this graph were measured using an experimental arrangement in which product ions were collected in a direction transverse to the reactant ion beam via an electrostatic repeller field. Since the collection efficiency of this arrangement need not be complete and will depend on the angular distribution of products, these points represent a possible lower limit to the total cross section. As shown in Fig. 17, reasonable agreement exists between experiment and the predictions of the statistical phase space model.

Summary

Examination of the reactions of inert gas ions with nitrogen has shown that the phase space model gives excellent agreement with observed measurements of the energy dependence of cross sections, as long as the product state is specified. The main feature missing in the formulation of the model is that there is no mechanism for discriminating between statistically available product electronic states, even though some states are not allowed and; therefore, are not observed experimentally. However, by making *a priori* restrictions on the allowed product electronic states, either using experimental observation or by correlating the states of the

complex with the electronic states of reactants and products, we find the agreement with experiment is satisfactory. In many cases certain product states are forbidden due to spin and/or symmetry effects (see Chapter V). In Chapter VII we consider the case of $He^+ + N_2$. Calculation of the potential energy of the complex and correlating the lowest state of the complex with the electronic states of the reactants and products shows that the $N_2^+(C^2\Sigma_u)$ state would be formed preferentially.

Once the product state is specified, the threshold and energy dependence of cross section is in good agreement with observed behavior. The dissociation process can be well represented in any case since the dissociation asymptote for all states is the same. Also, the phase space model successfully predicts vibrational population of a given product state as shown by comparison with observed kinetic energy distributions of product ions and with observed relative radiative intensities.

The model also indicates the correct dependence on initial internal energy. This dependence and the success of the model for dissociative charge transfer lead us to next consider the collision induced dissociation of excited O_2^+ and NO^+. These reactions offer the opportunity to examine fully the function of incident internal energy on thresholds and magnitudes of the cross section.

CHAPTER IV

COLLISION INDUCED DISSOCIATION OF EXCITED O_2^+ AND NO^+ IONS

In the previous section it was observed that the phase space model gave good results for dissociative charge transfer processes for inert gases on N_2. With this success we have compared calculated cross sections for production of O^+ and N^+ from collision induced dissociation of O_2^+ and NO^+ with experimental results of Tiernan and Marcotte (63). Using a tandom beam type (double stage) mass spectrometric apparatus with in-line geometry, they have examined the energetic thresholds and energy dependence of the cross section for the dissociative channels of reaction of O_2^+ and NO^+ ions with argon and neon atoms. They have shown that the cross section for this process depends strongly on the energy of the electrons producing the reactant ions. Since the energy of the ionizing electrons can effect the ion internal energy distribution in a calculable manner, one may estimate the population distribution of reactants in the various electronic and vibrational states and thus examine the participation of these degrees of freedom in the dissociative reaction pathway. Also, for NO^+ we can examine the competing N^+ and O^+ product channels.

Other experiments on dissociative ion-molecule reactions using a Cermak-Herman (60) type method showed efficient conversion of kinetic energy in the collision process (64); however, distinct separation of reactant ion translational and internal energy was difficult. Beam experiments (62) above 100 eV LAB kinetic energy using ground state reactant ions have shown that the most probable dissociation events in the reaction of diatomic ions with helium atoms product fragment ions with velocity approximating that of the original projectile ions. From this work (62) it was concluded that a stripping type model adequately describes the angular and velocity distributions of the reaction products. In this chapter we examine the applicability of the phase space model to the collision induced dissociation processes.

Collision Induced Dissociation of O_2^+

The various reaction channels for the interaction of O_2^+ ions with Ar atoms are

$$O_2^+(X^2\pi_g, v) + Ar \rightarrow \begin{cases} O_2^+(X^2\pi_g, v') + Ar & (64a) \\ O_2^+(A^2\pi_u, v') + Ar & (64b) \\ O_2(X^3\Sigma_g, v') + Ar^+ & (64c) \\ O(^3P) + O(^3P) + Ar^+ & (64d) \\ O^+(^4S) + O(^3P) + Ar & (64e) \end{cases}$$

The cross section for the dissociative channel of reaction Eq. (64e) has been calculated from phase space theory, and the results for the lower vibrational levels of the $O_2^+(X^2\pi_g,v)$ reactant ions are given by the dashed lines in Fig. 18. The points in Fig. 18 are those of Tiernan and Marcotte (63) for reactant ions produced by 13 eV electrons. Although the shape of the calculated cross section curves for individual vibrational levels are similar above 12 eV ion center of mass kinetic energy, they differ near the threshold kinetic energy. A comparison between theory and experiment should consider the vibrational population distribution in the reactant ion beam. We have estimated this distribution from Franck-Condon factors (64-66) for $O_2(X^3\Sigma_g,v=0) \rightarrow O_2^+(X^2\pi_g,v)$ transitions with the assumption that the cross section for electron-molecule ionizing collision is linear (67) with $(EE-E_{IP})$, where EE is the electron energy and E_{IP} is the minimum energy required to form ions in vibrational level v. Measurements of the probability for low energy electron impace ionization (68,69) and photoionization (70) are in agreement with those calculated from these Franck-Condon factors. Experimental data (71) has been obtained which show autoionization processes can also occur. Rydberg levels of O_2 are known (72) and observed in optical adsorption experiments (73), high energy electron scattering (74), and photoionization measurements (75,76). The main contribution of these autoionizing levels appears to be above

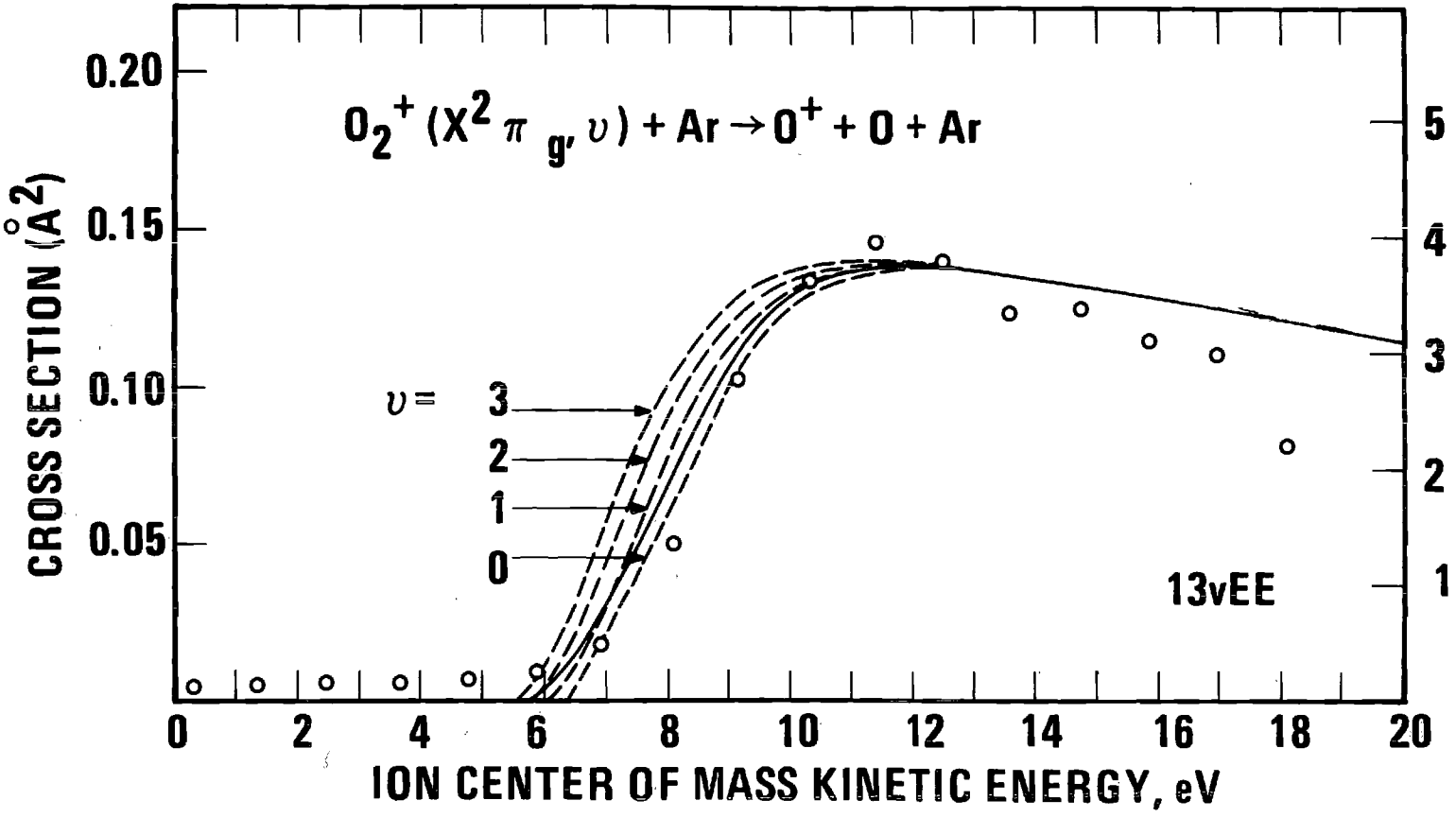

Figure 18. Cross Section for O^+ Production in O_2^+ - Ar Interactions as a Function of Ion Center of Mass Kinetic Energy. (The data points are from Ref. (63) for O_2^+ ions formed in 13 eV electron impact ionization (left ordinate scale). The dashed curves (left ordinate scale) are cross sections calculated for the various O_2^+ vibrational state and the solid curve is the weighted calculated cross section.)

13 volts energy (77), and one would expect the calculated $O_2(X^3\Sigma_g, v=0) \rightarrow O_2^+(X^2\pi_g, v=0,1,2,3)$ Franck-Condon factors to give a reasonable $O_2^+(X^2\pi_g)$ vibrational distribution for 13 eV electron impact ionization. The vibrational composition of the reactant $O_2^+(X^2\pi_g)$ ion beam computed in this manner has been used to weight the cross section for the collision-induced dissociation reaction calculated by the phase space model. This computed cross section is given by the solid curve in Fig. 18. In this figure the left hand ordinate scale pertains to the experimental points while the right hand ordinate is that for the calculated cross sections. Although there is a discrepancy between the absolute magnitude of the calculated and observed cross sections, the shape and energetic threshold of the cross section computed by the phase space treatment agrees with measurements of Tiernan and Marcotte (63). This agreement supports the application of the phase space model to dissociative reactions in which there is an effective conversion of translational energy.

The participation of reactant ion internal excitation energy in this type of collision has been examined experimentally (63) by increasing the energy of electrons that produce reactant O_2^+ ions. It is known that electronically excited $a^4\pi_u$, $A^2\pi_u$, $b^4\Sigma_g$ and $^2\Sigma_g$ states are produced in high energy electron impact ionization of O_2. From observed transition moments (78-80) the relative populations of the various

O_2^+ states are: 0.24, $X^2\pi_g$; 0.07, $a^4\pi_u$; 0.29, $A^2\pi_u$; 0.26, $b^4\Sigma_g$; and 0.14, $^2\Sigma_g$. Radiative transitions have been observed between the $^2\Sigma_g \rightarrow A^2\pi_u$; $A^2\pi_u \rightarrow X^2\pi_g$ and $b^2\Sigma_g \rightarrow a^4\pi_u$ states in time periods short compared with transit times for reactant ions to reach the collision region with the result that the $a^4\pi_u$ and $X^2\pi_g$ states are important for reaction (80). From the above estimates of initial state populations and radiative processes that occur prior to reaction, it is estimated that 33 per cent of the O_2^+ reactant ion beam is in the long lived $a^4\pi_u$ state (78-80). The vibrational distributions of O_2^+ reactant ions in both the $X^2\pi_g$ and $a^4\pi_u$ states have been calculated from Franck-Condon factors for direct electron impact ionization processes (64-66) weighted by respective transition moments and the Franck-Condon factors for the consequent spontaneous radiative processes (64,81). These internal state distributions, which have been calculated as a function of ionizing electron energy, have been used to weight the dissociative reaction cross sections calculated via the statistical phase space model. The processes considered for the electronically excited $O_2^+(a^4\pi_u, v)$ ions are

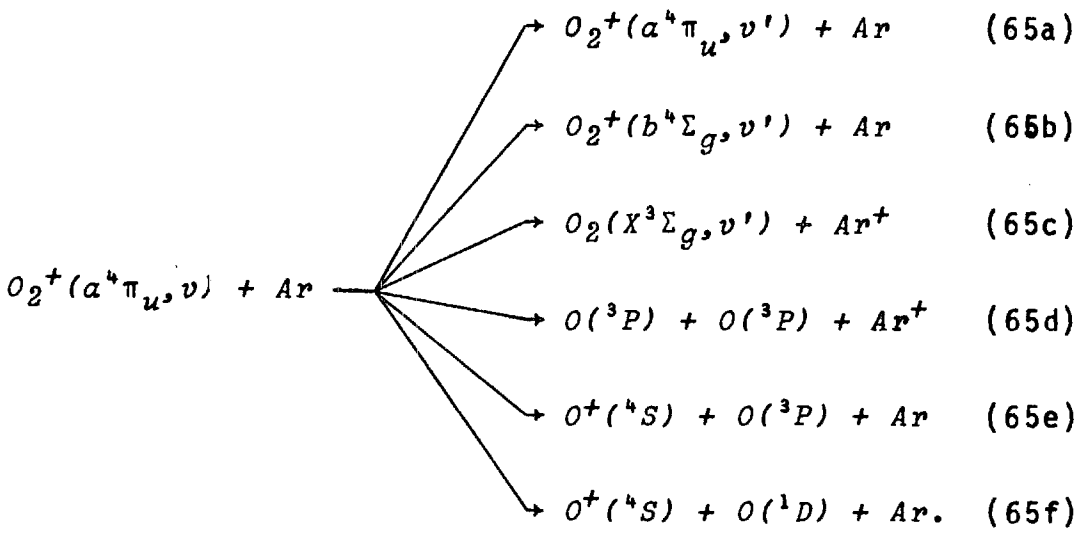

Total cross sections for dissociative channels leading to O^+ product ions are presented in Fig. 19 as a function of ion center of mass kinetic energy and compared with the experimental data of Tiernan and Marcotte (63). As shown in this figure, there is reasonably good agreement between calculated and measured dependences of the dissociative cross sections with reactant ion kinetic energy. The absolute magnitude of the computed cross sections (scale on the right of Fig. 19) is larger than those measured; however, the collection efficiency of the in-line configuration in the analyzing mass spectrometer is difficult to determine and the absolute values of the experimental cross sections are reported to be the order of ±100 per cent (63). Experimental data in Fig. 19 show dissociative processes are possible below 3 eV ion kinetic energy whereas the calculated cross sections are small and approaching zero. If higher O_2^+ vibrational levels

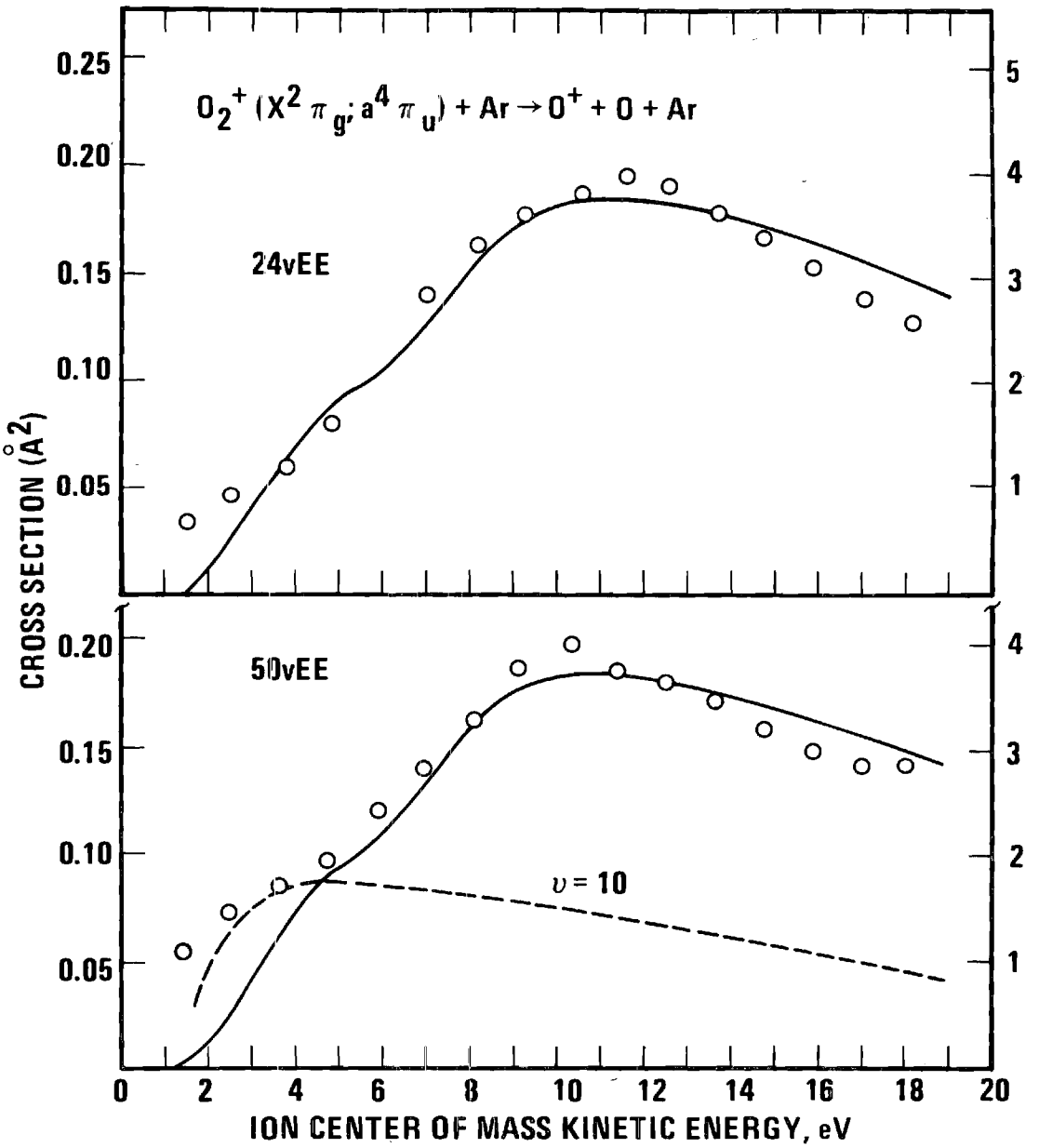

Figure 19. Cross Section for O^+ Production in O_2^+ - Ar Collisions for O_2^+ Reactant Ions Formed in 24 and 50 Volt Electron Impact Ionization. (The data points are from Ref. (63), and the solid lines are the calculated cross sections. The dashed line is that calculated for $O_2^+(a^4\pi_u)$ ions in the $v = 10$ level.)

are populated in electron impact ionization than are estimated from the direct ionization processes considered here, then dissociative ion-molecule reactions computed from the phase space model would extend to lower ion kinetic energies. The dashed curve in Fig. 19 is that estimated for ions in the $O_2^+(a^4\pi_u, v) + Ar$ reactions.

A further comparison between the statistical phase space model and experiment (63) is given in Fig. 20 for electronically excited O_2^+ + Ne dissociative reactions. Computed cross sections in Fig. 20 involving reactions of $O_2^+(a^4\pi_u, v)$ ions with Ne have been multiplied by 0.33 so that comparison can be made with the composite curves previously presented. As shown in Fig. 20, the experimental data for reactions of electronically excited ions are in harmony with participation of internal excitation energy in the dissociative reaction pathways as computed by the statistical phase space model.

Collision Induced Dissociation of NO^+

The effect of electronic and vibrational energy on collision-induced reactions has been examined for reactions of NO^+ ions. This is a particularly fruitful system for study since there is evidence (78,80,82) for long lived ionic states in the electron impact ionization of NO and relative abundance of these long lived states have been estimated (78,80,82) to comprise 28 to 45 per cent of the total number of NO^+ ions produced in high energy electron impact

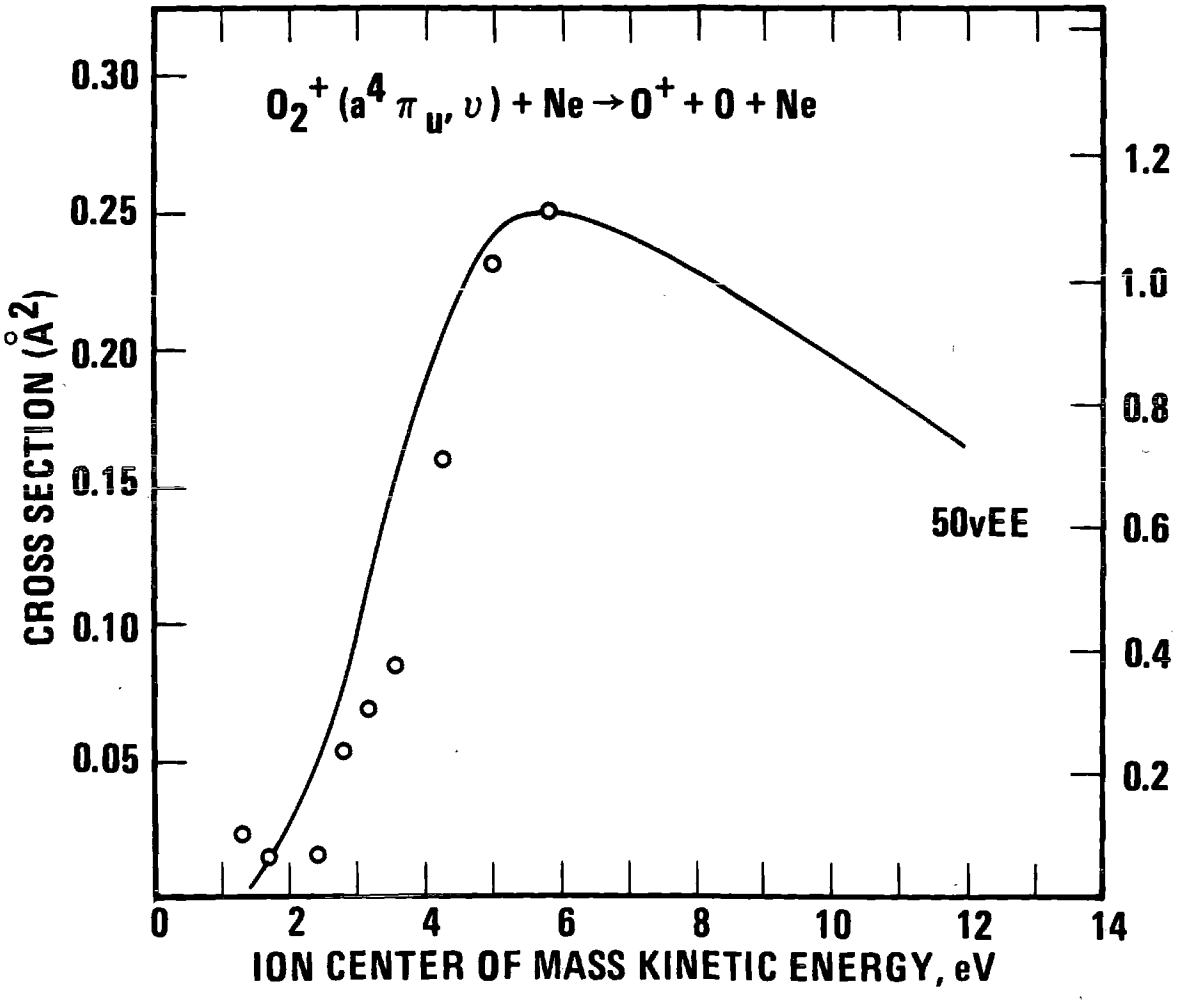

Figure 20. Cross Section for O^+ Production in O_2^{+*} - Ne Interactions. (The data are from Ref. (63) (left ordinate scale).)

ionization. The potential energy curves (46,83,84) for the ground and electronically excited NO^+ states have been computed from spectroscopic (46) constants and data taken from photoelectron experiments (83,84). The NO^+ triplet states are spin forbidden to convert to the $NO^+(X^1\Sigma, v)$ ground state via radiative transitions and these states can be considered long lived for ion-molecule reactions. The relative probabilities for populating NO^+ states are taken to be (78): *0.56*, $X^1\Sigma$; *0.32*, $^3\Delta$ and close triplet levels; *0.12*, $A^1\pi$. Vibrational distributions within the X and A states formed in the direct ionization processes have been taken from tabulated (65) Franck-Condon factors. Estimation of the similar distributions for the $NO^+(^3\Delta)$ state is approximate since spectroscopic parameters are not known. We have assumed r_e to be 1.225Å, and taken ω_e to be approximately 1600 cm^{-1}, and estimated $\omega_e x_e$ from the relation $D_e = \omega_e^2/4\omega_e x_e$ (27). Morse anharmonic oscillator wavefunctions (64) were constructed from these approximate molecular constants and the vibrational distribution within the $NO^+(^3\Delta)$ state taken from these computed Franck-Condon factors. This calculated distribution is in approximate accord with that observed in high resolution photoelectron spectroscopy measurements (83). Franck-Condon factors for $NO^+(A^1\pi) \rightarrow NO^+(X^1\Sigma)$ spontaneous radiative transitions (85) were also taken into account in our consideration of the $NO^+(X^1\Sigma)$ internal state distribution.

The statistical phase space model was used to compute

the cross sections for the possible reactions

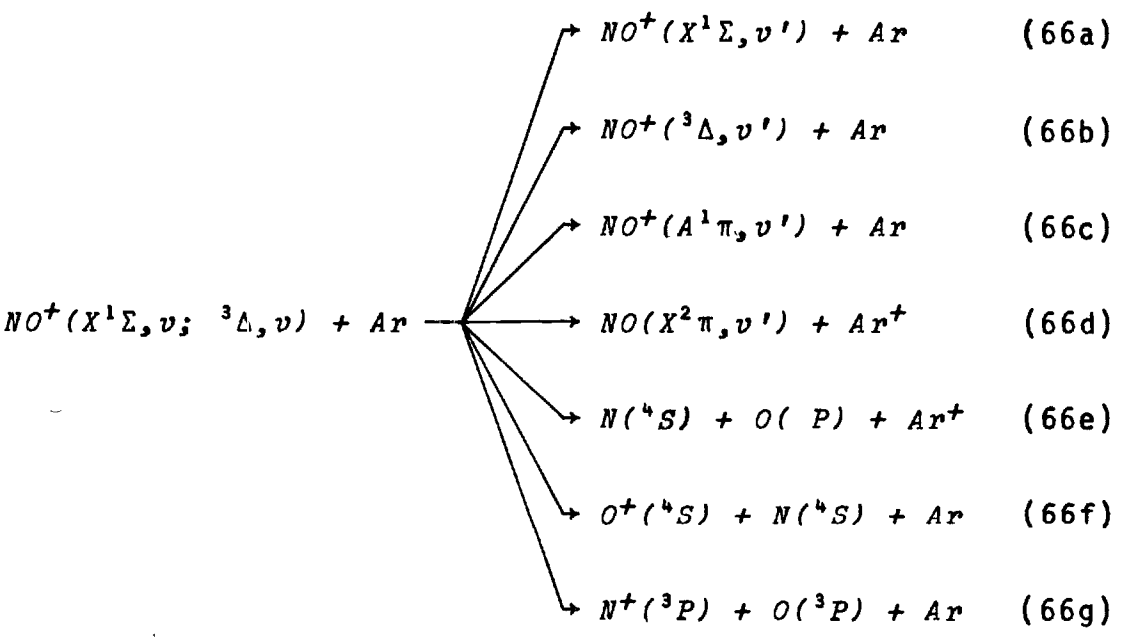

The cross section for the interaction channel Eq. (66g) leading to N^+ ions is presented in Fig. 21 as a function of ion center of mass kinetic energy along with the experimental points. The curve passing through the 13 volt data has been computed by considering only $NO^+(X^1\Sigma, v)$ ions as reactant since the 13 eV energy of the ionizing electron is below (83) the energetic thresholds for the electronically excited NO^+ states. The N^+ reaction cross section calculated for reactant NO^+ ions formed via 17 and 20 eV electron impact ionization have been weighted to account for the vibrational distributions in the $X^1\Sigma$ and $^3\Delta$ states as previously outlined. Agreement between calculated and experimental data on the dissociative N^+ reaction channel support use of the phase space model, and in particular, kinetic energy thresholds

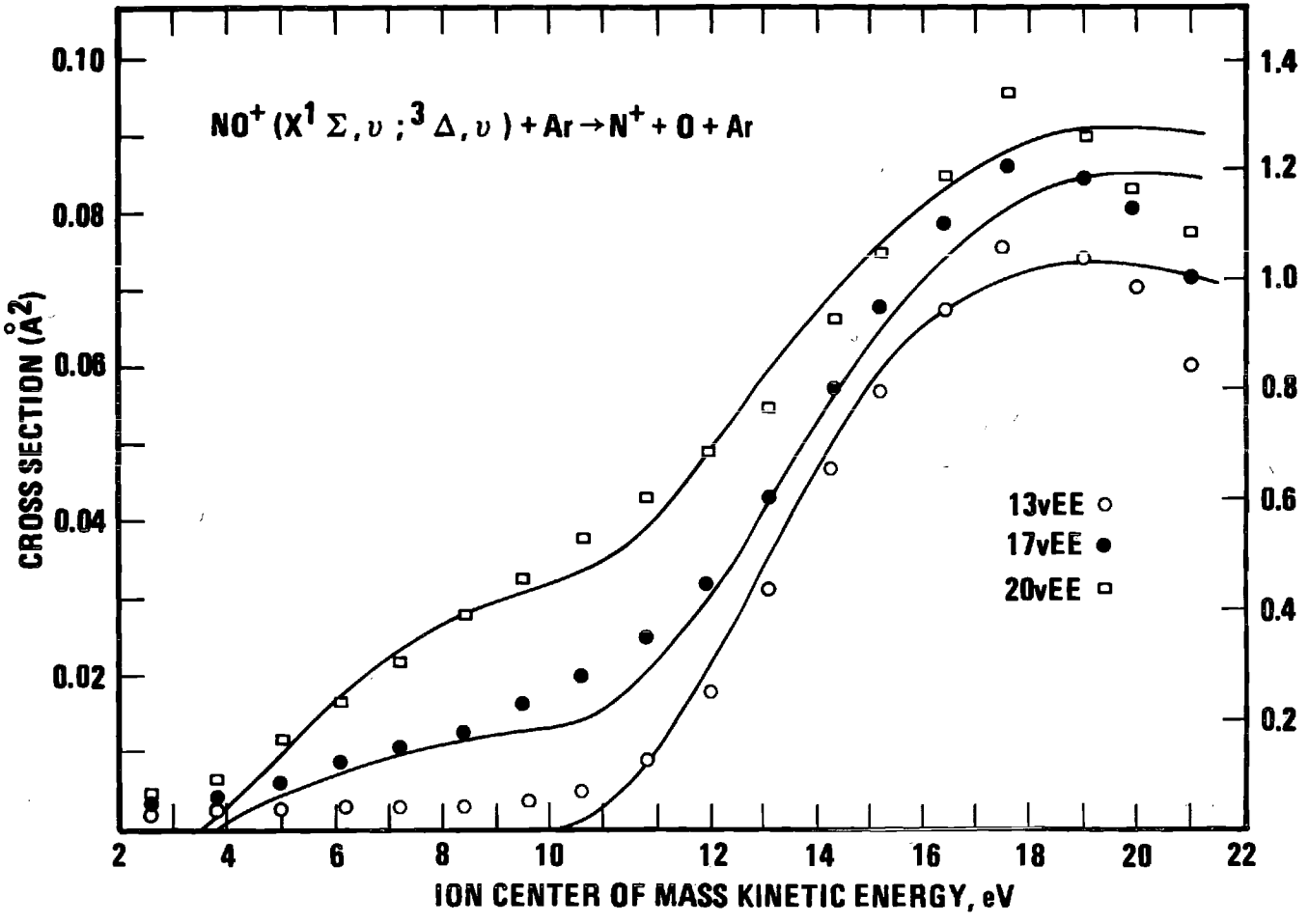

Figure 21. Cross Section for the Dissociative $NO^+ + Ar \rightarrow N^+$ Reactions as a Function of Ion Center of Mass Kinetic Energy. (The data points are from Ref. (63) for 13, 17, and 20 volt ionizing electron energy (left ordinate scale); and the lines are the calculated cross sections (right ordinate scale).)

given in Fig. 21 are consistent with those predicted for reactions of $NO^+(^3\Delta,v)$ ions. There is evidence from photoelectron spectroscopy (83) that $NO^+(^3\Sigma)$ and $^3\pi$ states are formed in ionization processes of neutral NO. Although the presence of these states in an NO^+ ion beam formed by electron impact ionization is somewhat speculative, these states have ionization potentials close to the $^3\Delta$ state; which would result in dissociative ion-molecule cross sections similar to that for $NO^+(^3\Delta,v)$, when computed from the statistical model. We have, therefore, considered $NO^+(^3\Delta,v)$ to be the only long lived electronically excited state for the calculated curves in Fig. 21 since agreement between calculation and experiment is evidenced. The corresponding O^+ product channel predicted using the phase space model is presented in Fig. 22 along with experimental data for this system. We have assumed for this calculation that dissociation to $O^+(^4S) + N(^4S)$ products are possible from both the $NO^+(X^1\Sigma)$ and $^3\Delta$ states although the asymptotic limit of the $^3\Delta$ state is correlated with $[N^+(^3P) + O(^3P)]$. It has been previously suggested (63,80) that spontaneous predissociative transitions from the $^5\Sigma$ or $^7\Sigma$ states, which are correlated with $O^+(^4S) + N(^4S)$ at large internuclear distances, are possible with excitations involving $NO^+(^3\Delta)$. Within the framework of the statistical model this predissociative type mechanism would give kinetic energy thresholds for O^+ formation similar to those calculated

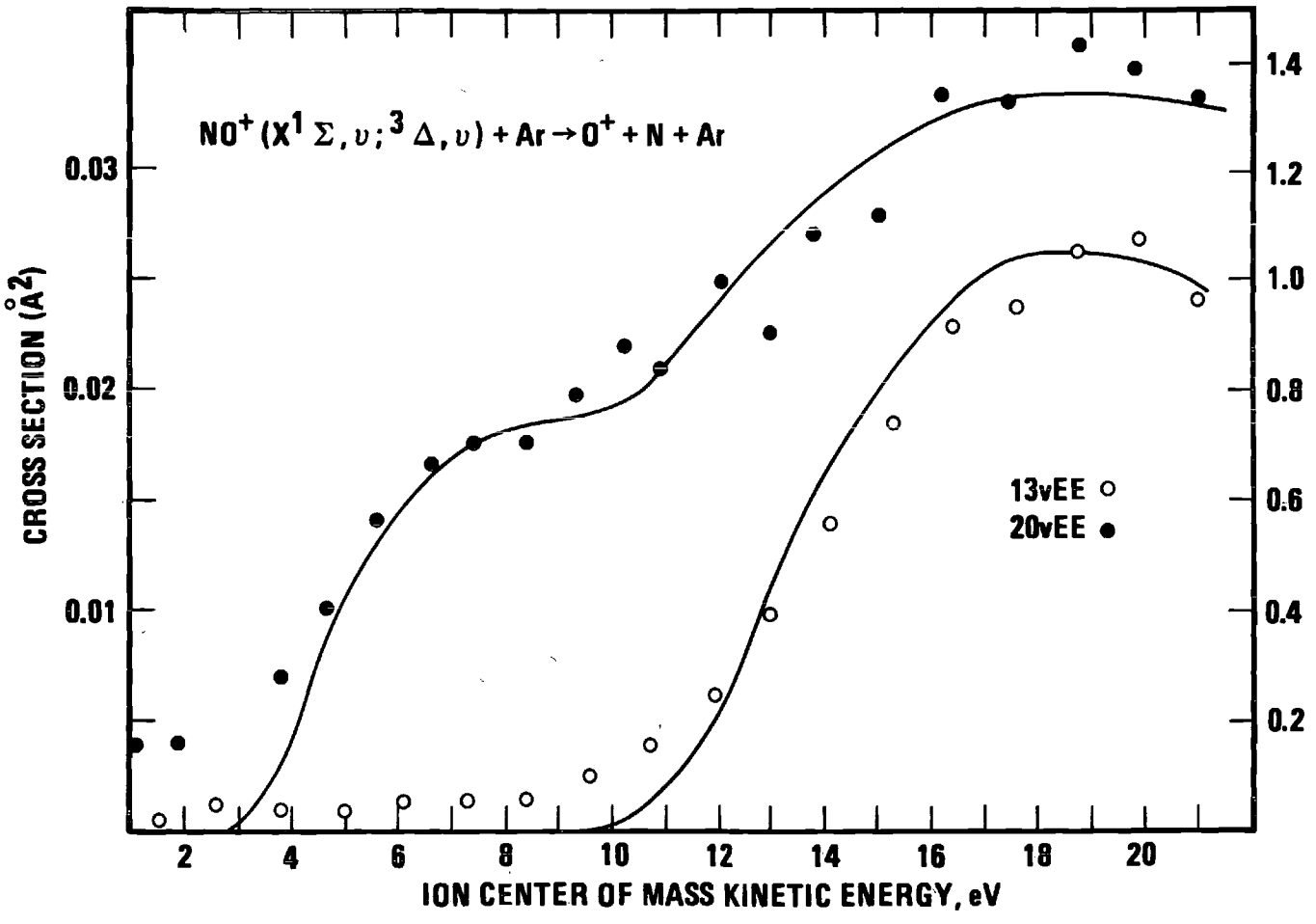

Figure 22. Cross Section for Dissociative $NO^+ + Ar \rightarrow O^+$ Reactions as a Function of Ion Center of Mass Kinetic Energy. (The data points are from Ref. (63).)

assuming mixing of $NO^+(^3\Delta, v)$ and high vibrational levels of $NO^+(X^1\Sigma)$ in collisions with corresponding dissociations producing O^+. A more detailed examination of this aspect of dissociative reaction pathways is given in Fig. 23 for reactions of electronica-ly excited NO^+ with Ar. Experimental points in Fig. 23 show both O^+ and N^+ to be formed in reactions of excited NO^+ and are in harmony with cross section curves obtained from the phase space treatment. Further evidence of the relevance of the statistical model to dissociative reactions is given in Fig. 24 for NO^+ - Ne reactions. Dissociative cross sections have been computed for this system using a set of reaction channels analogous to that for NO^+ - Ar collisions. As shown in Fig. 24, calculated curves are in reasonable agreement with the experimental points of Tiernan and Marcotte (63).

Summary

Preparation of the diatomic ion is very important in determination of the threshold and cross section dependence on ion kinetic energy. Given the preparation conditions, which *a priori* fix the reactant ion vibronic distribution, the phase space model reproduces observed thresholds and kinetic energy dependence for the collision induced dissociation. Also, for $NO^+(^3\Delta)$ which can dissociate forming both N^+ and O^+ (46) calculated results are in excellent agreement with experimental observation both in shape and relative

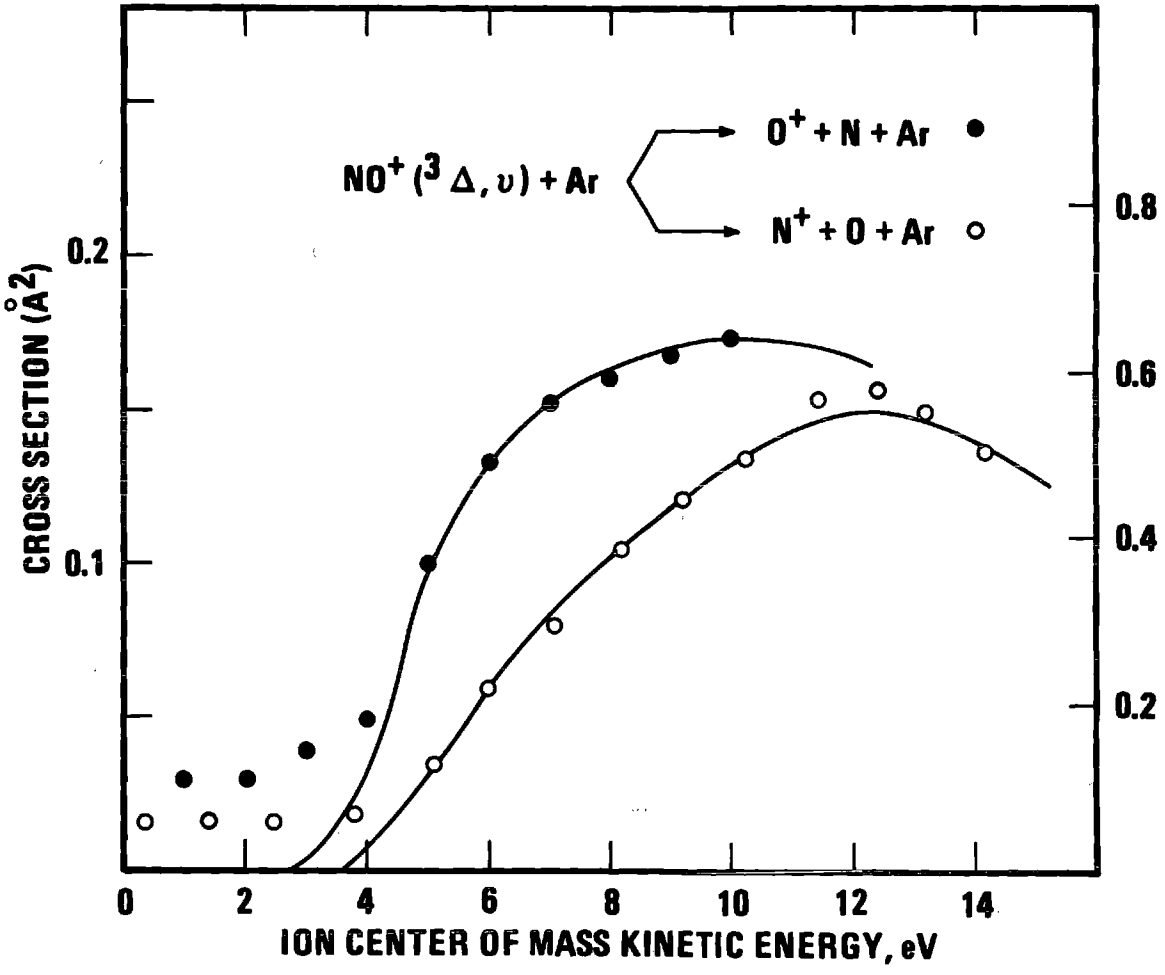

Figure 23. Cross Section for O^+ and N^+ Produced in Dissociative Reactions of Electronically Excited NO^+. (The data points are from Ref. (63).)

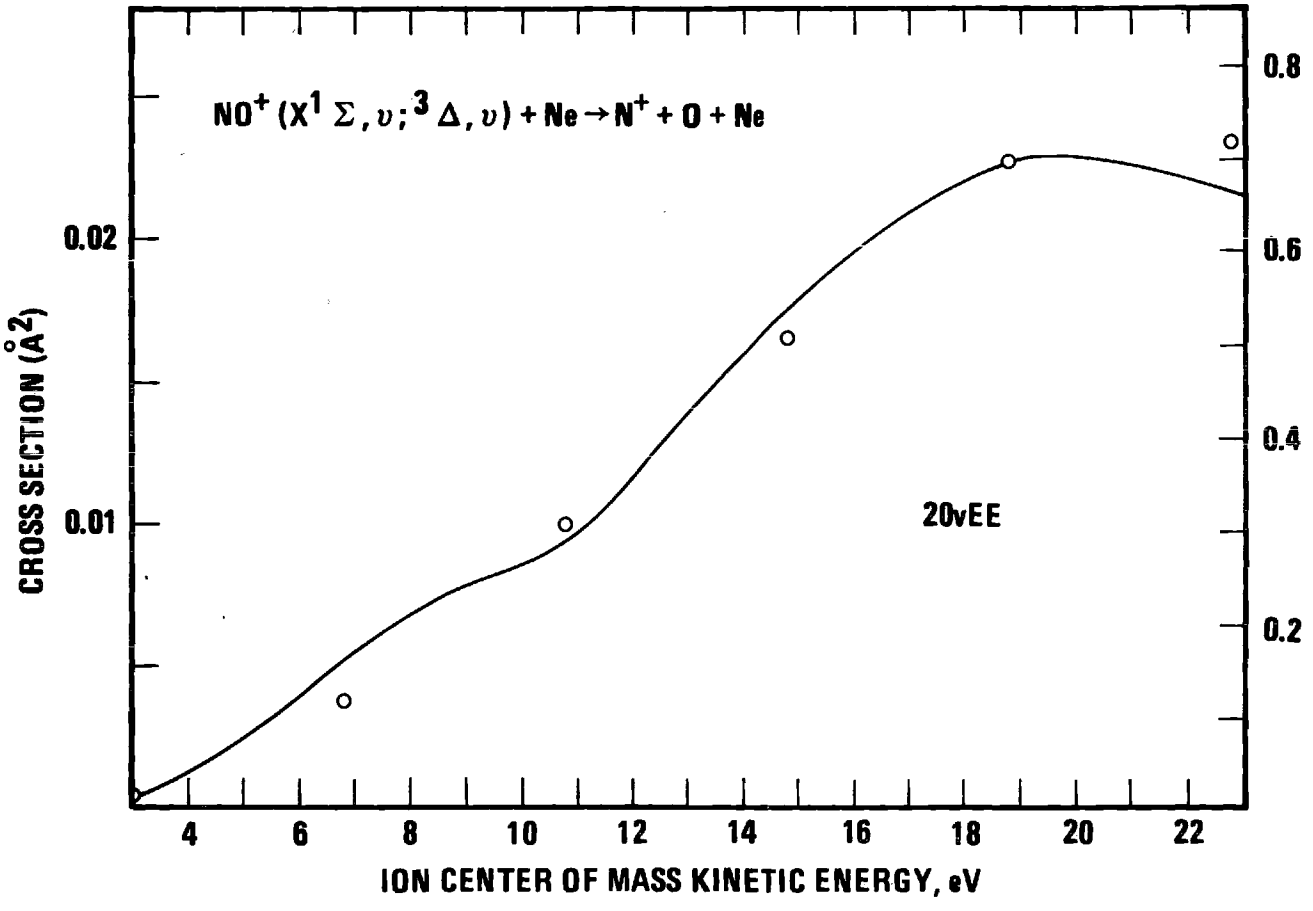

Figure 24. Cross Section for the Dissociative $NO^+ + Ne \rightarrow N^+$ Reactions as a Function of Ion Center of Mass Kinetic Energy. (The data points are taken from Ref. (63).)

production of N^+ and O^+. Although there is some discrepancy in absolute magnitude, it is expected that calculated cross sections using the ion-induced dipole potential are an upper bound; while the experimental cross sections may be low due to the in-line geometry of the experimental apparatus.

CHAPTER V

ION-MOLECULE REACTIONS OF C^+ WITH O_2 AND N_2

In this chapter we consider the applicability of the phase space model to the reactions of C^+ with O_2 and N_2. In addition to the charge transfer and dissociative charge transfer processes considered these reactions also have rearrangement (mass transfer) channels available. Also, we further test the role of internal energy and conservation principles not explicitly contained in the phase space model and find a strong dependence on spin conservation.

Reaction cross sections of C^+ and N_2 and O_2 have been studied by Lao, Rozett and Koski (86) using a tandem mass spectrometer. They examined the effect of C^+ excitation energy on reaction mechanisms by changing the ionizing electron energy in the source chamber of the first mass spectrometer. With this technique they were able to measure the translational energy dependence of cross sections for various reaction channels involving both ground state and electronically excited C^+ reactant ions. These measurements provide information on the role of translational and internal energy in reaction mechanisms and data with which to compare.

The energetics (in eV) and various ion-molecule reaction channels involving $C^+(^2P)$ and $C^+(^4P)$ reactant ions are

		^2P	^4P	
$C^+(^2P, ^4P) + N_2(X^1\Sigma_g)$	$\rightarrow C^+(^2P) + N_2(X^1\Sigma_g)$	0	5.331	(67a)
	$\rightarrow C^+(^4P) + N_2(X^1\Sigma_g)$	-5.331	0	(67b)
	$\rightarrow C(^3P) + N_2^+(X^2\Sigma_g)$	-4.312	1.019	(67c)
	$\rightarrow C(^3P) + N_2^+(A^2\pi_u)$	-5.429	-0.098	(67d)
	$\rightarrow C(^3P) + N_2^+(B^2\Sigma_u)$	-7.481	-2.150	(67e)
	$\rightarrow C(^3P) + N_2^+(C^2\Sigma_u)$	-12.311	-6.980	(67f)
	$\rightarrow N(^4S) + CN^+(^3\pi)$	-4.726	0.605	(67g)
	$\rightarrow N(^2D) + CN^+(^3\pi)$	-7.109	-1.778	(67h)
$C^+(^2P, ^4P) + O_2(X^3\Sigma_g)$	$\rightarrow C^+(^2P) + O_2(X^3\Sigma_g)$	0	5.331	(68a)
	$\rightarrow C^+(^4P) + O_2(X^3\Sigma_g)$	-5.331	0	(68b)
	$\rightarrow C(^3P) + O_2^+(X^2\pi_g)$	-0.793	4.538	(68c)
	$\rightarrow C(^3P) + O_2^+(a^4\pi_u)$	-4.825	0.506	(68d)
	$\rightarrow C(^3P) + O_2^+(A^2\pi_u)$	-5.563	-0.232	(68e)
	$\rightarrow C(^3P) + O_2^+(b^4\Sigma_g)$	-6.907	-1.576	(68f)
	$\rightarrow O(^3P) + CO^+(X^2\Sigma)$	3.228	8.559	(68g)
	$\rightarrow O(^3P) + CO^+(A^2\pi)$	0.699	6.030	(68h)

Columns labeled ^2P and ^4P give reaction energetics for the respective C^+ reactant ion states. Molecular and atomic parameters used to calculate these energetics are given in Appendix A. Lao, Rozett and Koski (86) were able to determine electronic state distribution of the reactant C^+ ions produced in electron impact ionization of neutral CO. They found that ground state $C^+(^2P)$ ions are predominately formed in 23 eV electron impact of CO while ionization by 70 eV electrons results in a C^+ beam composed of 72 per cent $C^+(^2P)$ and 28 per cent $C^+(^4P)$ ions. These workers were thus able to study ion-molecule reactions of $C^+(^2P)$ ions by using 23 eV electrons to produce the reactant ion beam. By measuring the ion-molecule interactions of C^+ ions produced at 23 eV and 70 eV electron energies, estimates of the contributions of both the C^+ ^2P and ^4P states to rearrangement reactions have been obtained.

Mass Transfer Reactions

The reaction cross section of C^+ ions with neutral nitrogen molecules leading to formation of $CN^+ + N$ products, Eqs. (67g) and (67h), have been computed using the statistical phase space model and the results of this calculation are given as a function of translational energy in Fig. 25 along with the experimental data (86) for this reaction channel. The open circles in Figs. 25a and 25c are the data obtained for reactions of C^+ ions formed in 23 eV and 70 eV

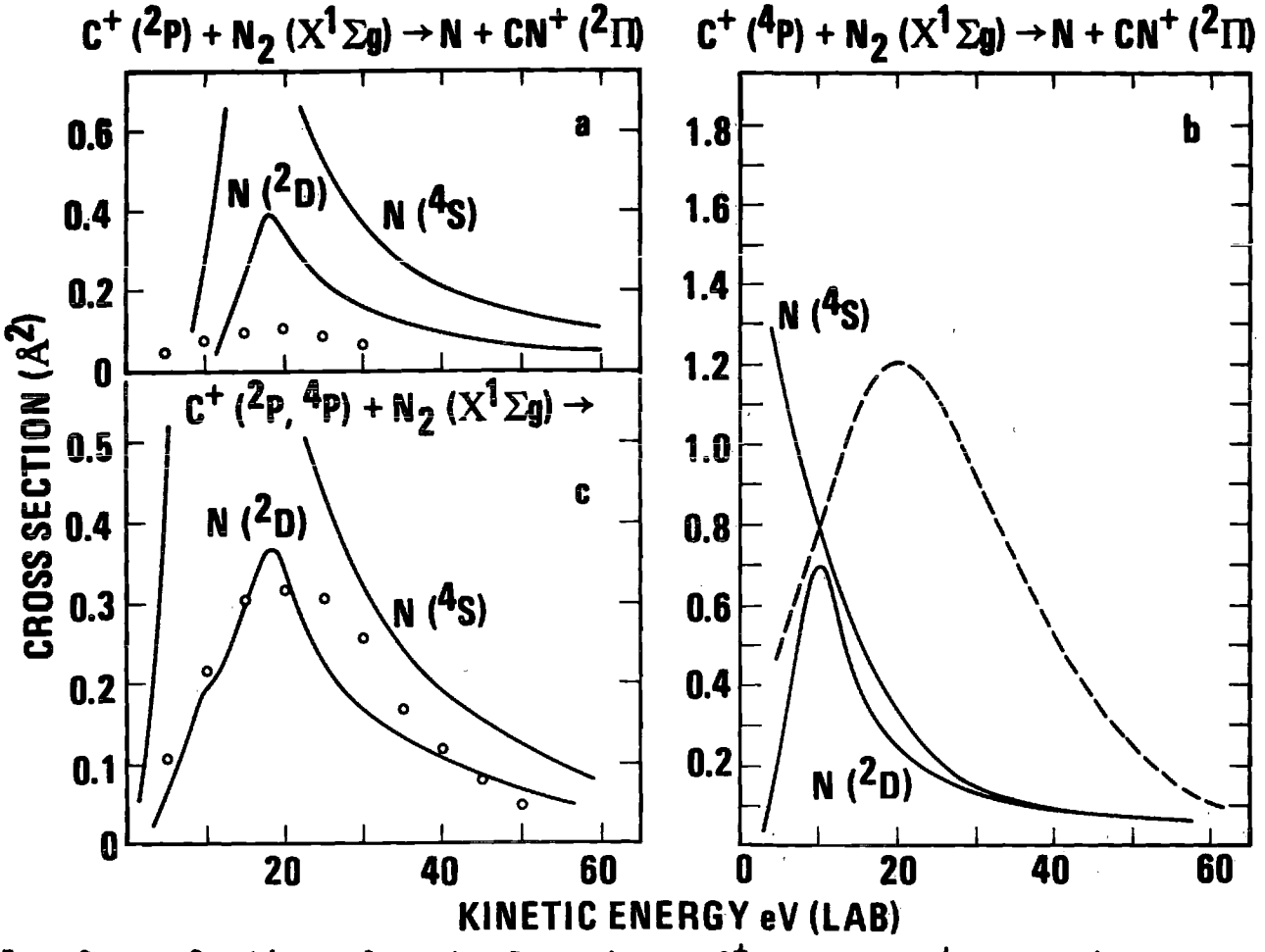

Figure 25. Cross Sections for the Reaction: $C^+ + N_2 \rightarrow CN^+ + N$. (The data points are from Ref. (86), and the dashed line is estimated from the other data points. The solid curves are the calculated cross sections.)

electron impact ionization respectively. Data obtained for C^+ ions produced by 23 eV electrons refer to the reactions of ground state $C^+(^2P)$ ions and are presented in Fig. 25a. In Fig. 25a a comparison of this data is made with computations using the phase space model which are given by the solid curves. Curves labeled $N(^4S)$ and $N(^2D)$ refer to computed cross sections for reactions, (67g) and (67h), respectively in which the product N atoms are considered in either the ground ^4S, or excited ^2D state. The energy dependences of the calculated cross sections in Fig. 25a for these two reactions are similar; however, the absolute magnitude of the computed curve in which $N(^2D) + CN^+(^3\pi)$ are considered products is in better agreement with the experimental data. The $C^+(^2P) + N_2(X^1\Sigma_g)$ reactions leading to $N(^2D) + CN^+(^3\pi)$ may be favored since the overall spin change would be less than the corresponding reaction in which $N(^4D)$ atoms are formed. As noted previously, the distribution of products among the various product ion states in the statistical model is primarily controlled by the energetics of reaction and no *a priori* account is made for activation energy barriers or spin selection rules. Further information on this point is given in Fig. 25b for the reactions of $C^+(^4P)$ with $N_2(X^1\Sigma_g)$ forming $N(^4S \text{ or } ^2P) + CN^+(^3\pi)$. The reaction producing $N(^4S)$ atoms is exothermic with the computed cross section steadily increasing as the reactant ion kinetic energy is lowered, while that for the endothermic reaction forming $N(^2D)$ atoms

goes through a maximum in agreement with experimental data given by the dashed line. We note that this latter reaction of $C^+(^4P)$ ions with $N_2(X^1\Sigma)$ giving $N(^2D) + CN^+(^3\pi)$ does not involve a net spin change while the analogous reaction producing $N(^4P)$ has a spin change of two. The experimental curve for $C^+(^4P)$ reaction was estimated from the 70 eV points in Fig. 25c by subtracting contributions from $C^+(^2P)$ reactions. Since this technique relies strongly upon accurate determination of the electronic state distribution of the C^+ ion beam and obtaining accurate values of cross sections at both high and low bombarding electron energies, the experimental data for reactions of $C^+(^4P)$ ions is somewhat uncertain; however, comparison between the experimental and calculated cross sections indicates the reaction pathway leading to $N(^2D)$ atoms, Eq. (67h), is preferred. A further comparison between experiment and the statistical model is presented in Fig. 25c where the reaction cross sections for C^+ produced in 70 eV ionization are given along with those computed for reactions (67g) and (67h) leading to CN^+. In order to compare theory and experiment in Fig. 25c, we have weighted the calculated cross sections for reactions involving ^2P and ^4P C^+ ions 0.72 and 0.28 respectively to account for the experimental reactant ion beam distribution. Satisfactory agreement between the measurements and the computed cross sections is obtained if reaction (67h) leading to $N(^2D) + CN^+(^3\pi)$ products is taken as the dominant atom trans-

fer channel for reactions of $C^+(^2P$ and $^4P)$ ions with nitrogen molecules.

The analogous mass transfer channels for reactions of C^+ and O_2 to give $CO^+ + O$ are presented in Fig. 26 with circles and dashed line representing the estimated experimental data of Ref. (86). Possible reactant and product states that we have considered in the phase space model of this reaction are outlined by Eqs. (68g) and (68h). The results of this calculation are given in Fig. 26a for reactant $C^+(^2P)$ ions with products $O(^3P)$ and $CO^+(X^2\Sigma$ and $A^2\pi)$ states. Comparison between the calculated curves and the experimental points indicate that either X or A product states of CO^+ can be considered possible within the framework of the statistical phase space model. We note that both these product ion states have the same multiplicity. The cross sections for reactions of excited $C^+(^4P)$ ions with O_2 are given in Fig. 26b and compared with those derived from the experimental data. We consider this data to have fairly large error limits since an estimate of this reaction pathway relies on extremely accurate cross section measurements made at two different ionizing electron energies. The apparent discontinuity of the curve in Fig. 26b reflects this error; however, the experimental data bound the cross sections calculated for both CO^+ (X and A) product states. Another comparison between experiment and theory is shown in Fig. 26c for the more accurate cross sections measured at 70 eV ionizing electron energies where

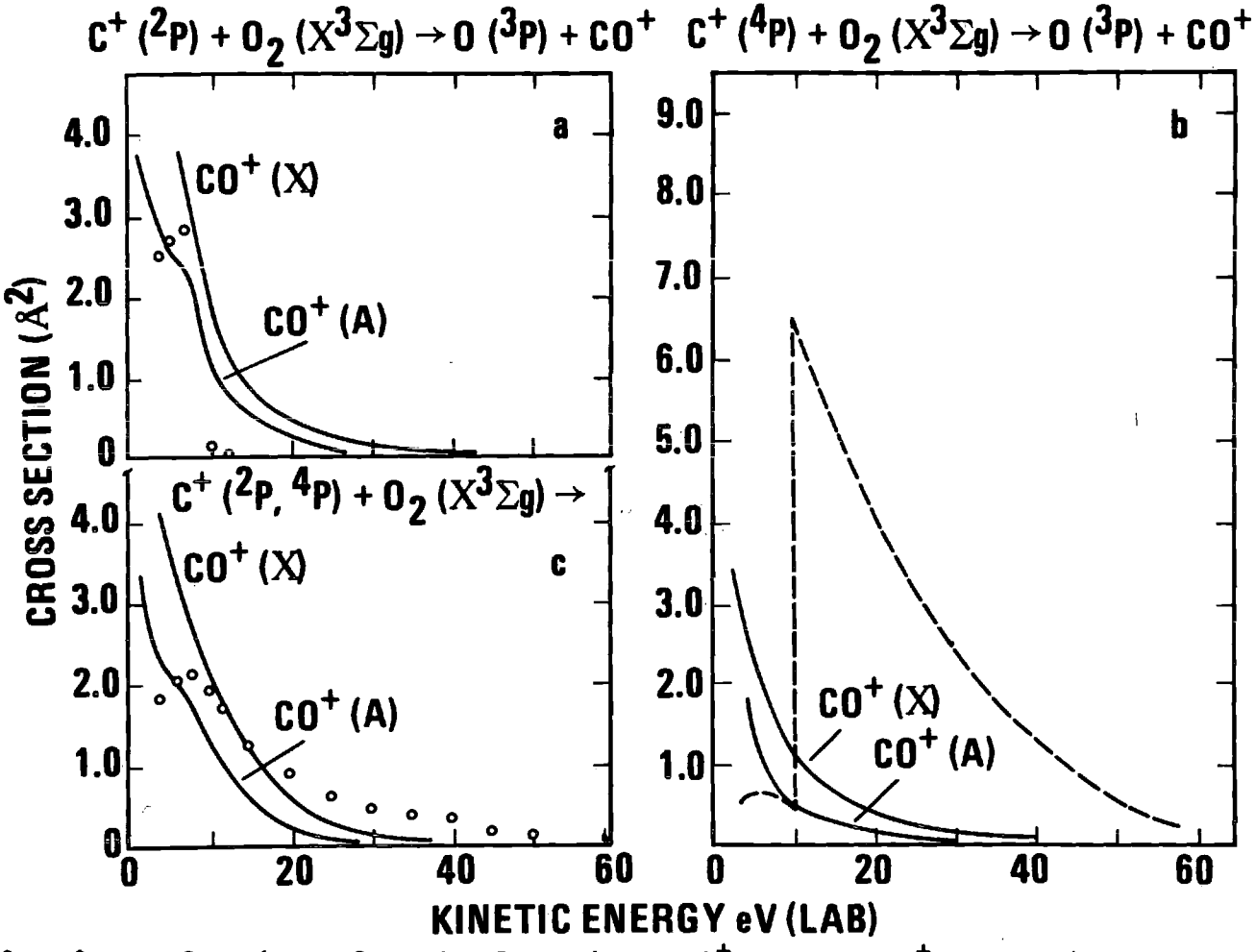

Figure 26. Cross Sections for the Reaction: $C^+ + O_2 \rightarrow CO^+ + O$. (The data points are from Ref. (86), and the dashed line is estimated from the other data. The solid curves are the calculated cross sections.)

both the $C^+(^2P$ and $^4P)$ reactant states contribute to reaction. Computed cross sections, weighted according to the reactant ion state distribution, compare favorably with the data and suggest that both $CO^+(X^2\Sigma$ *and* $A^2\pi)$ are possible product states.

Dissociative Charge Transfer Reactions

Previous calculations of dissociative charge transfer channels of reaction have shown the phase space theory accurately predicts translational energy dependences of reaction cross sections for both ground state and/or vibrationally excited reactant ions. Although cross sections obtained from the phase space model give correct energy dependences, it has been found that absolute magnitudes of the computed cross sections are in some cases larger than those experimentally determined. Dissociative channels for reactions of C^+ ions with N_2 molecules are presented in Fig. 27 where the circles and dashed line are estimated data of Ref. (86), and the solid curves are cross sections computed from the phase space model. These dissociative reactions for the $C^+(^2P) + N_2$ reactant system are presented in Fig. 27a; those for the $C^+(^4P) + N_2$ system are given in Fig. 27c; and those reactions involving both $C^+(^2P)$ and $C^+(^4P)$ ions are given in Fig. 27b. Computed cross sections in Fig. 27b are weighted to account for the $C^+(^2P)$ and $C^+(^4P)$ distributions in the reactant C^+ beam formed from high energy electron impact ionization of

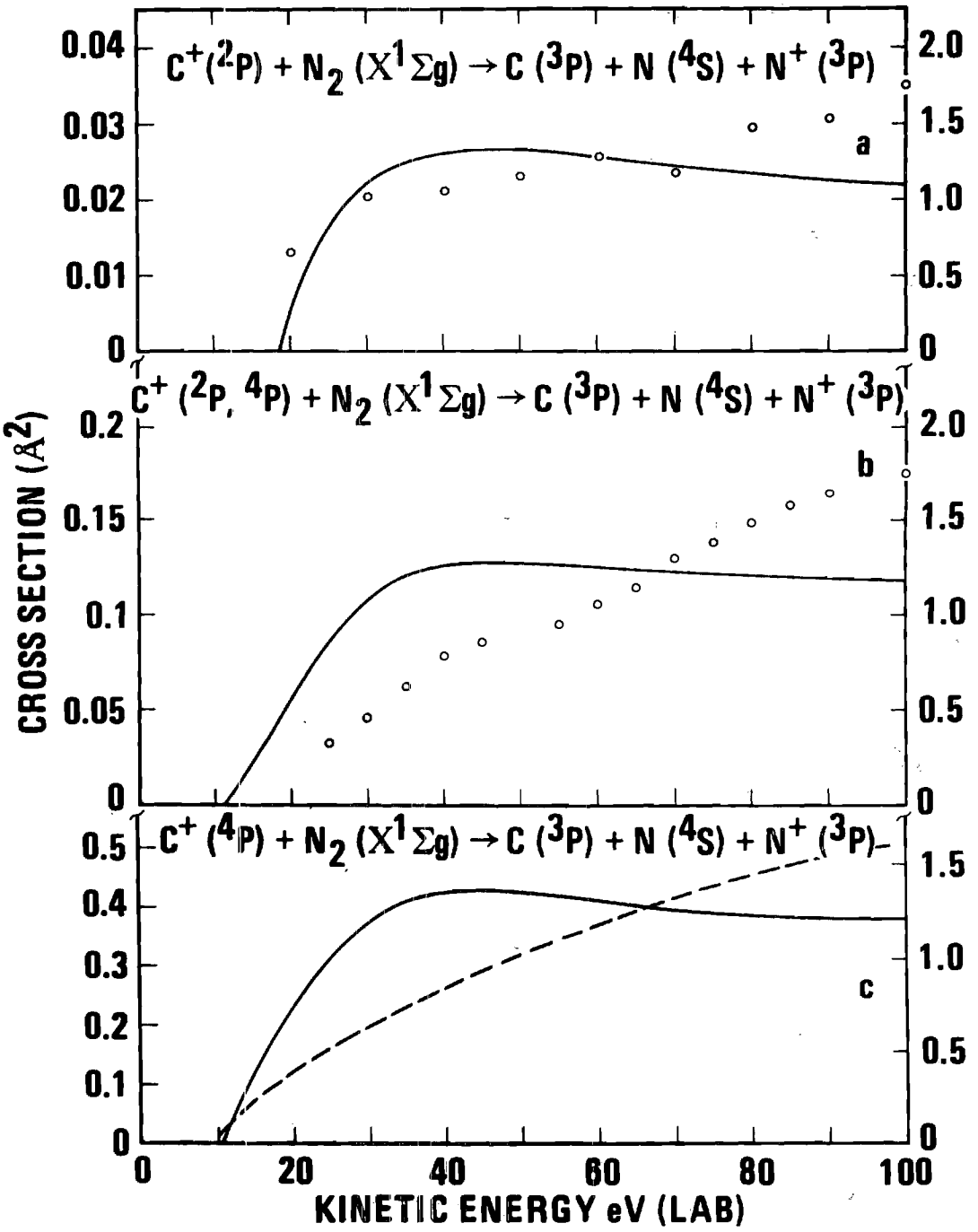

Figure 27. Cross Sections for $C^+ + N_2 \rightarrow N^+$ Reactions. (The data points are from Ref. (86), and the dashed line is that estimated from the other data. The solid curves are the calculated cross sections.)

CO so that direct comparison can be made with the experimental measurements. It is to be noted in all cases that the computed cross sections given in Fig. 27 are larger than those measured, but the energy dependences of the theoretical and experimental cross sections are in reasonable accord.

Similar presentations of data for the interactions of C^+ with O_2 are shown in Fig. 28. The reactions of $C^+(^2P)$ and $C^+(^4P)$ states are in Figs. 28a and 28c respectively with the weighted cross sections given in Fig. 28b. It is seen that the shape of the experimental and calculated cross sections are similar, but a significant difference in the absolute magnitude of the cross sections is evidenced. Measured angular distributions (62) and total cross sections (63) for atomic ions resulting from dissociation at high kinetic energies are consistent with the predominance of forward scattering. It is possible that not all charged particles from the dissociative processes investigated in Ref. (86) were collected by the second spectrometer which was at right angles to the primary ion beam. Repeller voltages were applied to accelerate products out of the interaction region into the analyzing mass spectrometer, but ionic products with momentum in the forward direction will not be collected with 100 per cent efficiency, leading to low experimental dissociative cross sections. The computed thresholds for atomic ion formation obtained from Figs. 27 and 28 approximate those measured and support the applicability of the phase space

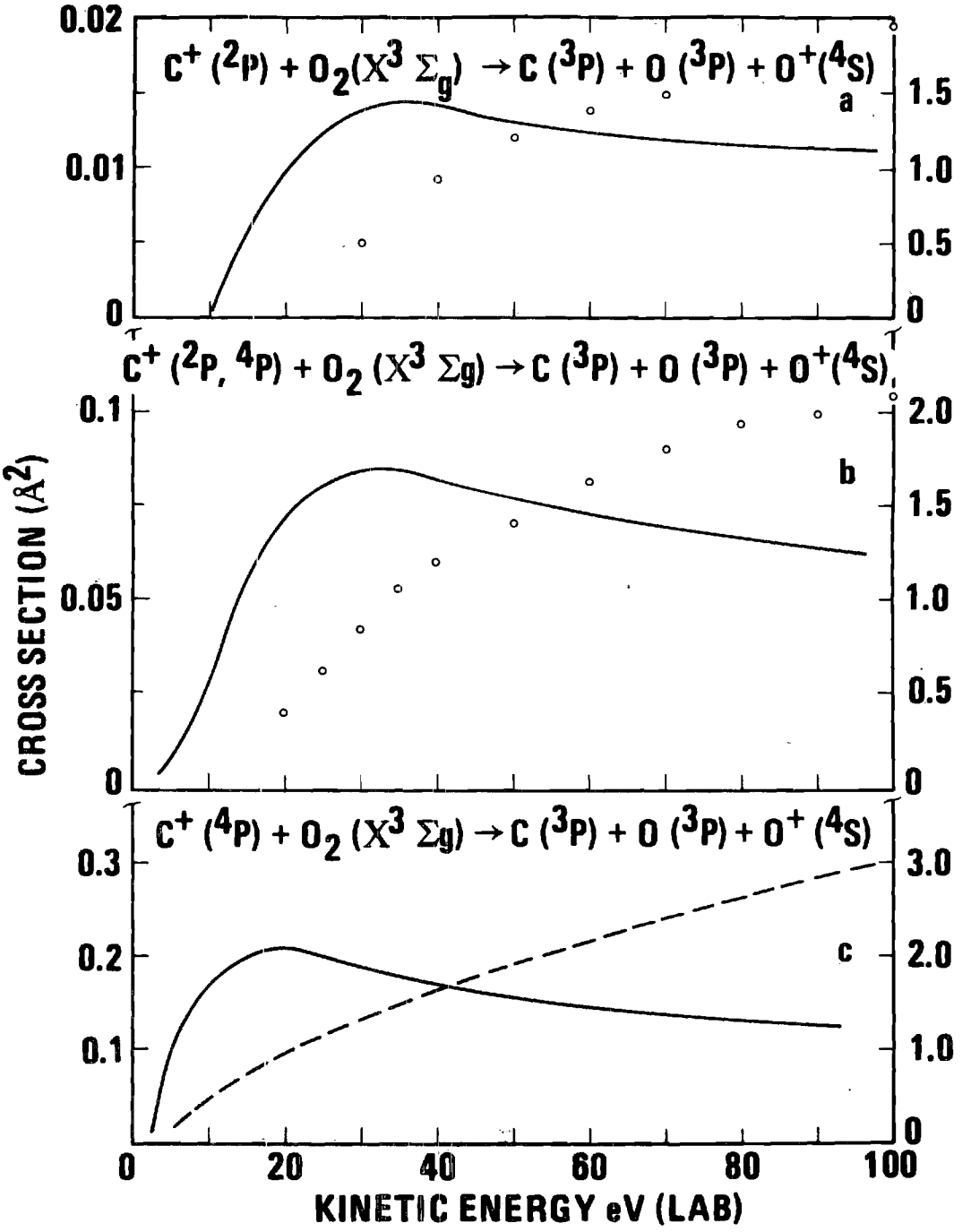

Figure 28. Cross Sections for $C^+ + O_2 \rightarrow O^+$ Reactions. (The data points are taken from Ref. (86), and the dashed line is estimated from the other data. The solid curves are the calculated cross section.)

model to energy conversion processes in these reaction channels.

Charge Transfer Reactions

The experimental charge transfer processes for C^+ reacting with N_2 are shown in Fig. 29 as the circles and dashed line. Fig. 29 gives the comparison with phase space calculations for various N_2^+ product states for the $C^+(^2P) + N_2$ reactant system. Similar comparisons are shown in Fig. 29c for the $C^+(^2P) + N_2$ system where the dashed curve is obtained from experimental data and the solid curve is total cross section for N_2^+ formation derived from the statistical model. A serious departure of the theoretical and experimental cross sections is evidenced in Fig. 29c with the result that the weighted cross sections computed for $C^+(^2P, ^4P) + N_2$ reactions in Fig. 29b are also in disagreement with experiment above 20 eV. Experimental cross sections for $C^+(^4P)$ reactions exceed the total cross sections calculated from the ion-induced dipole potential and suggest electron transfer occurs at impact parameters larger than those possible from Eq. (25). An alternate approach to the description of charge transfer processes is the one electron model (19) for asymmetric systems in which the cross section is dominated by "accidental resonance" conditions when the energy defect ΔE is small (20). $C^+(^4P)$ is in close resonance with $N_2^+(A^2\pi_u)$ and vibrationally excited $O_2^+(a^4\pi_u)$ in the corresponding oxygen system, and

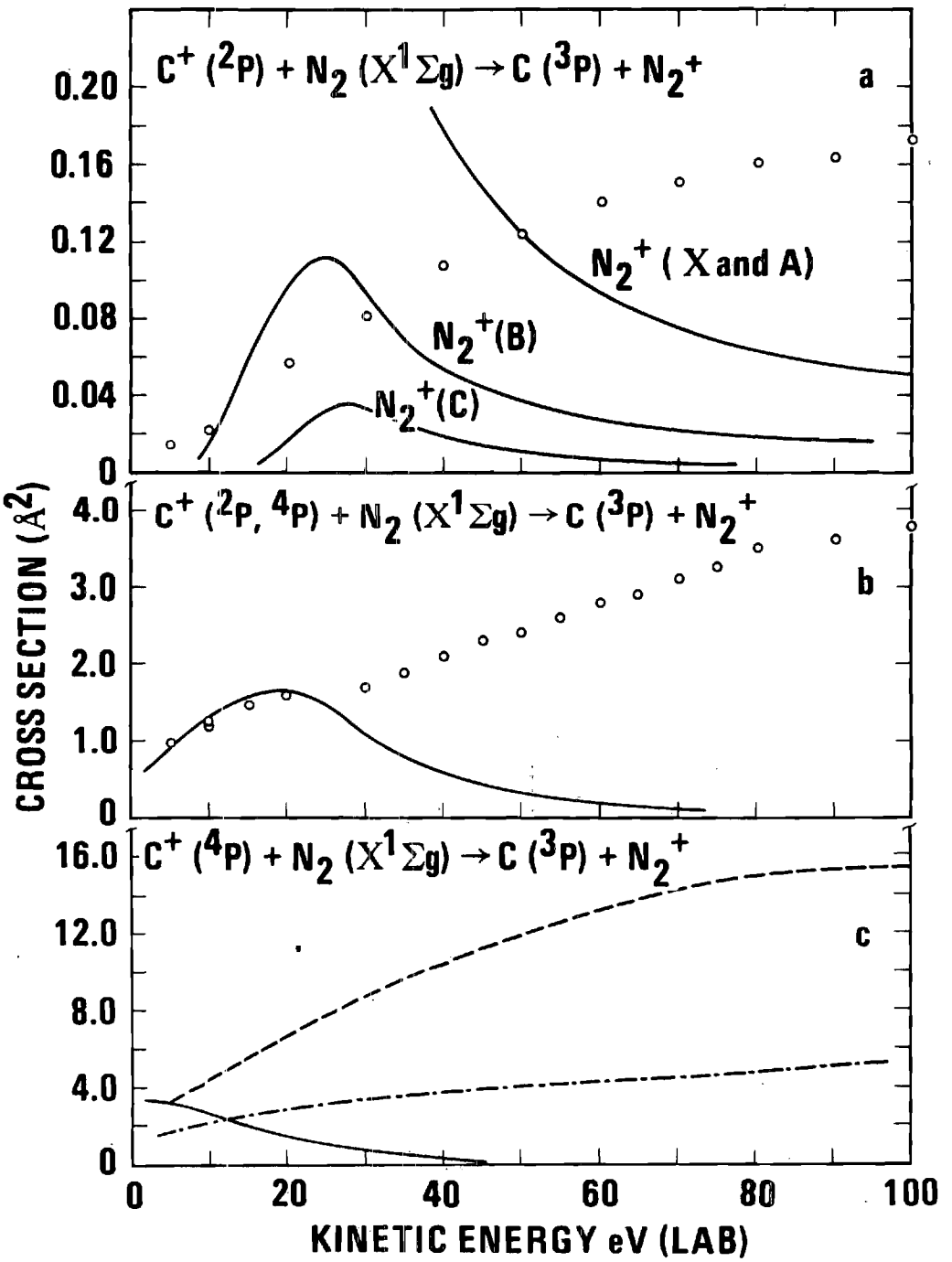

Figure 29. Cross Sections for $C^+ + N_2 \rightarrow N_2^+$ Reactions. (The data points are taken from Ref. (86), and the dashed line is estimated from the other data. The phase space calculation is given by the solid lines and the nearest resonance calculation by the dot-dash line.)

the charge transfer processes might be dominated by these accidental resonances. Bohme, Hasted, and Ong (21) have obtained an approximate expression for near resonant charge transfer processes for a given vibrational-rotational level of the reactant molecule

$$\sigma_{v,j}(v) = \sigma_m(v_m)\ \zeta\ exp\left[k'\left(1-\frac{\alpha|\Delta E|(v,j\rightarrow v',j')}{hv}\right)\right], v<v_m \quad (69a)$$

$$= \sigma_m(v_m)\ \zeta. \qquad v>v_m \quad (69b)$$

ζ is the square of the vibrational overlap integral (41) between states v and v'. Consistent with the assumptions of Bohme, Hasted, and Ong (21) α, the adiabatic parameter is taken to be 100Å; k', a measure of the 'sharpness' of the maximum in the cross section, is taken to be 2; and v_m, the velocity at which the maximum cross section is attained, is given by $h/|\Delta E| = \alpha/v_m$. The energy defect is given by

$$\frac{\Delta E}{hc}(v,j\rightarrow v',j') = \frac{\Delta E}{hc}(0,0\rightarrow 0,0) + [G(v) - G(0) + F_v(j)] - [G(v') - G(0') + F_{v'}(j')], \quad (70)$$

where the primes denote the product state. $\Delta E(0,0\rightarrow 0,0)$ is the energy defect for ground state products. The vibrational and rotational levels for the diatomics are given by (27)

$$G(v) = \omega_e(v+\tfrac{1}{2}) - \omega_e x_e(v+\tfrac{1}{2})^2; \quad (71)$$

$$F_v(j) = [B_e - \alpha_e(v+\tfrac{1}{2})]\ j(j+1). \quad (72)$$

To calculate $\sigma_m(v_m)$ we consider the interaction potential to be that given by Eq. (24) with the inclusion of a resonance potential which has the asymptotic form (12)

$$V_r = \pm Ar \exp\,[-Z(1+r)] \tag{73}$$

where $A = (e^2/2a_o)\,(Z^3 4^{1/Z})$. Z^2 is the ionization energy in Rydbergs, a_o is one Bohr radius, and r is expressed in units of a_o. Considering only the attractive portion of the potential, a maximum in the potential is reached when $r = r_*$ given by

$$(dV/dr)_{r=r_*} = 0. \tag{74}$$

From Eqs. (24), (73), and (74) in atomic units $L^2(r_*)$ is given by

$$L^2(r_*) = 2\mu\alpha/r_*^2 + \tfrac{1}{2}\mu A(Zr_*-1)r_*^3 \exp\,[-Z(1+r_*)] \tag{75}$$

which then gives for the potential at its maximum

$$V_* = \alpha/r_*^4 + \tfrac{1}{2}r_*\,A(Zr_*-3)\exp\,[-Z(1+r_*)]. \tag{76}$$

Since (d^2V/dr^2) must be less than zero at the maximum, all $r_* > r_m$ will lead to formation of a maximum in V where r_m is given by $(5 + \sqrt{13})/2Z$ (12). For intimate interactions the barycentric kinetic energy cannot be less than V_*. Thus, setting $E = V_*$ will uniquely define r_* and $L(r_*)$ from which the cross section is obtained

$$\sigma = \pi L^2/(\mu v)^2. \tag{77}$$

However, in cases for $E > V_*$ at $r = r_*$, the orbital angular momentum is given by (12)

$$L^2 = L^2(r_*=r_m) + \mu r_m^2 \, [E - V_*(r_*=r_m)]. \qquad (78)$$

$\sigma_m(V_m)$ is obtained by solving Eqs. (75), (76), and (78) for L^2 at $v = v_m$. Bohme, Hasted, and Ong (21) have shown that only the six closest exothermic resonances make significant contributions to the total cross section. The total charge transfer cross section for a given ion velocity is then given by

$$\sigma(v) = \sum_{v,j} \sum_{n=1}^{6} \sigma_{v,j}(v) f(v,j) \Big/ \sum_{v,j} f(v,j), \qquad (79)$$

where $f(v,j)$ is the distribution function for reactant diatomic molecules

$$f(v,j) = \frac{(2j+1)}{Q_v Q_r} \exp\,[-\{G(v)-F_v(j)\}hc/kT]. \qquad (80)$$

Q_v and Q_r are the partition functions for the vibrational and rotational states respectively. We have used this near resonance formalism to describe the interactions of the $C^+(^4P) + N_2(X^1\Sigma_g)$ system since it is in close energy balance with the $N_2^+(A^2\pi_u, v=0,1) + C(^3P)$ product channel. Results of this computation given by the dot-dash line in Fig. 29c are to be compared with the experimental curve. The functional dependence of the measured charge transfer cross section is in harmony with the nearest resonance calculations; however, the

absolute value of the computed cross section is lower than indicated by the experimental estimate. It is to be noted that the vibrational wavefunctions used to calculate the overlap integrals were those involving infinite N_2 and N_2^+ separation, whereas a more complete description would take into account the perturbation of the vibrational motion during the heavy particle collision. Also, the large error noted in the subtraction technique to obtain the curve suggests an overestimate of the experimental cross section, and the resonance calculation gives the correct energy dependence of cross section.

Similar reactions involving the $C^+(^2P$ and $^4P) + O_2$ systems are presented in Fig. 30 with the experimental data given by the circles and dashed line. Cross sections predicted by the statistical phase space model are given by the solid curves in this figure. Computed cross sections for the reactions of $C^+(^2P)$ ions are given for channels involving different O_2^+ electronic states. The calculated cross sections for $C^+(^2P)$ ions in Fig. 30a are of the same order of magnitude as the experimental data, but quantitative agreement is not evidenced. A more serious deficiency of the phase space model in describing these electron transfer reactions is shown in Fig. 30c for $C^+(^4P)$ ions where computed total O_2^+ cross section is low with an apparent incorrect energy dependence, which also has a corresponding effect on the weighted $C^+(^2P, ^4P)$ data in Fig. 30b. A more realistic

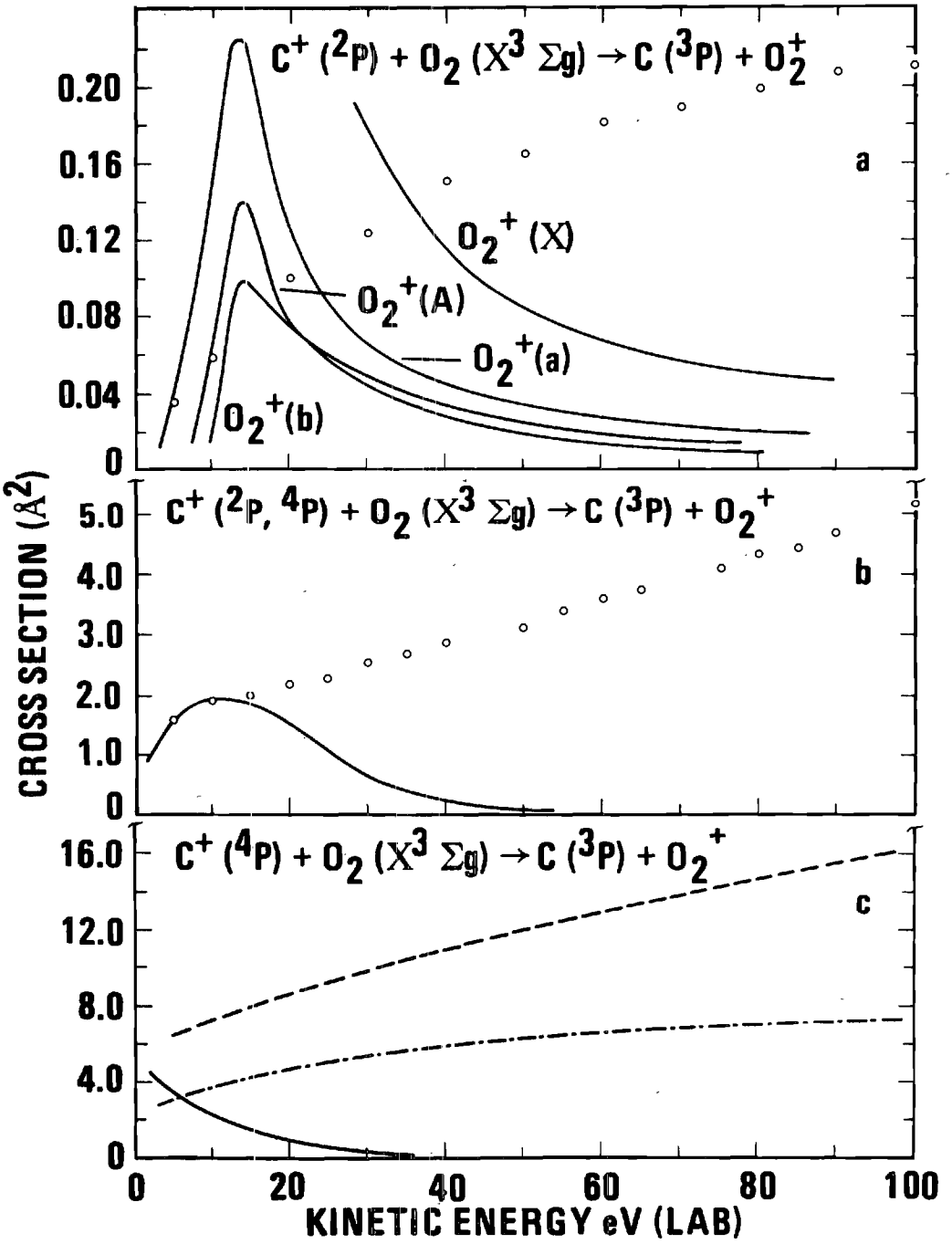

Figure 30. Cross Sections for $C^+ + O_2 \rightarrow O_2^+$ Reactions. (The data points are taken from Ref. (86), and the dashed line is estimated from the other data. The phase space calculation is given by the solid lines and the nearest resonance calculation by the dot-dash line.)

description of the $C^+(^4P) + O_2(X^3\Sigma_g)$ interactions is embodied in the nearest resonance model in which we have taken the $C(^3P) + O_2^+(a^4\pi_u)$ as products. This particular channel does not involve a net spin change and the energy balance between reactant and product system is obtained at approximately the $v=5$ level of $O_2^+(a^4\pi_u)$. Computation using the nearest resonance model, which is presented in Fig. 30c, shows the cross section to be of the right magnitude; and the variation of the cross section with reactant ion kinetic energy is similar to experimental observation.

Summary

The cross sections for chemical rearrangement reactions of low energy C^+ ions with N_2 and O_2 leading to CN^+ and CO^+ respectively are in reasonable agreement with the predictions of the statistical phase space model. However, quantitative comparison between the results using this model and experimental data indicates that product states do not necessarily mix statistically; and spin and/or symmetry requirements play a role in determining the product states. Translational energy dependences of dissociative reactions as determined from the statistical model appear to be correct, but the statistical treatment overestimates the magnitude of this channel. Competative charge transfer processes with close energy balance between initial and final states are better described by the nearest resonance model, where

electron transfer may occur over large distances, with the statistical approach limited to close coupled collisions. It is noted that the phase space results for Figs. 29b and 30b are in good agreement at energies below 20 eV, the energy where b_{max} becomes approximately equal to the hard core diameter of the target specie. Above this energy the Langevin cross section and, thus, the partial cross sections fall off faster than is indicated by experimental measurements.

CHAPTER VI

ROTATIONAL EXCITATION OF N_2^+ PRODUCED IN CHARGE TRANSFER REACTIONS WITH INERT GAS IONS

In this chapter we wish to investigate further the internal energy distribution of product diatomics using the phase space model. In Chapter III we showed that the phase space model gives a good representation of the relative population of the various vibrational states of diatomic ions produced in charge transfer reactions. In treating the internal energy distribution, vibrations were treated quantum mechanically while integrating over rotational states. We now consider the classical phase space model applied to internal rotational population where we treat rotations quantum mechanically. We will examine the rotational distributions within a given vibrational state of N_2^+ formed in low energy charge transfer reactions of inert gas ions with N_2.

In Chapter III we noted that Inn (31) observed significant deviations in both vibrational and rotational distributions from that predicted by a Boltzmann distribution for $N_2^+(C^2\Sigma_u)$ formed in charge transfer of $He^+ + N_2$. He obtained rotational populations on the basis of observed radiative intensities of the N_2^+ second negative transitions corresponding to

$$N_2^+(C^2\Sigma_u) \rightarrow N_2^+(X^2\Sigma_g) + h\nu. \qquad (81)$$

In other studies of low energy charge transfer processes, the population of higher vibrational and rotational states of product diatomics is significantly higher than that predicted on the basis of the Franck-Condon principle (87-93). Moore and Doering have investigated the first negative system of N_2^+ corresponding to the radiative transitions

$$N_2^+(B^2\Sigma_u) \rightarrow N_2^+(X^2\Sigma_g) + h\nu \qquad (82)$$

where $N_2^+(B^2\Sigma_u)$ ions are formed in charge transfer processes. They find vibrational (87) and rotational (88) relative band intensities agree with those predicted from the Franck-Condon principle at high energies, while at ion velocities below 10^8 cm/sec significant enhancement of higher rotational and vibrational states is observed. Similar behavior has been observed by Polyakova et al. (89) and Liu (90). Also, CO^+ formed in charge transfer processes has shown anomalous vibrational distributions (91,92) at low energies.

In this laboratory Moran and Fullerton (94) observed a similar departure from the Franck-Condon principle in the collision induced dissociation of H_2^+. The dissociation process may be described in terms of an electronic transition from the $H_2^+(^2\Sigma_g)$ bound state to the $H_2^+(^2\Sigma_u)$ repulsive curve. At 2 keV ion energy the electronic transition resulting in the formation of H^+ was adequately described by the Franck-

Condon principle, but as the ion energy was lowered, deviation from the Franck-Condon principle became significant resulting in H^+ ion having a much lower velocity than would be expected. Presumably, these deviations may be attributable to longer collision times resulting in a perturbation of the internuclear separation of the diatomic. At low ion kinetic energies this perturbation may be described by invoking complex formation, which would then allow a representation of these processes by the phase space model.

Previous results of applying the phase space model to rotational populations (4-7) have shown that the model predicts high rotational enhancement of the diatomics produced in neutral-neutral reactions. Pechukas et al. (4) examined internal energy distributions for reactions of potassium with hydrogen halides and found reasonable agreement with experiment. They noted that in reactive collisions that most of the angular momentum is converted to product rotation. Disagreement was noted at the threshold indicating a small energy barrier. Lin and Light (5) then studied the same reaction by incorporating a potential barrier in the phase space model and found better agreement with experiment. Truhlar and Kuppermann (6) investigated the internal energy distribution for the reactions of atomic hydrogen with deuterium halides and observed a very marked dependence on initial energy and angular momentum. As the energy is raised, the relative energy of the reactants provides more

energy and angular momentum to the complex so that energy and angular momentum from internal modes is less important and rotational distributions become broader. Their predicted ratios of product vibrational and rotational states compare favorably with experiment. More recent calculations of Truhlar (95) applying the phase space model to inelastic processes for the beam reaction K + HCl predict a high ratio of inelastic collisions to reactive scattering. Product diatomics are predicted to be highly rotationally excited in substantial agreement with experiment. There have been no comparisons of rotational distributions for ion-neutral collisions, presumably due to the lack of data with which to make comparison. With the improvement of experimental resolution in recent years data from spectroscopic sources have become available with which to compare phase space predictions.

The phase space for forming a given rotational state is given by integrating the phase space integral, Eq. (38), over M_z (see Eq. (36)). This gives

$$\Gamma(E,K,v,m) = 2M, \qquad M<|M_1|; \quad (83a)$$

$$= M - K + (8e^2\alpha\mu^2\varepsilon)^{1/4}(1 - M^2/2I\varepsilon)^{1/4} \qquad M>|M_1|. \quad (83b)$$

If we write

$$M^2 = m(m+1)\,\hbar^2 = 2IE_{rot}$$

defining product rotational energy and angular momentum, we find the phase space for forming a diatomic product defined by total energy, E; total angular momentum, K; vibrational

quantum number, v; and rotational quantum number, m. The probability for forming a product in vibrational state v and rotational state m is then

$$P_r(E,K,v,m) = [\Gamma(E,K,v,m) / \sum_m \Gamma(E,K,v,m)] P_i(E,K,v). \quad (85)$$

We multiply the probability for a given rotational state within a given vibrational state by the probability for forming the vibrational state, $P_i(E,K,v)$, in order to insure that the sum of the probabilities of forming that vibrational state.

Low energy charge transfer processes for the reaction

$$He^+ + N_2(X^1\Sigma_g) \rightarrow He + N_2^+(C^2\Sigma_u) \quad (86)$$

show anomalously high rotational and vibrational enhancement (31,43). (See Chapter III for a discussion of the vibrational distribution, Fig. 3). This enhancement was attributed to the fact that high rotational states of the $v=3$ level are in exact resonance with He^+ (31). We have calculated the rotational distributions of N_2^+ formed by Eq. (86) and the results are shown in Figs. 31 and 32. In Fig. 31 the vibrational-rotational distribution of $N_2^+(C^2\Sigma_u)$ formed by He^+ with thermal velocity and 1.0 eV translational energy are presented; Fig. 32 shows the distributions for 5.0 and 10.0 eV He^+ ions. As the ion kinetic energy is increased, the rotational distribution becomes broadened. At thermal energy and low values of rotational angular momentum the

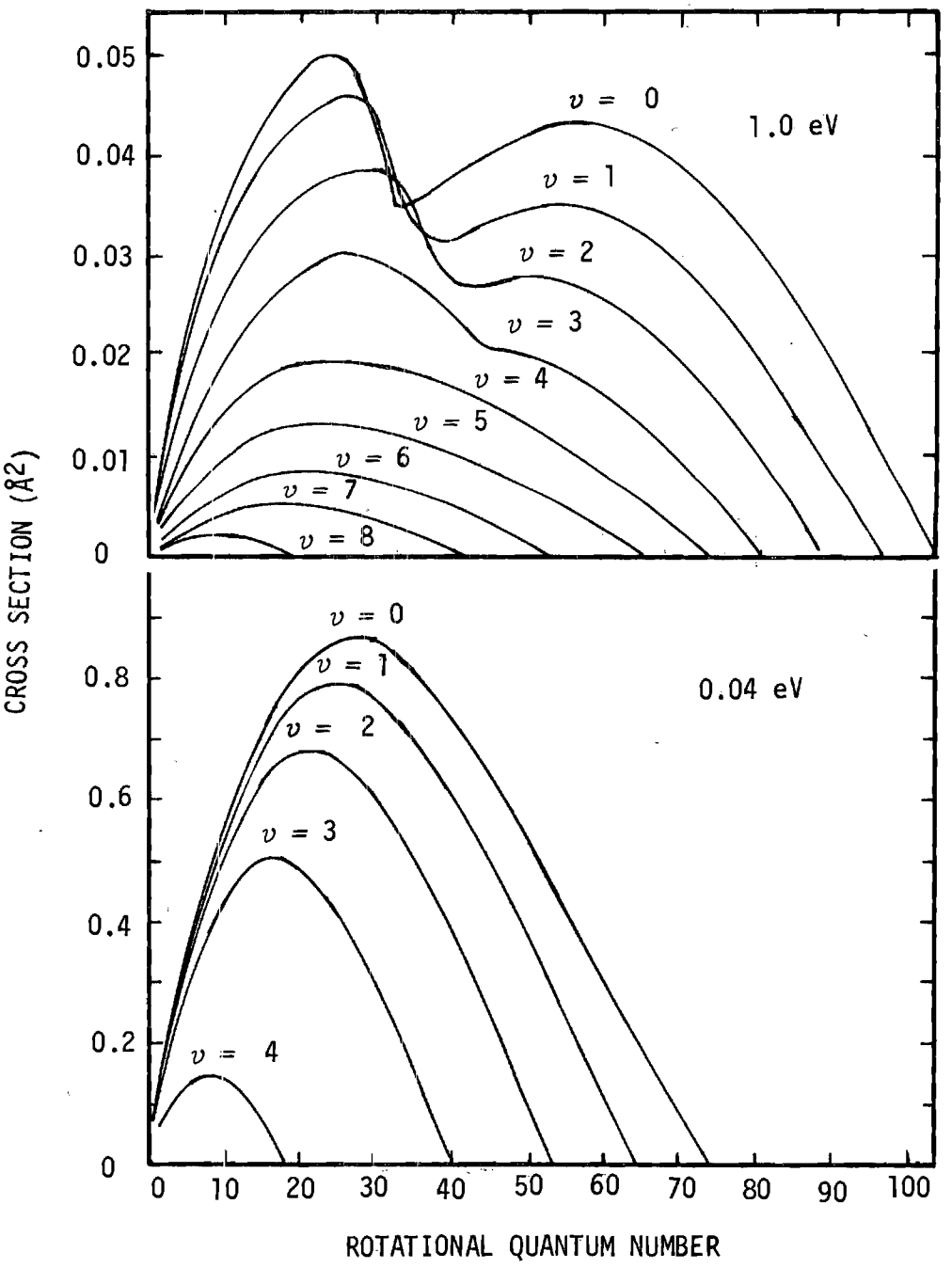

Figure 31. Rotational-Vibrational Distribution of $N_2^+(C^2\Sigma_u)$ Formed with 0.04 and 1.0 eV He^+ Ions.

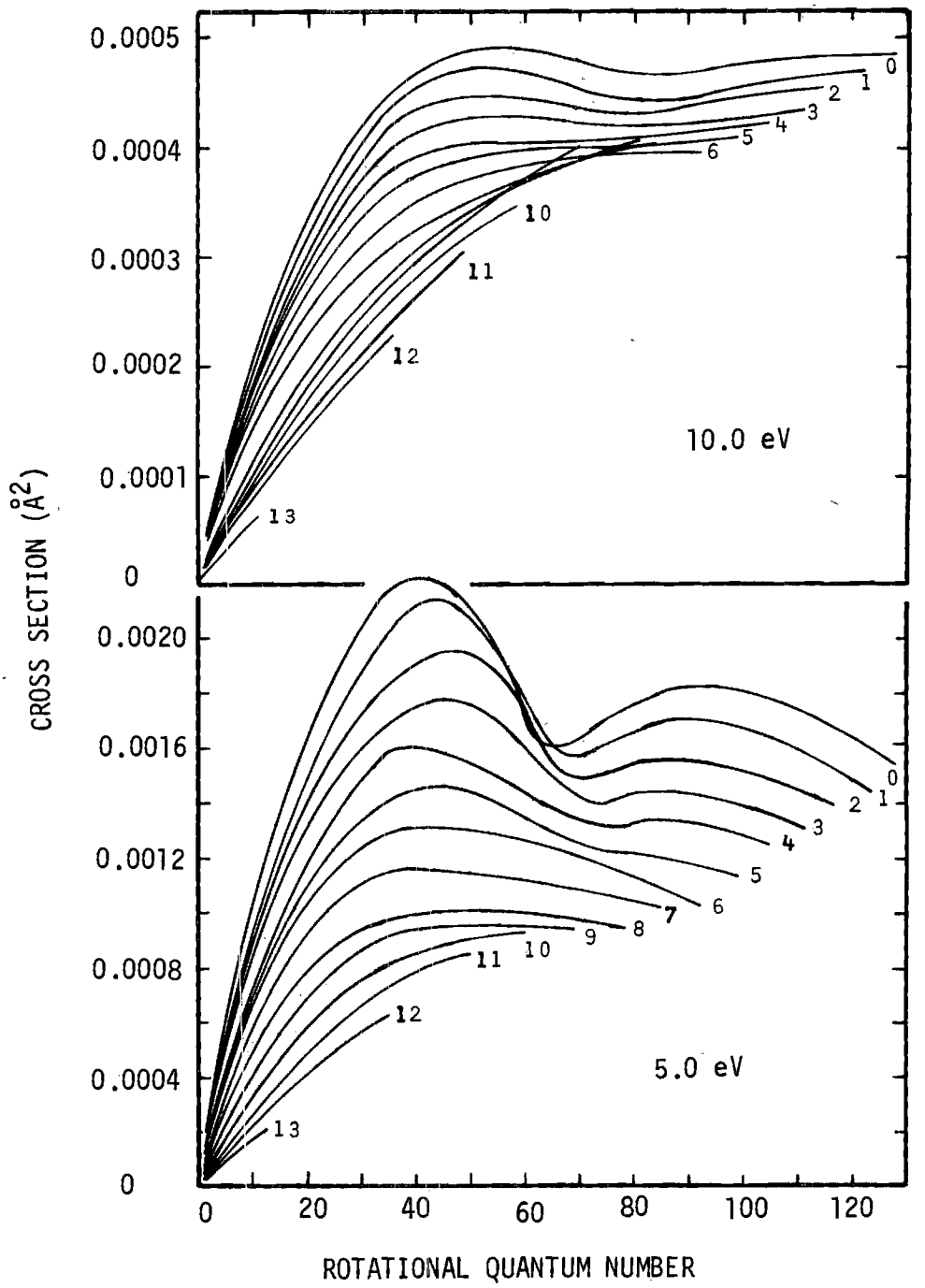

Figure 32. Rotational-Vibrational Distribution of $N_2^+(C^2\Sigma_u)$ Formed with 5.0 and 10.0 eV He^+ Ions.

rotational intensity is proportional to $2M$, Eq. (83a). Due to conservation of angular momentum, states with higher than a certain rotational angular momentum cannot be formed from all incident partial waves. As the energy is increased, the initial orbital angular momentum increases allowing more rotational states to be populated. But, due to angular momentum considerations, the intensity of higher rotational states is given by Eq. (83b) resulting in the two-peaked structure shown for 1.0 eV ion kinetic energy. Thus, the total intensity is given by a composite of the two conditions. At higher energies the two-peaked structure becomes less evident, but we note a further limitation. We require that the rotational energy be less than the dissociation energy from the given vibrational state, and we note a sudden fall off in the rotational cross section corresponding to the point at which the rotational energy equals the dissociation energy. The cross sections presented in Figs. 31 and 32 are smoothed out over the undulations present in the calculated cross section.

In Fig. 33 we show the actual cross sections calculated for each rotational state in the $v=0$ vibrational level for ion kinetic energies of 0.04, 1.0, 5.0, and 10.0 eV. As the energy increases to 5.0 eV, we note an increase in the undulations, and the two-peaked structure becomes more evident. At higher energies essentially a constant distribution is observed and the two-peaked structure is not as

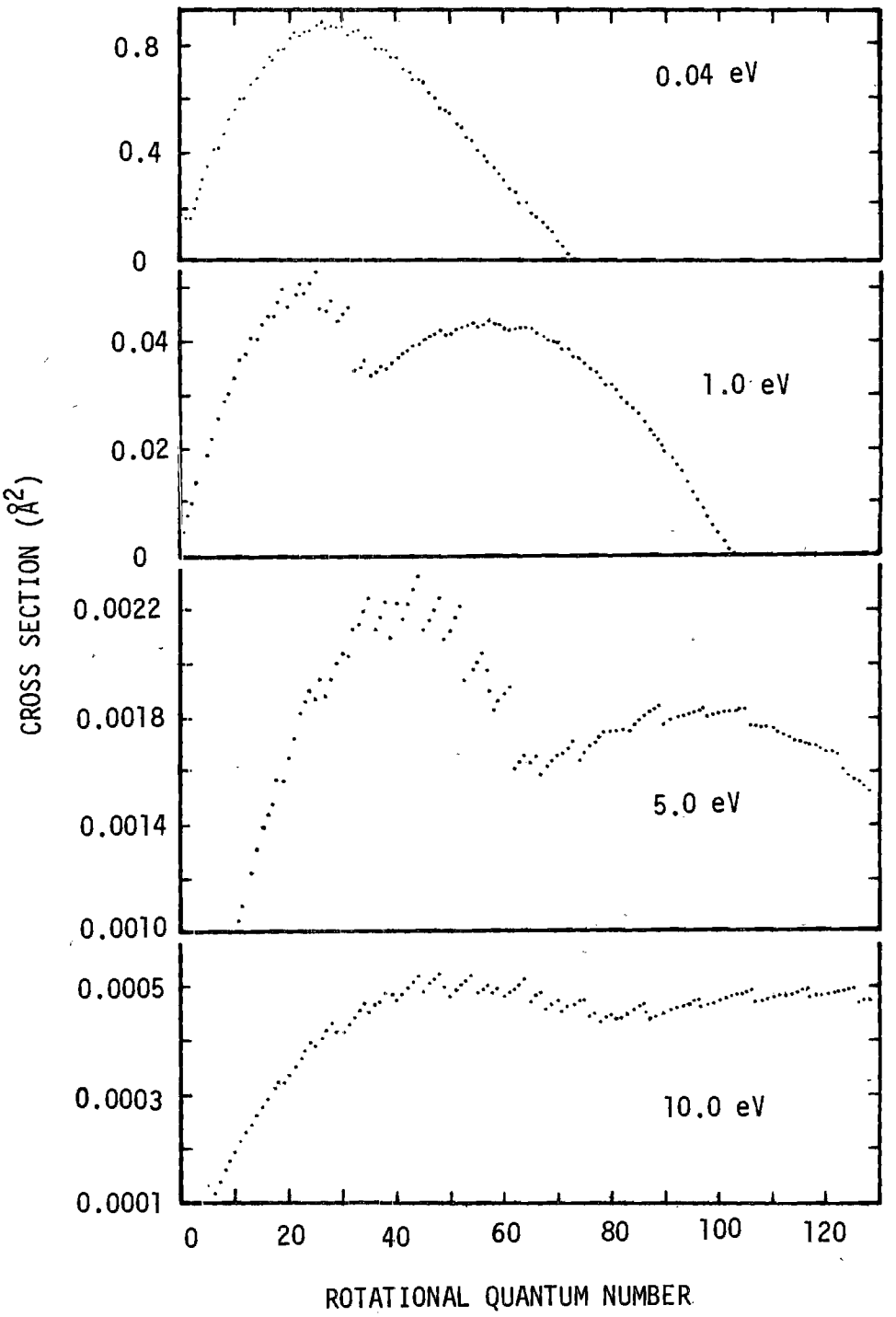

Figure 33. Rotational Cross Sections for Formation of $N_2^+(C^2\Sigma_u, v=0)$.

evident. A double peak such as predicted has never been observed experimentally, and it would require careful selection of ion energy in order that it ever be observed; but it would make an interesting experiment.

In the following figures the calculated rotational intensitiies will be presented as smoothed out curves drawn through an average of the calculated cross sections for each rotational state.

In Figure 34 the rotational distribution of the $v=3$ and 4 states are shown with the relative spectral intensities for the second negative transitions, Eq. (81), estimated from the data of Inn (31). Inn attempted to fit the distribution with a Boltzmann distribution at 610°K for rotational states above $m=10$ but found only approximate agreement. For the lower rotational states it was difficult to obtain a good estimate of the intensity due to poor resolution of the P and R branch transitions which overlap in this region (31). For the comparison we have assumed that the calculated cross sections for the rotational states is directly proportional to the relative intensity when multiplied by the Franck-Condon factor for the transitions from $v=3$ and 4. For the (3,9) and (4,10) bands presented by Inn (31), the Franck-Condon factors are 0.3330 and 0.3693 respectively (50). For the higher rotational states of the $v=3$ level, where the P and Q transitions are resolved, the calculated relative intensities give a very good representation of the observed spectral intensity for

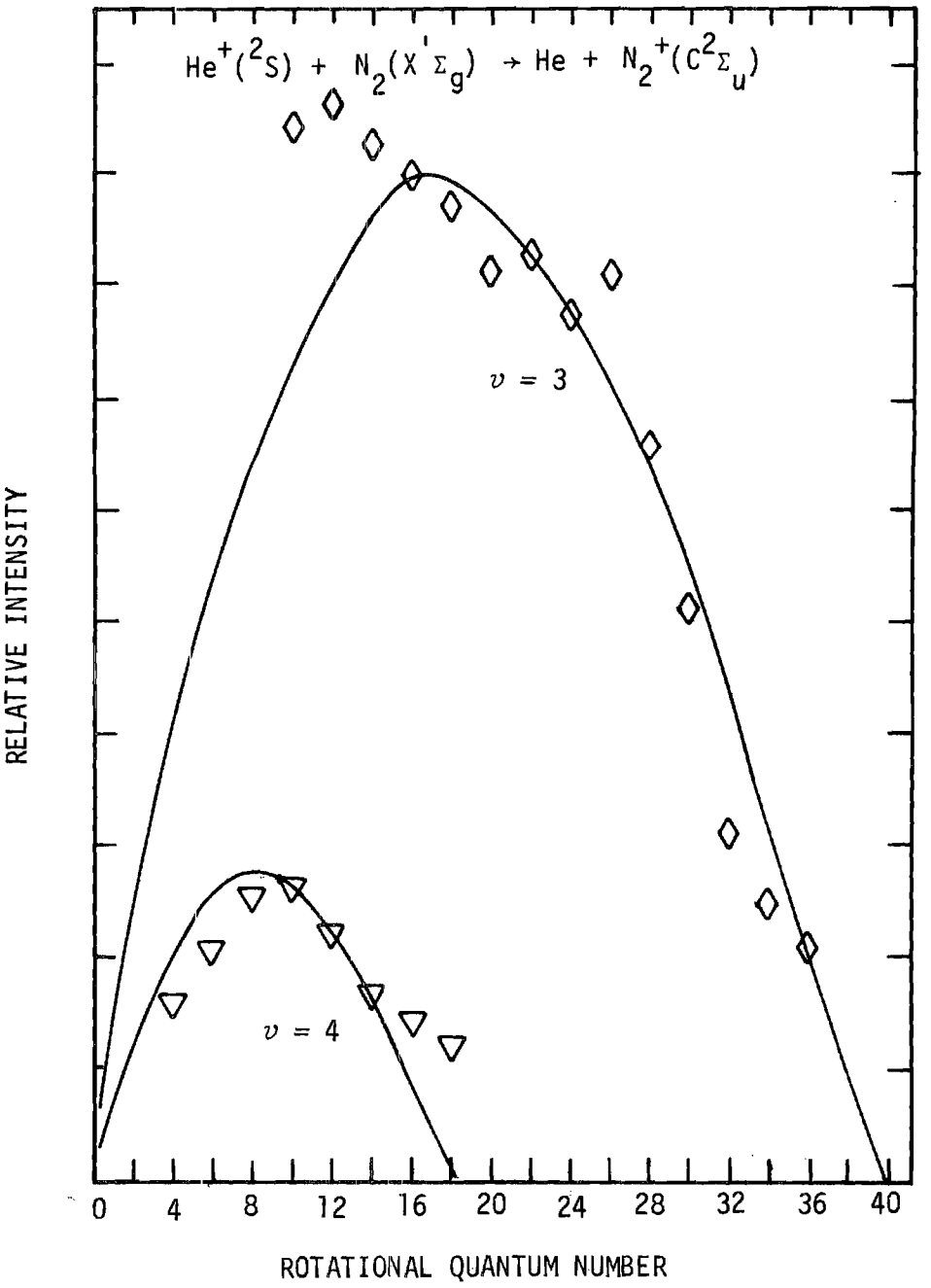

Figure 34. Relative Rotational Intensity of $N_2^+(C^2\Sigma_u, v=3,4)$ Formed by Ion Impact with He^+. (The data points are taken from Ref. 31.)

P branch transitions. For the $v=4$ vibrational state only the lowest rotational states are populated at thermal energies and, thus, have a much lower relative intensity. From the intensities estimated from the spectrum of Inn (31) relative to the intensities for the $v=3$ vibrational state the phase space prediction of the spectral maximum and the relative magnitudes is in accord with observed intensities. Previously, we showed that the phase space model gave good vibrational product state ratios. From Fig. 34 we see that the model also gives good ratios of product diatomic rotational states within a given vibrational state and of relative intensities from different vibrational states.

Kassal and Fishburne (93) have obtained rotational distributions of $N_2^+(B^2\Sigma_u)$ ions formed in charge transfer reactions of the type

$$I^+(i) + N_2(X^1\Sigma_g) \rightarrow I(j) + N_2^+(B^2\Sigma_u) \qquad (87)$$

which then radiate according to Eq. (82). $I(j)$ corresponds to an inert gas atom in state j formed from the corresponding ion in state i. The spectrometer they used was connected to the collision chamber into which the gases were mixed. The electron gun used to ionize the gas operated at voltages above 5 keV, and pressure on the order of microns was maintained in the chamber. Using this high energy electron beam, inert gas ions could be formed in many possible states. (See Moore (96) for a tabulation of the possible states.)

Most of these states have short lifetimes, but some of the quartet metastable state are relatively long-lived. Hagstrum (97) has estimated that these metastable states have lifetimes greater than one second and, thus, would not decay in a time short compared with the collision time for the high pressure maintained in the collision chamber (93). For Ar^+, Kr^+, and Xe^+ it is necessary to consider these metastable states as reactant ions in that the ground states of the ions are not capable of exciting N_2 at thermal temperatures. In Table 3 we give some of the metastable states of the inert gas ions considered and the corresponding exothermicities resulting in forming the atom in a low excited state for the charge transfer process represented by Eq. (87). Also shown are the corresponding ground state exothermicities to illustrate the disfavor of these reactions.

For the reaction of N_2 with Kr^{+*} we have taken the two lowest metastable states to be dominant and of equal probability. In Fig. 35 we present the calculated probability for rotational population of the $v=1$, 2, and 3 levels of $N_2^+(B^2\Sigma_u)$ along with the experimental intensity given by Kassal and Fishburne (93). We have used an energy scale to present the results using band heads reported by Wallace (48) in order that we make a direct comparison with the observed intensity, since the broad spectrum observed could not be resolved into contributions from each vibrational level except for the $v=0$ state. The corresponding rotational

Table 3: Energy States of Rare Gases and Exothermicities for Charge Transfer Reactions $I^+ + N_2(X^1\Sigma_g) \rightarrow I + N_2^+(B^2\Sigma_u)$

	State	Energy	Exothermicity to Ground State Atom	Exothermicity to Excited State Atom
Ar	$^1S_0$	0		
Ar*		13.075		
Ar^+	$^2P_{3/2}$	15.755	-2.990	-15.897
Ar^{+*}	$^4D_{7/2}$	32.161	13.416	0.341
	$^4F_{9/2}$	33.384	14.639	1.564
Kr	$^1S_0$	0		
Kr*		9.860		
Kr^+	$^2P_{3/2}$	13.996	-4.749	-14.609
Kr^{+*}	$^4D_{7/2}$	28.900	10.155	0.295
	$^4F_{9/2}$	29.618	10.873	1.013
Xe	$^1S_0$	0		
Xe*		8.315		
Xe^+	$^2P_{1/2}$	12.127	-6.618	-14.933
Xe^{+*}	$^4D_{7/2}$	23.960	5.215	-3.101
	$^4F_{7/2}$	24.379	5.634	-2.681
	$^4F_{9/2}$	24.451	5.706	-2.609
	$^2F_{7/2}$	26.374	7.629	-0.686
	$^4D_{1/2}$	27.056	8.311	-0.004

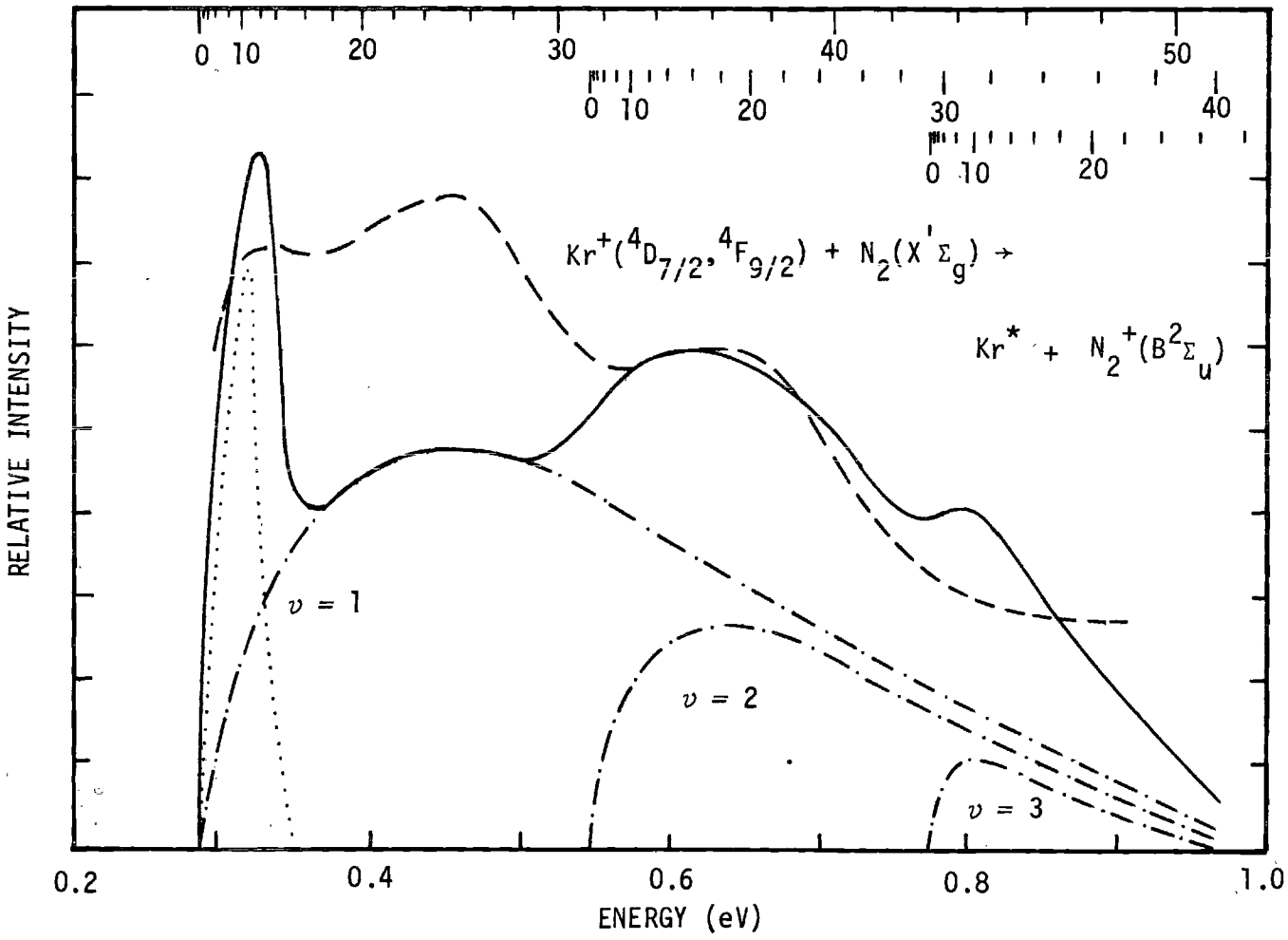

Figure 35. Relative Rotational Intensity of $N_2^+(B^2\Sigma_u)$ Formed by $Kr^{+*} + N_2$. (The solid line is the calculated intensity, and the dashed line is the observed intensity taken from Ref. 93.)

quantum numbers for the $v=1$, 2, and 3 states are shown at the top of Fig. 34. We have multiplied the calculated cross sections for each vibrational state by the corresponding Franck-Condon factor (50) for the individual spontaneous radiative $B - X$ transitions given by Eq. (81). (See Table 2 for these values.) In Fig. 35 the calculated rotational distribution for the individual vibrational states multiplied by the Franck-Condon factor for the $B - X$ transition of $N_2^+(B^2\Sigma_u)$ formed by reaction of N_2 with $Kr^+(^4D_{7/2})$ is given by the dotted line and those due to reaction with $Kr^+(^4F_{9/2})$ by the dash-dot curves. The total calculated intensity obtained by summing over all vibrational states is given by the solid line. The dashed line is the experimental distribution given by Kassal and Fishburne (93).

The $^4D_{7/2}$ state contributes very little at thermal velocities since only the lowest rotational states of the $v=1$ vibrational level are populated, and it is obvious that most of the rotational structure observed must be due to the $^4F_{9/2}$ state, but evidence for both states is noted. The discrepancy in relative magnitude of the peak observed at 0.4 eV may be due to high rotational states of the $v=0$ band which are not completely resolved in the experiment of Ref. (93). Also, the relative importance of the $v=3$ state appears to be overestimated which may be due to experimental resolution. The overall agreement with experiment is reasonable within experimental error of determining the absolute

intensity, again showing that the phase space model gives a good representation of product internal energy distribution.

Fig. 36 shows the corresponding distribution for the Ar^+ reaction. As before, we have considered the lower two metastable states to dominate; and the individual rotational distributions multiplied by the appropriate Franck-Condon factor (50) are shown. The dotted curves correspond to $N_2^+(B^2\Sigma_u)$ formed in the various vibrational states by reaction with $Ar^+(^4D_{7/2})$ and the dot-dash lines by reaction with $Ar^+(^4F_{9/2})$, and we have considered the contributions from both metastable ions to be equal. The solid line is the total calculated intensity obtained by summing over all contributing vibrational states. The experimental data, given as the dashed line, does not extend to the lower rotational states in that the P and Q branches were not resolvable (93). Comparison with the experimental intensity indicates that the contribution due to reaction with $Ar^+(^4F_{9/2})$ may be less than that due to $Ar^+(^4D_{7/2})$. Also, the contribution of the $v=1$ vibrational state appears to be less than we calculate. This may be due to the fact that we have not considered any broadening of the calculated intensities but have considered the calculated cross sections multiplied by the appropriate Franck-Condon factor to be directly proportional to the intensity. Experimental intensities for the $B - X$ transition and the phase space predictions both show that the dominate reaction is $Ar^+(^4D_{7/2}) + N_2 \rightarrow N_2^+(B^2\Sigma_u, v=0)$.

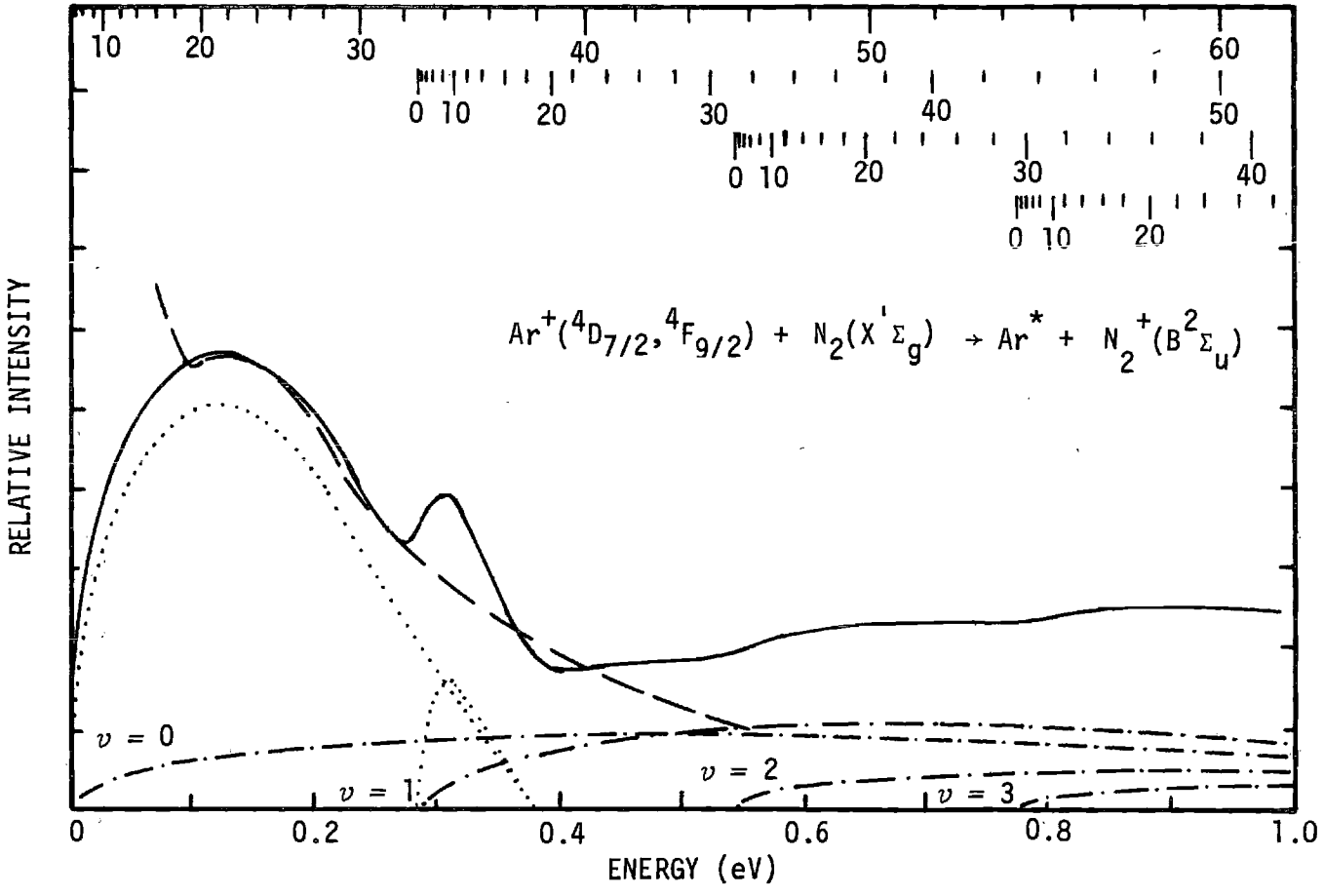

Figure 36. Relative Rotational Intensity of $N_2^+(B^2\Sigma_u)$ Formed by $Ar^{+*} + N_2$. (The solid line is the calculated intensity, and the dashed line is the observed intensity taken from Ref. 93.)

For the reaction of N_2 with Xe^+ forming $N_2^+(B^2\Sigma_u)$ the only metastable state that is energetically feasible is $Xe^+(^4D_{1/2})$. However, even with this state some additional energy must be supplied. In Fig. 37 we show the rotational distribution calculated for an ion kinetic energy of 0.15 eV as the solid line along with the experimental intensity given by Kassal and Fishburne (93) as the dashed line. For this presentation we use rotational quantum number as the abscissa in that only the $v=0$ state is populated. In the experimental arrangement some ions produced would be expected to have a small amount of translational energy. Also, some of the N_2 may possess a certain amount of internal energy which could make up the energy deficit. By assuming this additional energy, we obtain a good representation of the observed spectral distribution. The small bump observed at approximately $m=24$ is not explained by this mechanism. At the high pressure maintained in the collision chamber, some higher states of Xe^+ may be formed and undergo charge transfer before they decay. This could explain both the energy deficit and the additional maxima observed by Kassal and Fishburne (93).

In the calculation of rotational distributions of product diatomic species the severe restrictions imposed due to angular momentum conservation are very evident. In the cases examined the overall energy defects (including internal, translational, and exothermicity) were small, and

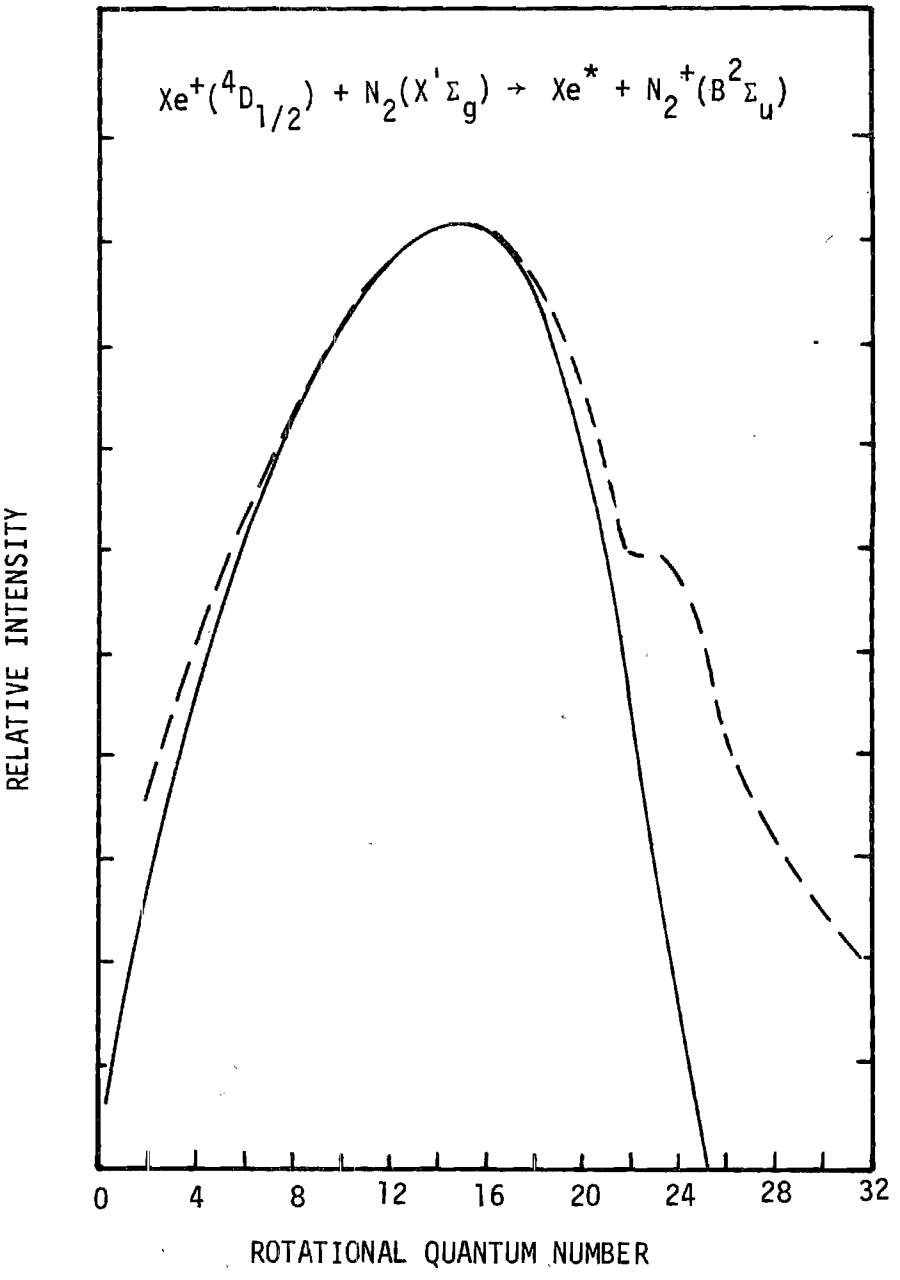

Figure 37. Relative Rotational Intensity of $N_2^+(B^2\Sigma_u)$ Formed by $Xe^{+*} + N_2$. (The solid line is the calculated intensity, and the dashed line is the observed intensity taken from Ref. 93.)

we obtained good agreement with experimentally observed product internal energy distributions. In its basic form the phase space model gives good results when used to predict relative internal energy distributions of ion-molecule reactions.

In some cases, however, conservation of energy and angular momentum, while being necessary conditions, are not sufficient to describe the interaction. To provide a tractable model, in addition to conservation of energy and angular momentum, other quantities, such as spin, must be conserved. In other cases spin conservation will not explain the process. In the following chapter we examine the $He^+ + N_2$ reaction in an effort to provide the additional *a priori* information that $N_2^+(C^2\Sigma_u)$ is the preferred electronic state of the product.

CHAPTER VII

FURTHER CONSIDERATIONS OF THE $He^+ + N_2$ REACTION

Two main problems were noted in our adaptation of the statistical phase space model. One problem arises when the most energetically favored product channel is not observed experimentally. In Chapter III we made the assumption based on experimental evidence that $N_2^+(C^2\Sigma_u)$ is the dominant product electronic state formed in charge transfer reactions of He^+ with N_2. In Chapter V in order to achieve an adequate description of the reactions of C^+ with O_2 and N_2, it was necessary to consider conservation of spin in addition to conservation of energy and angular momentum. Kaufman and Koski (98) have argued that it is necessary to consider conservation of spin in formation of the complex in addition to conservation of spin in going from reactants to products.

For a detailed study of the collision problem it is necessary to have an accurate potential energy surface with which the various reactant and product electronic states can be correlated. This approach has been used successfully to describe the reaction $O^+ + N_2 \rightarrow NO^+ + N$. This reaction is exothermic by 6.7 eV, and NO^+ production would be expected to have a variation with energy similar to that given by the Langevin expression where the cross section decreases with

increasing energy (see the phase space calculation of Wolf (8)). However, experimental results in the energy range 1-30 eV show the cross section rising with energy and going through a broad maximum at 10 eV (99). In the thermal energy range it was found that the rate of reaction increased rapidly with N_2 vibrational temperature (36). Kaufman and Koski (98) have calculated a potential energy surface for the N_2O^+ complex and, by correlating the electronic states of the complex with separated particle electronic states, show that a minimum reaction energy (or activation energy) of about 0.9 eV is required for the reaction to occur. This is consistent with experimental observations (36,99). This approach is often difficult because good molecular wave functions and electron configurations are not always available. In the next section we consider the $He^+ + N_2$ reaction and give a qualitative proof that $N_2^+(C^2\Sigma_u)$ is the preferred product electronic state using correlation considerations.

The ion-induced dipole potential is not adequate to describe the interactions between ions and molecules above several electron volts. At higher energies calculated cross sections decrease faster than experimentally measured cross sections. We will consider a potential description that is more suitable over a wider energy range. The potential we consider includes long range dispersion forces and short range repulsive forces in addition to the ion-induced dipole potential considered previously.

Correlation Considerations for the $He^+ + N_2$ Interaction

Wigner and Witmer (27,100,101) have derived rules for determining the molecular states that result from given states of the separated atoms and/or molecules. These correlation rules have been derived under the assumption of an adiabatic change of internuclear distance. When two species with orbital angular momentum $\vec{L}$ and spin angular momentum $\vec{S}$ are brought together, the resultant angular momentum about the line connecting the nuclei is given by

$$\Lambda = |M_{L_1} + M_{L_2}| \tag{88}$$

where M_L is the magnetic quantum number corresponding to orbital angular momentum $\vec{L}$. In addition we must have for the total spin in the molecule

$$\vec{S} = \vec{S}_1 + \vec{S}_2 \tag{89}$$

where $\vec{S}_1$ and $\vec{S}_2$ are the spins of the separated species.

For the reaction

$$He^+(^2S) + N_2(X^1\Sigma_g) \rightarrow HeN_2^+ \tag{90}$$

Eqs. (88) and (89) give that the state of HeN_2^+ must be $^2\Sigma$. For the decomposition of HeN_2^+,

$$HeN_2^+(^2\Sigma) \rightarrow He(^1S) + N_2^+, \tag{91}$$

the above considerations give that the N_2^+ product state

must be $^2\Sigma$.

In Table 4 we give the electron configuration for $N_2(X^1\Sigma_g)$ and the more important N_2^+ electronic states (46,47). Herzberg (100,101) has argued that electronic states of triatomic molecules can be obtained by consideration of the corresponding states of the united atom or molecule. In Table 5 the expected electron configurations for the lowest states of HeN_2^+ are shown. The ground state of HeN_2^+ is expected to be the $^2\Pi$ electronic state (100), which is the lowest state of the united molecule NO. The other electron configurations shown in Table 5 are some of the lower excited state configurations of NO (46). In Tables 4 and 5 only the valence electrons are shown.

Since the complex formed between He^+ and N_2 must have the designation $^2\Sigma$, the corresponding electron configuration for the reactant intermediate would be $\sigma^2\sigma^2\sigma^2\pi^3\pi^1\sigma^1$. Since the neutral decomposition product is $He(^1S)$, it is reasonable to assume that He removes a pair of σ electrons. This leaves an electron configuration for N_2^+ of $\sigma^2\sigma^2\pi^3\pi^1\sigma^1$. This electron configuration corresponds to $N_2^+(C^2\Sigma_u)$ and suggests that the C state would be the dominant charge transfer product state. However, due to strong interactions between the C state and the B state of N_2^+ (43), some ambiguity exists as to the exact electronic distribution at large internuclear separation (46); and it is not surprising that a certain fraction of the charge transfer also forms $N_2^+(B^2\Sigma_u)$.

Table 4: Electron Configurations of Nitrogen
(only valence shell electrons are given)

Molecule	State	Electron Configuration
N_2	$X^1\Sigma_g$	$(2\sigma_g)^2(2\sigma_u)^2(1\pi_u)^4(3\sigma_g)^2$
N_2^+	$X^2\Sigma_u$	$(2\sigma_g)^2(2\sigma_u)^2(1\pi_u)^4(3\sigma_g)^1$
	$A^2\Pi_u$	$(2\sigma_g)^2(2\sigma_u)^2(1\pi_u)^3(3\sigma_g)^2$
	$B^2\Sigma_u$	$(2\sigma_g)^2(2\sigma_u)^1(1\pi_u)^4(3\sigma_g)^2$
	$C^2\Sigma_u$	$(2\sigma_g)^2(2\sigma_u)^2(1\pi_u)^3(3\sigma_g)^1(1\pi_g)^1$
	$D^2\Pi_u$	$(2\sigma_g)^2(2\sigma_u)^2(1\pi_u)^2(3\sigma_g)^2(1\pi_g)^1$

Table 5: Electron Configurations of HeN_2^+
(only valence shell electrons are given)

State	Electron Configuration
$^2\Pi$	$\sigma^2\sigma^2\sigma^2\pi^4\pi^1$
$^4\Pi, ^2\Pi$	$\sigma^2\sigma^2\sigma^2\pi^3\pi^2$
$^2\Sigma, ^4\Sigma, ^2\Delta, ^4\Delta$	$\sigma^2\sigma^2\sigma^2\pi^3\pi^1\sigma^1$
$^2\Sigma, ^4\Sigma, ^2\Delta, ^4\Delta$	$\sigma^2\sigma^2\sigma^1\pi^4\pi^2$
$^2\Sigma$	$\sigma^2\sigma^2\sigma^2\pi^4\pi^1$

Evidence of this was given in Chapter III.

Although this proof is only qualitative, it does suggest a reasonable method of analyzing ion-molecule interactions where certain anomalies exist. As more accurate wave functions are obtained, better potential energy surfaces will be obtained which will allow a more thorough description of the collision process.

Consideration of Dispersion and Short Range Forces in the Phase Space Model

The problem of calculating the interaction energy between two species reduces in principle to a solution of the Schrödinger equation using a Hamiltonian, which consists of the sum of the Hamiltonians for the isolated species, plus the coulomb interactions between all charges in specie 1 and those in specie 2. The accurate evaluation of an intermolecular potential is essential for a detailed understanding of energy transfer in molecular collisions (102). The usage of a potential energy surface is twofold. First, it can serve to visualize what happens in an atomic or molecular process. Secondly, it can be used as input data in a theory of the collision process. However, calculations of accurate potential energy surfaces are very limited due to consideration of the coulombic interactions, which manifest themselves at intermediate internuclear distance. Intermolecular forces at large internuclear separation have been considered in

some detail (103-107) and various treatments presented.

The long range behavior for the interaction of an ion and a neutral specie may be given as (104)

$$V(r,\theta) = v_{elec} + v_{ind} + v_{disp}. \tag{92}$$

The interaction potential given by Eq. (92) represents the electric interaction between the two species. The electrostatic energy represents the interaction energy determined by the permanent electric moments of the species and is given by (107)

$$v_{elec} = r^{-3} q \Theta_n P_2(\cos\theta). \tag{93}$$

Θ_n is the quadrapole moment of the neutral particle, q is the charge on the ion, and θ the angle of inclination of the diatomic specie relative to the trajectory of the free particle. The permanent moments producing a distortion of the electronic structure in neighboring molecules gives the induction energy (107),

$$v_{ind} = -r^{-4} q^2 \left[\tfrac{1}{2}\alpha_n + \tfrac{1}{3}(\alpha_{\parallel} - \alpha_{\perp})_n P_2(\cos\theta)\right], \tag{94}$$

where α_n, $\alpha_{\parallel}$, and $\alpha_{\perp}$ are the polarizabilities of the neutral particles. The London dispersion energy represents the interaction between the two induced charge distributions and is given as (103,107)

$$v_{disp} = -r^{-6}\left[3 I_i \alpha_i I_n \{\alpha_n + \tfrac{1}{3}(\alpha_{\parallel} - \alpha_{\perp})_n P_2(\cos\theta)\}/\ 2(I_i + I_n\right], \tag{95}$$

where I_i and I_n are the ionization energies of the ion and neutral species, respectively, and α_i is the polarizability of the ion. The potential given by Eq. (92) was obtained from perturbation theory (104,107) and has been shown (108) to give a good representation of the accurate Hartree-Fock *ab initio* calculation for the reaction of $Li^+ + H_2$ at large internuclear separation.

In addition to the potential given in Eq. (92) we consider a short range repulsive potential of the form

$$v(12) = d\, r^{-12}. \tag{96}$$

In Figs. 38, 39, and 40 we present the potential for the interactions of $He^+ + N_2$ and $He + N_2^+$ for 0°, 45°, and 90° collisions. The data for the potential given by Eq. (92) are presented in Table 6. The polarizability of He^+ was estimated from the relation (104)

$$\alpha = n^4 a_o^3/4Z^4. \tag{97}$$

Z is the nuclear charge, n is the principle quantum number, and a_o is one Bohr radius.

To estimate the values for d in Eq. (96) we have calculated the energy dependence of He - N_2 distance for the HeN_2^+ complex using the semiempirical LCAO-SCF-INDO method developed by Pople et al. (112). Ref. (113) gives the details of the calculation. There are serious deficiencies in this method. One inadequacy noted is that the method

Table 6: Potential Parameters for He, N_2, and the Corresponding Ions (References are given in parenthesis)

	He	He^+	N_2	N_2^+
Θ	0.0		-1.52×10^{-10} esuÅ^2 *(109)*	
α	0.205Å^3 *(110)*	0.037Å^3	1.76Å^3 *(104)*	1.76Å^3
$\alpha_{\parallel}$			2.38Å^3 *(104)*	
$\alpha_{\perp}$			1.45Å^3 *(104)*	
I	24.580eV *(96)*	54.403eV *(96)*	23.575eV *(111)*	19.925eV *(111)*

Table 7: *v(12)* Parameters for He - N_2 Interactions (in eV Å^{12})

	0°	45°	90°
$He^+ + N_2$	1537.87	283.89	17.059
$He + N_2^+$	1120.77	469.48	201.07

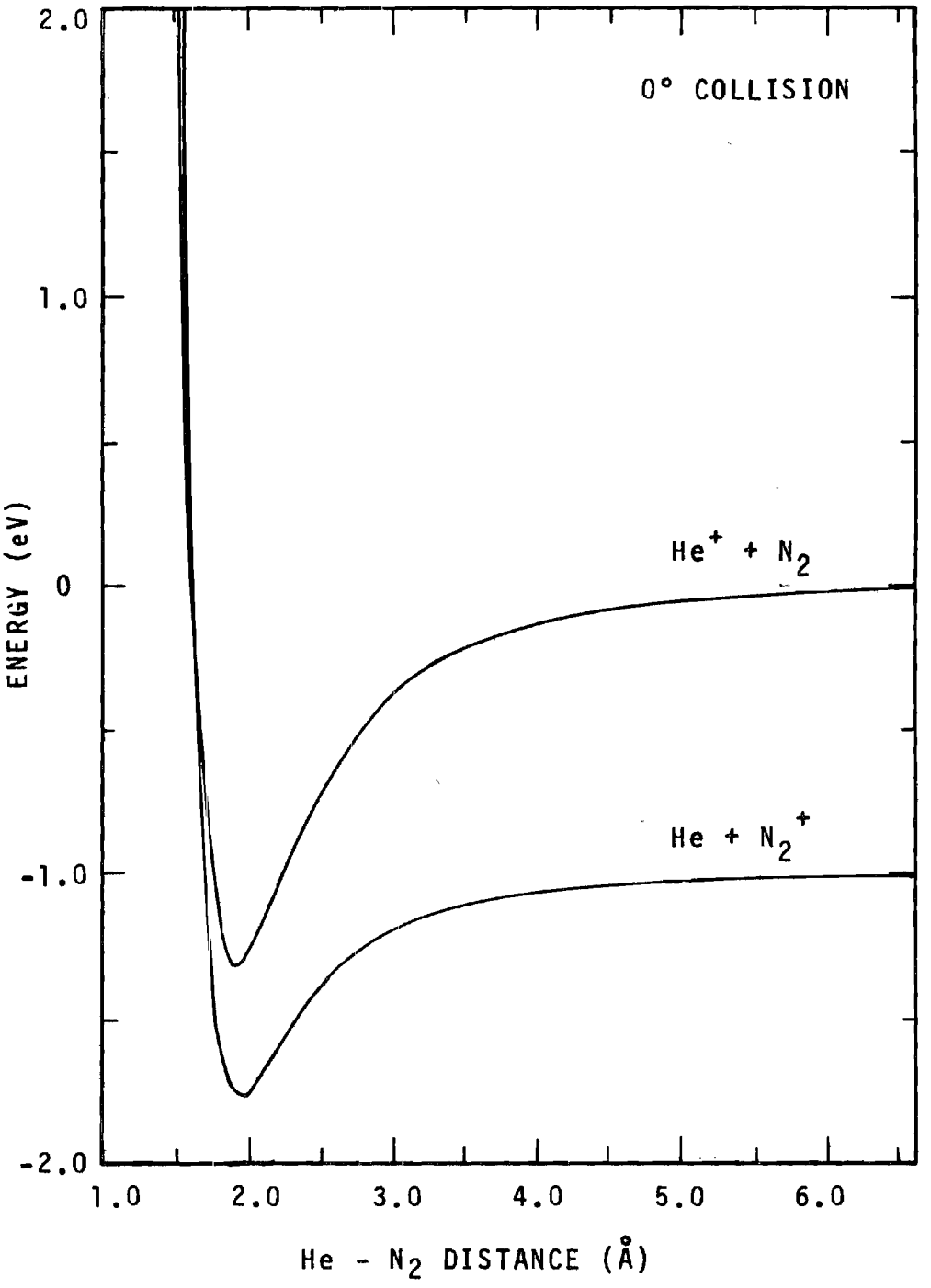

Figure 38. Interaction Potentials for $He^+ + N_2$ and $He + N_2^+$: 0° Collision.

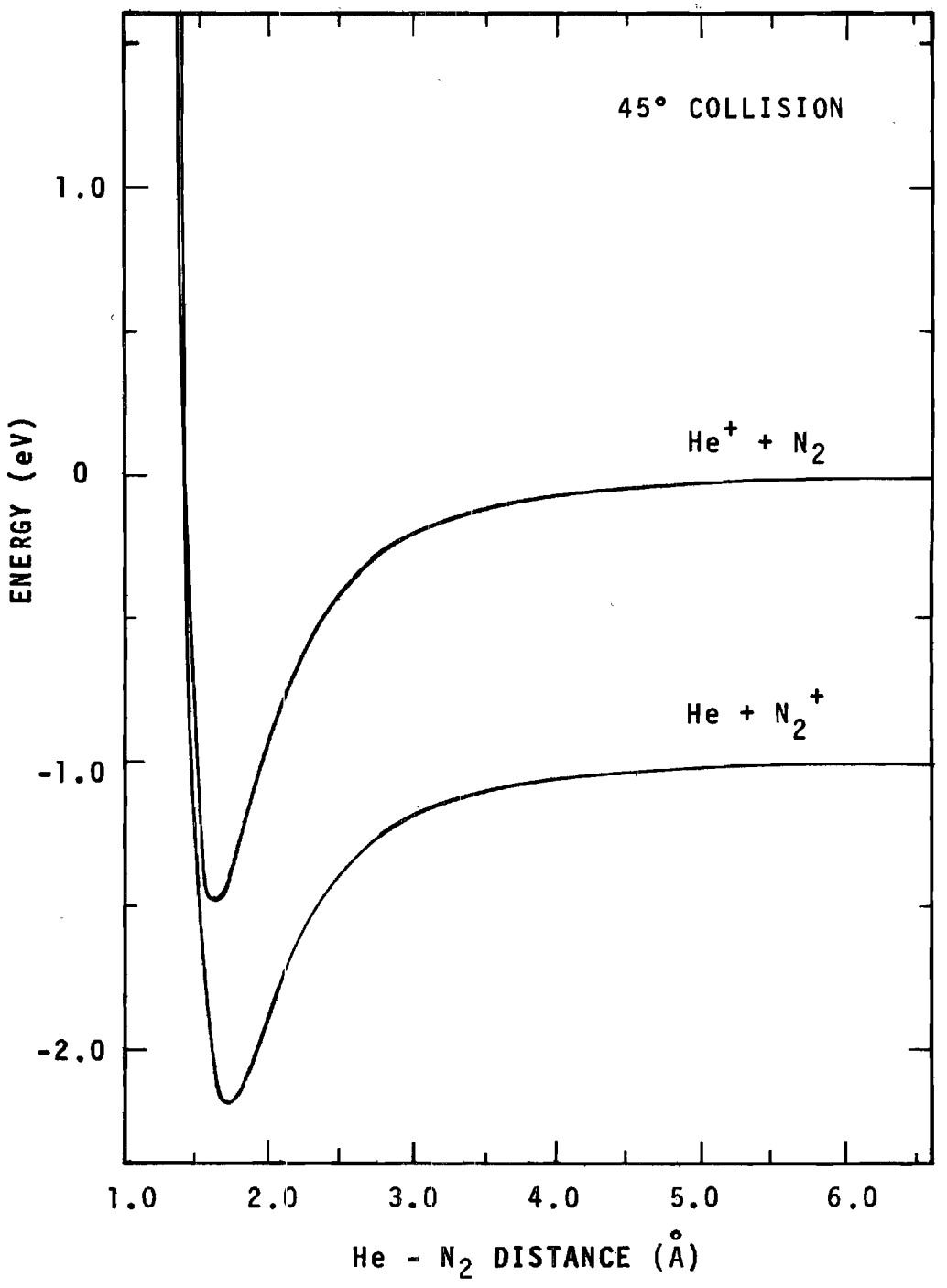

Figure 39. Interaction Potentials for $He^+ + N_2$ and $He + N_2^+$: 45° Collision.

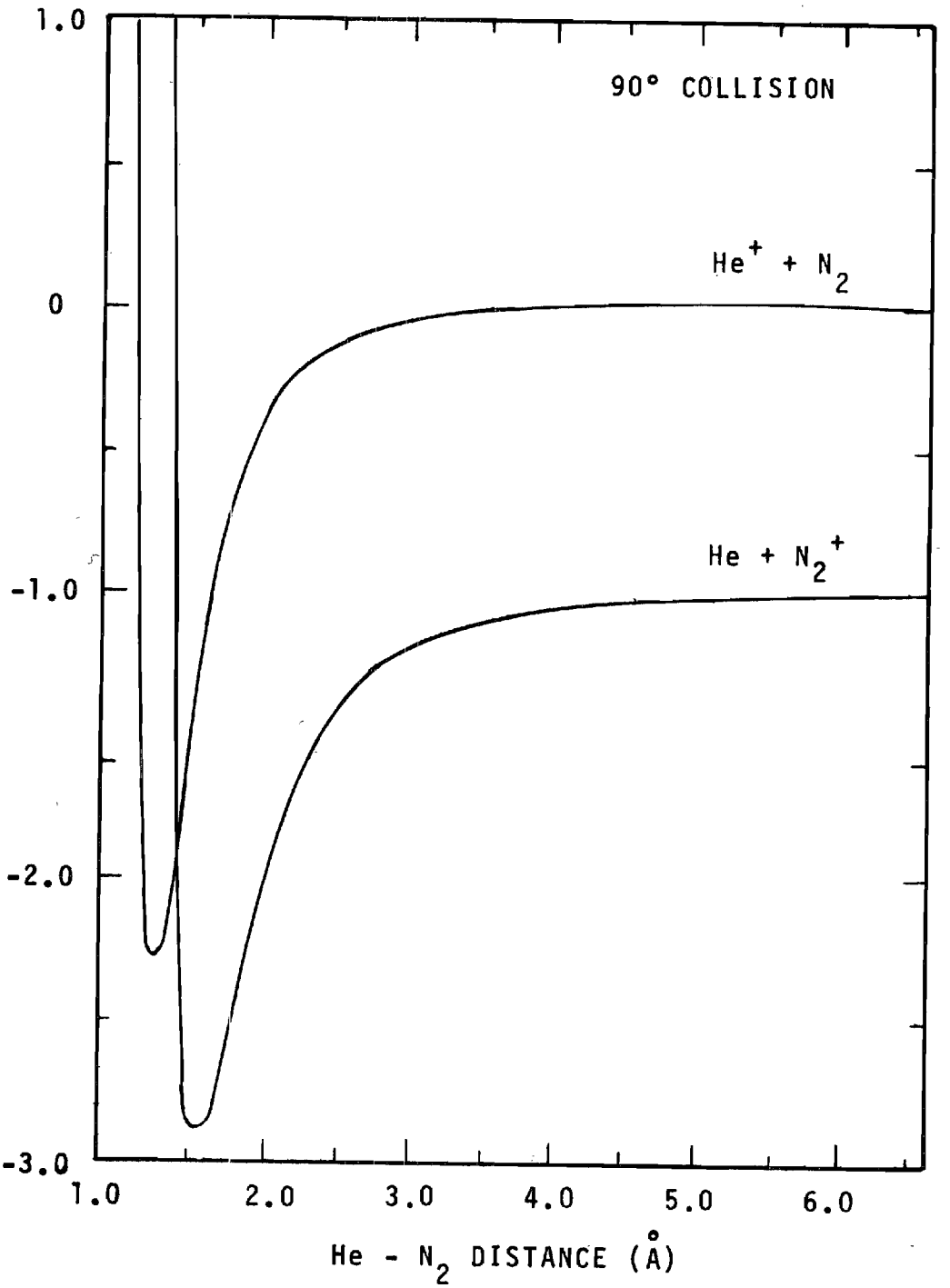

Figure 40. Interaction Potentials for $He^+ + N_2$ and $He + N_2^+$: 90° Collision.

does not give the correct ordering of molecular orbitals (114). Also, the INDO method is not adequate for excited state calculations of molecules and ions (115). However, it does give good representations of molecular geometries and relative energies (112). Therefore, the energies determined for small He - N_2 distances should be reasonably accurate and give a good representation of the repulsive barrier. The calculations indicate that HeN_2^+ should be linear in accord with the predictions made on the basis of Walsh's rules (116) indicating a collinear collision would be preferred. The values of d were estimated from the slope of the repulsive portion of the curve calculated from the INDO method. By requiring the potential given by Eqs. (92) and (96) to have the same slope as that computed by the INDO method for the repulsive curve at a given He - N_2 distance, we obtained the estimated values of d given in Table 7 for 0°, 45°, and 90° collisions.

The potential calculated using Eqs. (92) and (96) is shown in Figs. 38, 39, and 40 and shows the 90° approach having the deepest well, but there is a small repulsive barrier at large internuclear distance. Also, the species involved in the collision would have to penetrate the electron clouds of each other in order to interact intimately. At intermediate distances the electron clouds of the interacting particles overlap, and the energy due to chemical bonding forces is not included in the potential. However, the short range

repulsive forces and long range attractive forces are adequately represented, and the detailed features of the potential near the minimum are not necessary in the phase space model. Figs. 38, 39, and 40 show the He + N_2^+ potential curve located at 1.005 eV below the He^+ + N_2 curve. This difference corresponds to the exothermicity of the charge transfer process.

The effective potential, V_{eff}, is the apparent potential energy governing the relative motion of the particles and is composed of the static potential given by Eqs. (92) and (96) plus the centrifugal energy of the molecule (106). The effective potential is given by

$$V_{eff} = L^2/2\mu r^2 + a/r^3 - b/r^4 - c/r^6 + d/r^{12} \qquad (98)$$

where a, b, and c are defined by Eqs. (93), (94), and (95) respectively. We have incorporated this potential into the phase space model.

The potential given by Eq. (98) will pass through a maximum at some distance r_*. At the maximum we have $dV/dr = 0$. The orbital angular momentum at the maximum is then given by

$$L^2(r_*) = \mu[-3a/r_* + b/r_*^2 + 2c/r_*^4 - 12d/r_*^{10}], \qquad (99)$$

which gives for the potential at its maximum

$$V(r_*) = -a/2r_*^3 + b/r_*^4 + 2c/r_*^6 - 5d/r_*^{12}. \qquad (100)$$

In order to calculate the angular momentum of the complex, we must first determine r_*. For complex formation the initial translational energy must be greater than the potential at the maximum. Therefore, the minimum translational energy for complex formation is

$$E_{trans}(min) = -a/2r_*^3 + b/r_*^4 + 2c/r_*^6 - 5d/r_*^{12}. \quad (101)$$

Setting the initial translational energy equal to $V(r_*)$ will uniquely define r_* and $L^2(r_*)$. However, for $E_{trans}>V(r_*)$ we may have $r_*<r_m$, where r_m is the distance of closest approach for a given impact parameter. The distance of closest approach is given by (117)

$$dr/d\phi = \pm(r^2/b^2)\ [1 - V(r)/E_{trans} - b^2/r^2]. \quad (102)$$

At $r = r_m$ the classical turning point is reached, and $dr/d\phi = 0$. Thus, we have

$$1 - V(r_m)/E_{trans} - b^2/r_m^2 = 0. \quad (103)$$

We can write $L = \mu v b$, and from Eqs. (99) and (103) obtain the angular momentum of the complex for a given initial kinetic energy;

$$L^2 = L^2(r_*), \qquad r_*>r_m; \quad (104a)$$

$$L^2 = 2\mu r_m^2\ [E_{trans} - V(r_m)], \qquad r_*<r_m. \quad (104b)$$

To determine r_m we set the initial translational energy equal to the static potential which uniquely defines r_m.

From Eq. (104) we find the maximum impact parameter and the maximum cross section for complex formation given as

$$b_{max} = L/(2\mu E_{trans})^{1/2}; \tag{105}$$

$$\sigma_{max} = L^2/(2\mu E_{trans}). \tag{106}$$

We assume that the total angular momentum of the complex is equal to the initial orbital angular momentum given by Eq. (104). In order that we have product separation, the final translational energy, E_f, must be greater than the value of the potential evaluated at the maximum. E_f is given by

$$E_f = \varepsilon(1 - M^2/2I\varepsilon) \geq V(r_*); \tag{107}$$

and we have

$$\varepsilon(1 - M^2/2I\varepsilon) \geq -a/2r_*^3 + b/r_*^4 + 2c/r_*^6 - 5d/r_*^{12}. \tag{108}$$

To evaluate r_* for product separation, we set an upper bound on M^2. We must have $M^2 \leq 2I\varepsilon$ and $M^2 < K^2$. Whichever of these conditions is the more restrictive will impose an upper bound on M^2, and will define the maximum value of r_* from Eq. (108). From Eqs. (99), (107), and (108) the upper bound on orbital angular momentum is given by

$$L^2 < 2\mu r_*^2 \left[\varepsilon(1-M^2/2I\varepsilon) - a/r_*^3 + b/r_*^4 + c/r_*^6 - d/r_*^{12}\right]. \tag{109}$$

However, r_* cannot be less than r_m determined for the

reactant system. If r_* calculated from Eq. (108) is less than r_m, we set $r_* = r_m$. If we define

$$F(r_*) = 2\mu r_*^2 \left[\varepsilon - a/r_*^3 + b/r_*^4 + c/r_*^6 - d/r_*^{12}\right], \quad (110)$$

Eq. (109) is written as

$$L^2 \leq -\mu r_*^2 M^2/I = F(r_*). \quad (111)$$

From conservation of angular momentum, $K^2 + M^2 - 2KM_z = L^2$, the upper bound on M_z is found to be

$$M_z \geq \left[K^2 + (1 + \mu r_*^2/I)M^2 - F(r_*)\right]/2K. \quad (112)$$

To obtain the limits of integration for the phase space volume element given by Eq. (38), we need to find the roots of the equation

$$(K - M)^2 + 2\mu r_*^2 M^2/I - F(r_*) = 0. \quad (113)$$

The roots are

$$M_\pm = \frac{K \pm \sqrt{F(r_*) + (2\mu r_*^2/I)\left[F(r_*) - K^2\right]}}{(2\mu r_*^2/I + 1)}. \quad (114)$$

The phase space integral is

$$\Gamma = \int_{\phi_2}^{M_+} \int_{\phi_1}^{M} \left[1 + (M/K)^2 - 2M_z/K\right]^{-1/2} dM_z dM, \quad (115)$$

and the limits of integration are

$$\phi_1 = \begin{cases} -M, & M < |M|; \\ \text{Eq. (112)}, & M > |M|; \end{cases}$$

$$\phi_2 = M_- H(M_-);$$

where M_+ and M_- are the roots given by Eq. (114). Applying these limits, the phase space volume element is

$$\Gamma = \int_{|M_-|}^{M_+} [F(r_*) - \mu r_*^2 M^2/2I]^{1/2} dM +$$

$$[K|M_-| + \tfrac{1}{2}M_-^2]H(-M_-) + [\tfrac{1}{2}M_+^2 - KM_+]\, S(K-M_+) +$$

$$[K|M_-| - \tfrac{1}{2}M_-^2]H(M_-)\, S(K-M_-) - K^2\, H(M_+ - K)\, H(K-M_-) \quad (116)$$

Eq. (116) reduces to Eq. (47) obtained previously if we consider only the inductive portion of the potential. Since Eq. (115) contains the phase space available for dissociation, we must then apply Eq. (40), (48), and (49) to obtain the desired phase space elements and the corresponding probabilities. The cross section for a given channel is then given by

$$\sigma = 2\pi \int_0^{b_{max}} P\, b\, db \quad (117)$$

where P is the probability for formation of the channel and b_{max} is given by Eq. (105).

Fig. 41 shows the total cross sections for the reaction between He^+ and N_2. The dashed line is the total cross section calculated using the ion-induced dipole potential only. The dot-dash curves are the total cross sections calculated using Eqs. (104) and (106). Results are presented for 0°, 45°, and 90° collisions. The solid curve is the average of the three total cross sections. At low ion

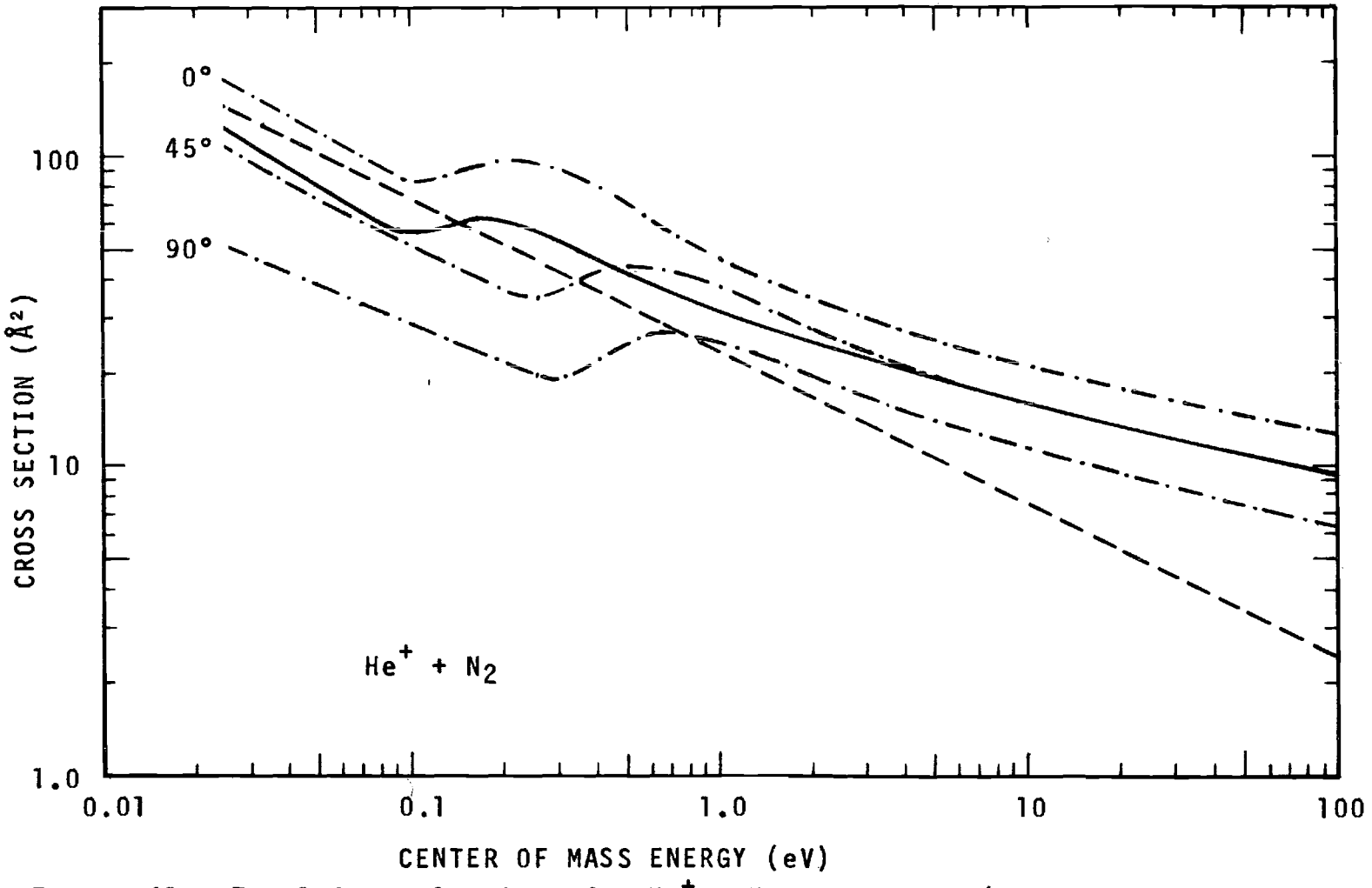

Figure 41. Total Cross Sections for $He^+ + N_2$ Reaction. (The dashed line is calculated from the ion-induced dipole potential. The solid line is the average of the curves calculated at the various collision angles.)

kinetic energies the cross sections behave substantially the same as the cross section computed using the ion-induced dipole potential. At approximately 0.1 eV center of mass kinetic energy the cross section rises and then decreases with ion kinetic energy. This is approximately the energy at which r_* becomes less than r_m. Above this energy the total cross section and the partial cross sections are higher than those calculated using only the ion-induced dipole potential. This is due mainly to inclusion of short range repulsion forces. The use of the more accurate potential will not substantially alter the relative magnitudes for production of a given product state. The partial cross sections computed using the potential given by Eq. (98) will not decrease as rapidly with increasing kinetic energy as those calculated considering the inductive portion of the potential only.

Figs. 42 and 43 show the cross sections for the formation of N_2^+ and N^+ computed using the phase space model. The dashed line is calculated using the inductive portion of the potential (see Figs. 4 and 5). The solid curves are those computed using the potential given by Eq. (98) and are averages of the cross sections calculated for 0°, 45°, and 90° collisions. In Chapter III we discussed the predissociation mechanism of $N_2^+(C^2\Sigma_u)$ to form N^+. The N^+ curve presented in Fig. 43 was computed by taking all $N_2^+(C^2\Sigma_u)$ ions in the $v = 2$ state and one-half of the ions in the

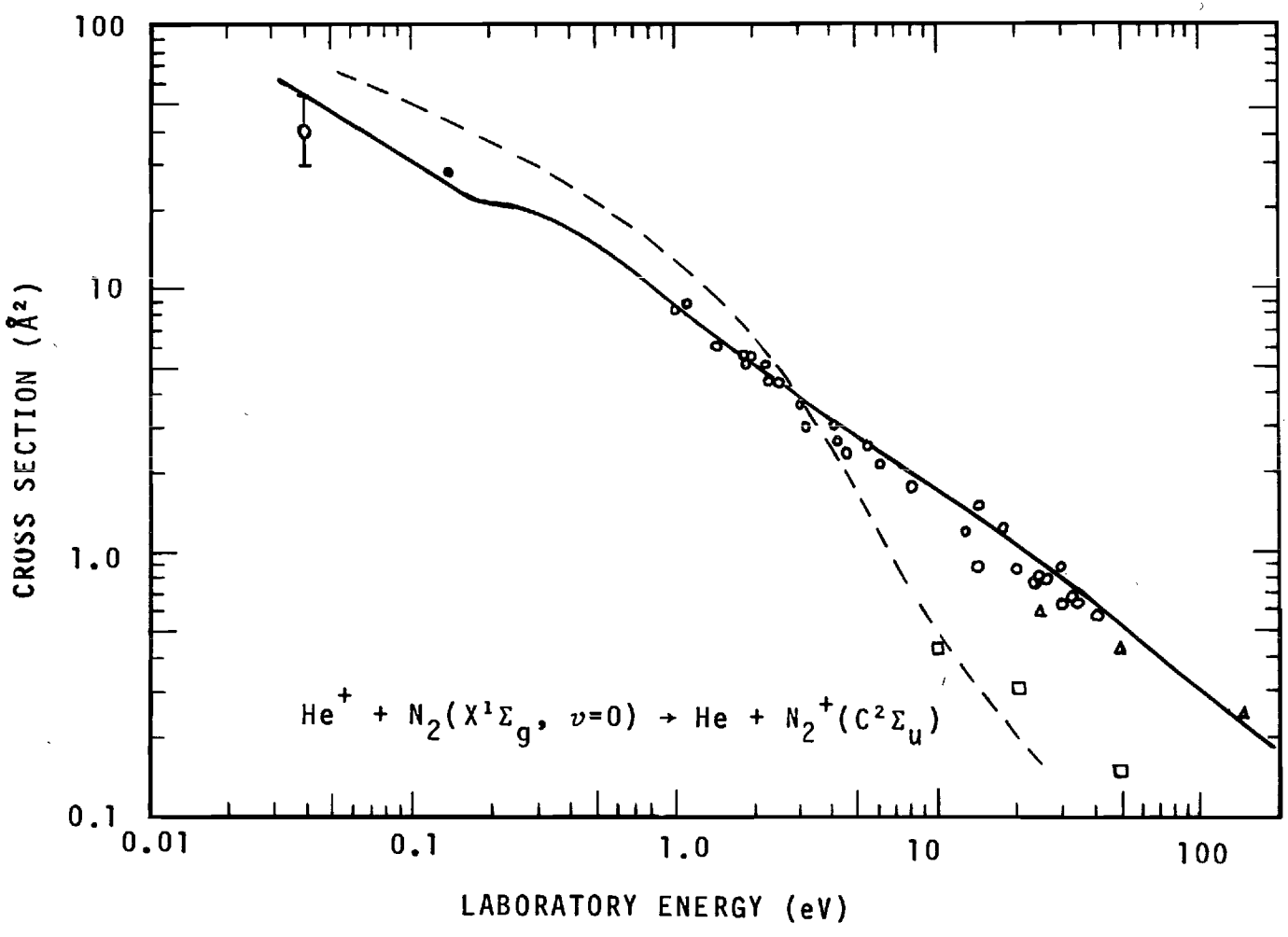

Figure 42. Cross Section for Formation of $N_2^+(C^2\Sigma_u)$ as a Function of He^+ Kinetic Energy. (The data points are from Ref. (28) O ; Ref. (40) □ ; Ref. (39) △ ; Ref. (32) ● ; Ref. (29-36) I represents the average of the thermal data.)

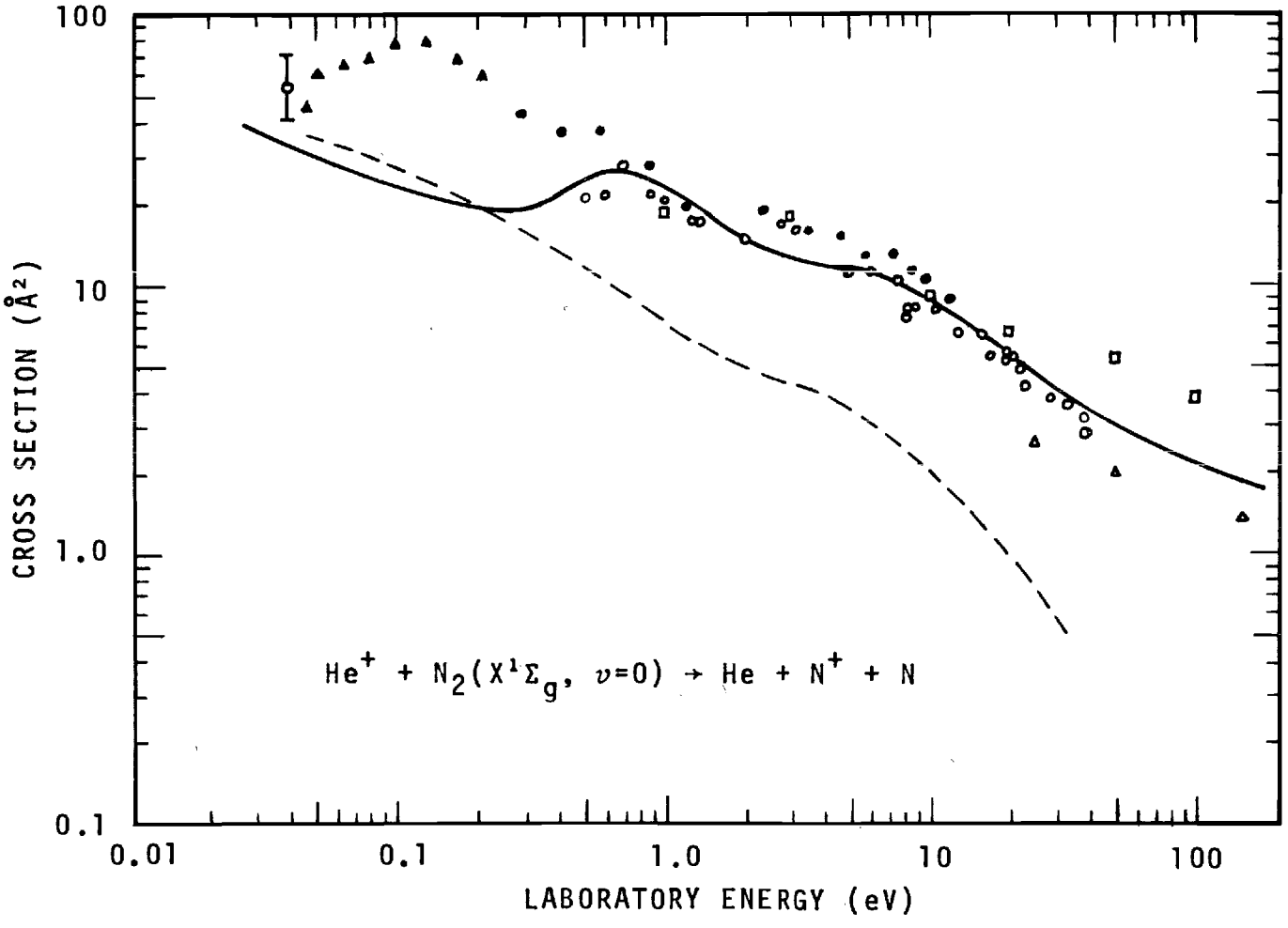

Figure 43. Cross Section for Formation of N^+ as a Function of He^+ Kinetic Energy. (The data points are: Ref. (28) ○ ; Ref. (41) ● ; Ref. (40) □ ; Ref. (39) △ ; Ref. (42) ▲ ; Ref. (29-36) represents the average of the thermal data.)

$v = 3$, 4, 5, and 6 levels to predissociate giving N^+. Also included in the curve is N^+ produced from direct dissociation of $N_2^+(C^2\Sigma_u)$. The N_2^+ curve presented in Fig. 42 is the cross section calculated with the predissociating states removed. Also shown in the figures are experimentally determined cross sections.

Agreement between experimentally determined cross sections and cross sections computed from the phase space model is substantially improved by including a more accurate potential. At energies above 1.0 eV inclusion of the repulsive portion of the potential is necessary to adequately describe the interaction.

CHAPTER VIII

CONCLUSIONS

The phase space model assumes that a collision complex is formed in the reaction between an ion projectile and a neutral target. The decomposition of the complex into the various reaction channels is governed only by conservation of total energy and total angular momentum. For large separation of the particles the potential energy surfaces are dominated by the strong polarization forces, whose potential decreases as the inverse fourth power of the separation. At small particle separations the nuclei are regarded as moving adiabatically on a many-dimensional potential energy surface. The statistical assumption avoids the calculation of the adiabatic potential energy surface.

Avoidance of the details of the potential poses a severe deficiency of the statistical assumption. The statistical assumption describes a chemical process as a transition from the potential energy surface of the reactants to that of the complex. The various states of the complex are populated statistically and decompose to all available product states. In chemical processes where an electronic transition occurs, the statistical assumption may not be valid. By using experimental or theoretical evidence to

determine accessible product states, additional details describing the interaction are provided; and qualitative agreement between computed and experimentally determined cross sections is obtained.

Dissociative processes are generally well described using the statistical approach. The phase space treatment of the dissociative processes presented in this work is different from the treatments used previously. Previous treatments have taken the difference between the reactive channels and the total cross section as the cross section for dissociation. The treatment presented in this work allows separation of collision induced dissociation and dissociative charge transfer processes resulting from the same interaction. Also, dissociation of heteronuclear diatomic ion to give different product states can be investigated. The energy dependence of cross sections, thresholds and relative magnitudes of the dissociative channels are well described using the statistical model.

Internal energy distributions of diatomic ions produced in charge transfer processes are well represented by the statistical model. Since there are more states available to form a lower vibrational state than to form a higher state, the vibrational population of reaction products decreases monotonically with increasing vibrational state. Evidence cited indicates that this is observed experimentally. The rotational population within a given vibrational

state increases with rotational quantum number, goes through a maximum, and then decreases according to conservation of angular momentum. These predictions are in accord with observed relative radiative intensities.

APPENDIX A

ATOMIC AND MOLECULAR PARAMETERS

Table A1: Spectroscopic Constants of Diatomic Molecules and Ions[a]

Molecule	$\omega_e (cm^{-1})$	$\omega_e x_e (cm^{-1})$	$r_e (\mathring{A})$	$D_o (eV)$	Recombination Energy (eV)
$N_2(X^1\Sigma_g)$	2358.07	14.19	1.0976	9.756	
$N_2^+(X^2\Sigma_g)$	2207.19	16.14	1.118	8.724	15.576
$N_2^+(A^2\pi_u)$	1902.84	14.91	1.177	7.607	16.693
$N_2^+(B^2\Sigma_u)$	2419.84	23.19	1.078	5.555	18.745
$N_2^+(C^2\Sigma_u)$	2061.	11.	1.262	3.105	23.575
$O_2(X^3\Sigma_g)$	1580.4	12.1	1.2074	5.12	
$O_2^+(X^2\pi g)$	1876.4	16.5	1.1227	6.48	12.06
$O_2^+(a^4\pi_u)$	1035.7	10.4	1.3813	2.53	16.02
$O_2^+(A^2\pi_u)$	900.	13.4	1.4089	1.76	16.79
$O_2^+(b^4\Sigma_g)$	1196.8	17.9	1.2795	2.43	18.04
$NO(X^2\pi)$	1904.0	13.9	1.1508	6.51	
$NO^+(X^1\Sigma)$	2377.1	16.3	1.0619	10.84	9.27
$NO^+(^3\Delta)$	1600.	15.5	1.225	4.14	16.86
$NO^+(A^1\pi)$	1608.9	23.3	1.1926	2.60	18.33
$CO(X^1\Sigma)$	2170.21	13.461	1.1282	11.091	

Table A1: (Continued)

Molecule	$\omega_e (cm^{-1})$	$\omega_e x_e (cm^{-1})$	$r_e (\mathring{A})$	$D_o (eV)$	Recombination Energy (eV)
$CO^+(X^2\Sigma)$	2214.24	15.164	1.1151	8.345	14.009
$CO^+(A^2\pi)$	1562.06	13.532	1.2437	5.815	16.538
$CN(X^2\pi)$	2068.71	13.144	1.1718	8.48	
$CN^+(^3\pi)$	1641	16.45	1.3117	5.068	14.66

a. N_2 data are taken from Ref. (47); $NO^+(^3\Delta)$ parameters and estimates, and the other data from Ref. (27).

Table A2: Rotational Constants of Diatomic Molecules and Ions (Ref. 27)

Molecule	$B_e(cm^{-1})$	$\alpha_e(cm^{-1})$
$O_2(X^3\Sigma_g)$	1.4457	0.01579
$O_2^+(X^2\pi_g)$	1.6722	0.01984
$O_2^+(a^4\pi_u)$	1.1047	0.01575
$O_2^+(A^2\pi_u)$	1.0617	0.1906
$O_2^+(b^4\Sigma_g)$	1.2873	0.02206
$N_2(X^1\Sigma_g)$	2.010	0.0187
$N_2^+(X^2\Sigma_g)$	1.9322	0.0202
$N_2^+(A^2\pi_u)$	1.740	0.018
$N_2^+(B^2\Sigma_u)$	2.083	0.195
$N_2^+(C^2\Sigma_u)$	1.65	0.05

Table A3: Polarizabilities of Diatomic Molecules (Ref. 104)

Molecule	Polarizability ($\AA^3$)
N_2	1.76
O_2	1.60
NO	1.69
CO	1.95
CN	1.77

Table A4: Atomic Parameters

Atomic State	Polarizability[a] ($Å^3$)	Ionization Energy[b] (eV)	Ion State
$C(^3P)$	2.1	11.264	$C^+(^2P)$
		16.595	$C^+(^4P)$
$N(^4S)$	1.13	14.545	$N^+(^3P)$
$N(^2D)$	1.13	12.162	$N^+(^3P)$
$O(^3P)$	0.77	13.614	$O^+(^4S)$
$He(^1S)$	0.205	24.580	$He^+(^2S_{1/2})$
$Ne(^1S)$	0.395	21.559	$Ne^+(^2P_{3/2})$
		21.656	$Ne^+(^2P_{1/2})$
$Ar(^1S)$	1.64	15.755	$Ar^+(^2P_{3/2})$
		15.933	$Ar^+(^2P_{1/2})$
$Kr(^1S)$	2.48	13.996	$Kr^+(^2P_{3/2})$
		14.662	$Kr^+(^2P_{1/2})$

a. Ref. 110, *b*. Ref. 96

APPENDIX B

DESCRIPTION OF THE COMPUTER CALCULATION

The phase space integral, Eq. (38) can be written as

$$\Gamma/A = \int_{\phi_2}^{X_2}\int_{\phi_1}^{X} [1 + (X/Z)^2 - 2X_z/Z]^{-1/2} dX dX_z, \qquad (B1)$$

where

$$A = 2I\epsilon$$

$$X^2 = M^2/A$$

$$Z^2 = K^2/A$$

$$\phi_1 = \begin{cases} -X, & X < |X_1| \\ [Z^2 + X^2 - C(1 - X^2)^{1/2}]/2Z, & X > |X_1| \end{cases}$$

$$\phi_2 = |X_1| H(X_1)$$

$$C = 2e^2\alpha\mu^2/I^2\epsilon$$

and X_1 and X_2 are the roots of

$$(Z - X)^2 - C(1 - X^2)^{1/2} = 0. \qquad (B2)$$

We have divided each equation by A, which gives the equation in reduced variables and thus gives

$$X^2 \leq 1. \qquad (B3)$$

The calculation is greatly simplified using the above equations. The phase space integral becomes

$$\Gamma/A = C^{1/2} \int_{|X_1|}^{X_2} (1 - X^2)^{1/4} dX \; +$$

$$[Z|X_1| + \tfrac{1}{2}X_1^2]\, H(-X_1) - [ZX_2^2 - \tfrac{1}{2}X_2^2]\, S(Z-X_2) +$$

$$[Z|X_1| - \tfrac{1}{2}X_1^2]\, H(X_1)\, S(Z-X_1) - Z^2\, H(X_2-Z)\, H(Z-X_1) \qquad (B4)$$

These equations are used in place of the ones given in Chapter II.

The following is an outline of the program used in the phase space calculations.

1. Input: Spectroscopic parameters, dissociative energies, equilibrium internuclear distances of diatomic species, force constants, masses, energy range and step sizes, and vibrational population distributions of reactant diatomic.
2. Calculate vibrational energy levels, reduced masses, dissociation energies, and moments of inertia of diatomic species.
3. For each energy determine energy dependent constants for each vibrational state and the maximum impact parameter.
4. Compute total phase space volumes for each channel and vibrational state. Compute phase space volumes for stable diatomic products and that for dissociation from that vibrational state. Sum to obtain total phase space. Convert to probabilities.

(a) The roots of Eq. (B2) are obtained from an iterative procedure.

(b) The integral in Eq. (B4) was evaluated using Simpson's one-third rule.

5. Use Simpson's one-third rule to evaluate the integral $\int P\ b\ db$ to obtain the partial cross sections.

6. Sum over all product and reactant vibration states to obtain total cross sections for a given channel.

7. Write partial and total cross sections.

LITERATURE CITED*

1. P. Langevin, Ann. Chim. Phys. 5, 245 (1905); See E. W. McDaniel, *Collision Phenomena in Ionized Gases* (John Wiley & Sons, New York, 1964) p. 701 for a translation of this paper.

2. J. C. Light, J. Chem. Phys. 40, 3221 (1964).

3. P. Pechukas and J. C. Light, J. Chem. Phys. 42, 3281 (1965).

4. P. Pechukas, J. C. Light and C. Rankin, J. Chem. Phys. 44, 794 (1966).

5. J. Lin and J. C. Light, J. Chem. Phys. 45, 2545 (1966).

6. D. G. Truhlar and A. Kupperman, J. Phys. Chem. 73, 1722 (1969).

7. J. C. Light and J. Lin, J. Chem. Phys. 43, 3209 (1965).

8. F. A. Wolf, J. Chem. Phys. 44, 1619 (1966).

9. O. B. Firsov, Zh. Eksperim. i Teor. Fiz. 42, 1307 (1962) [Soviet Phys. - JETP 15, 906 (1962)].

10. E. E. Nikitin, Teor. i Eksperim. Khim. Acad. Nauk Ukr. S. S. R. 1, 135 (1965) [Theor. Exptl. Chem. 1, 83 (1965)].

11. E. E. Nikitin, Teor. i Eksperim. Khim. Acad. Nauk Ukr. S. S. R. 1, 428 (1965) [Theor. Exptl. Chem. 1, 275 (1965)].

12. F. A. Wolf and J. L. Haller, J. Chem. Phys. 52, 5910 (1970).

13. G. Gioumousis and D. P. Stevenson, J. Chem. Phys. 29, 294 (1958).

---

*The abbreviations used herein conform to those adopted by the IUPAC and AIP as described in the List of Periodicals, Chem. Abstr. 55, 1J (1961) and later supplements.

14. J. C. Light, Disc. Faraday Soc. 44, 14 (1968).

15. L. M. Tannenwald, Proc. Phys. Soc. (London) 87, 109 (1966).

16. S. Watanabe, T. Kasuga and T. Horie, Prog. Theor. Phys. 39, 564 (1968).

17. T. Horie, S. Watanabe and K. Kurata, J. Chem. Phys. 31, 783 (1959).

18. T. Horie and T. Kasuga, J. Chem. Phys. 40, 1683 (1964); J. Phys. Soc. Japan 19, 1194 (1964).

19. D. Rapp and W. E. Francis, J. Chem. Phys. 37, 2631 (1962).

20. P. H. Edmonds and J. B. Hasted, Proc. Phys. Soc. (London) 84, 99 (1964).

21. D. K. Bohme, J. B. Hasted, and P. P. Ong. J. Phys. B 1, 879 (1968).

22. P. Pechukas, *Thesis* (University of Chicago, 1966).

23. A. O. Barut, *The Theory of the Scattering Matrix* (Macmillan, New York, 1967).

24. E. W. McDaniel, V. Čermák, A. Dalgarno, E. E. Ferguson and L. Friedman, *Ion-Molecule Reactions* (Wiley-Interscience, New York, 1970).

25. B. C. Eu and J. Ross, J. Chem. Phys. 44, 2467 (1966).

26. H. Goldstein, *Classical Mechanics* (Addison-Wesley, Reading, Massachusetts, 1950).

27. G. Herzberg, *Molecular Spectra and Molecular Structure I. Spectra of Diatomic Molecules* (D. Van Nostrand, Princeton, New Jersey, 1950).

28. W. B. Maier, II, Planet. Space Sci. 16, 477 (1968).

29. D. B. Dunkin, F. C. Fehsenfeld, A. L. Schmeltekopf, and E. E. Ferguson, J. Chem. Phys. 49, 1365 (1968).

30. E. E. Ferguson, F. C. Fehsenfeld, D. B. Dunkin, A. L. Schmeltekopf, and H. I. Schiff, Planet. Space Sci. 12, 1169 (1964).

31. E. C. Y. Inn, Planet. Space Sci. 15, 19 (1967).

32. P. Warneck, J. Chem. Phys. 47, 4279 (1967).

33. R. C. Bolden, R. S. Hemsworth, M. J. Shaw and N. D. Twiddy, J. Phys. B 3, 45 (1970).

34. V. Aquilanti and G. G. Volpi, Ric. Sci. Rend. 36, 359 (1966).

35. J. Sayers and D. Smith, Disc. Faraday Soc. 37, 167 (1964).

36. J. Heimerl, R. Johnsen and M. A. Biondi, J. Chem. Phys. 51, 5041 (1969).

37. A. L. Schmeltekopf, E. E. Ferguson, and F. C. Fehsenfeld, J. Chem. Phys. 48, 2966 (1968).

38. F. C. Fehsenfeld, A. L. Schmeltekopf, P. D. Golden, H. I. Schiff and E. E. Ferguson, J. Chem. Phys. 44, 4087 (1966).

39. E. Gustafsson and E. Lindholm, Ark. Fys. 18, 219 (1960).

40. R. F. Stebbings, J. A. Rutherford and B. R. Turner, Planet. Space Sci. 13, 1125 (1965).

41. T. F. Moran and L. Friedman, J. Chem. Phys. 45, 3837 (1966).

42. P. P. Ong and J. B. Hasted, J. Phys. B 2, 91 (1969).

43. P. K. Carroll, Can. J. Phys. 37, 880 (1959).

44. D. L. Albritton, A. L. Schmeltekopf and E. E. Ferguson, Bull. Am. Phys. Soc. 13, 212 (1968).

45. R. L. Champion and L. D. Doverspike, J. Chem. Phys. 49, 4321 (1968).

46. F. R. Gilmore, J. Quant. Spectry. Radiative Transfer 5, 369 (1965).

47. A. Lofthus, *The Molecular Spectrum of Nitrogen* Spectry. Rept. 2, Dept. Phys., U. of Oslo, Blindern, Norway, 1960.

48. L. Wallace, Astrophys. J. Suppl. 6, 445 (1962).

49. R. W. Nichols, J. Res. Natl. Bur. Std. 65A, 451 (1961).

50. D. C. Jain and R. C. Sahni, Int. J. Quantum Chem. 1, 721 (1967).

51. R. S. Hemsworth, R. C. Bolden, M. J. Shaw, and N. D. Twiddy, Chem. Phys. Lett. 5, 237 (1970).

52. W. B. Maier, II, J. Chem Phys. 41, 2174 (1964).

53. H. Schlumbohm, Z. Naturforsch. 24, 1720 (1969).

54. H. Schlumbohm, Z. Naturforsch. 23, 1386 (1968).

55. P. Warneck, J. Chem. Phys. 46, 513 (1967).

56. P. Mahadevan and G. D. Magnuson, Phys. Rev. 171, 103 (1968).

57. A. Galli, A. Giardini - Guidoni and G. G. Volpi, Nuovo Cimento 31, 1145 (1964).

58. R. C. Amme and H. C. Hayden, J. Chem. Phys. 42, 2011 (1965).

59. M. M. Shabin, Advan. Chem. Ser. 58, 315 (1966).

60. V. Cermak and Z. Herman, Nucleonics 19, 106 (1961).

61. T. F. Moran and J. R. Roberts, J. Chem. Phys. 49, 3411 (1968).

62. M. H. Cheng, M. Chiang, E. A. Gislason, B. H. Mahan, C. W. Tsao and A. S. Werner, J. Chem. Phys. 52, 5518 (1970).

63. T. O. Tiernan and R. E. Marcotte, J. Chem. Phys. 53, 2107 (1970).

64. T. F. Moran and L. Friedman, J. Chem. Phys. 42, 2391 (1965).

65. D. C. Jain and R. C. Sahni, Int. J. Quantum Chem. 2, 325 (1968).

66. R. K. Asundi and Ch. V. S. Ramachandrarao, Chem. Phys. Lett. 4, 89 (1969).

67. M. R. H. Rudge, Rev. Mod. Phys. 40, 564 (1968); M. R. H. Rudge and M. J. Seaton, Proc. Phys. Soc. 83, 680 (1964); J. W. McGowan and E. M. Clarke, Phys. Rev. 167, 43 (1968); L. J. Kieffer and G. H. Dunn, Rev. Mod. Phys. 38, 1 (1966).

68. C. E. Melton and W. H. Hamill, J. Chem. Phys. 40, 2995 (1964).

69. C. E. Brion, J. Chem. Phys. 40, 2995 (1964).

70. D. W. Turner and D. P. May, J. Chem. Phys. 45, 471 (1966).

71. J. W. McGowan, E. M. Clarke, H. P. Hanson and R. F. Stebbings, Phys. Rev. Letters 13, 620 (1964).

72. E. Lindholm, Arkiv. Phys. 40, 117 (1969).

73. R. E. Huffman, Y. Tanaka and J. C. Larrabee, Disc. Faraday Soc. 37, 159 (1964).

74. E. N. Lassettre, A. Skerbele, M. A. Dillon and K. J. Ross, J. Chem. Phys. 48, 5066 (1968).

75. V. H. Dibeler and J. A. Walker, J. Opt. Soc. Am. 57, 1007 (1967).

76. A. J. C. Nicholson, J. Chem. Phys. 39, 954 (1963).

77. C. E. Brion and G. E. Thomas, Int. J. Mass Spectrometry Ion Phys. 1, 25 (1968).

78. D. Vance, Phys. Rev. 169, 263 (1968).

79. B. R. Turner, J. A. Rutherford and D. M. J. Compton, J. Chem. Phys. 48, 1602 (1968).

80. T. F. Moran, F. C. Petty and A. F. Hedrick, J. Chem. Phys. 51, 2112 (1969).

81. R. W. Nicholls, Can. J. Phys. 43, 1390 (1965).

82. R. F. Mathis, B. R. Turner and J. A. Rutherford, J. Chem. Phys. 49, 2051 (1968).

83. O. Edqvist, E. Lindholm, L. E. Selin, H. Sjögren and L. Åsbrink, Arkiv. Phys. 40, 439 (1970).

84. J. E. Collin and P. Natalis, Int. J. Mass Spectrometry Ion Phys. 1, 483 (1968).

85. R. W. Nicholls, J. Phys. B. 1, 1192 (1968).

86. R. C. C. Lao, R. W. Rozett, and W. S. Koski, J. Chem. Phys. 49, 4205 (1968).

87. J. H. Moore and J. P. Doering, Phys. Rev. 177, 218 (1969).

88. J. H. Moore and J. P. Doering, Phys. Rev. 182, 176 (1969).

89. G. N. Polyakova, Ya. M. Fogel', V. F. Erko, A. V. Zats, and A. G. Tolstolutskii, Zh. Eksp. Teor. Fiz. 54, 374 (1968) [Sov. Phys.-JETP 27, 201 (1969)].

90. C. Liu, J. Chem. Phys. 53, 1295 (1970).

91. G. N. Polyakova, V. F. Erko, A. V. Zats, Ya. M. Fogel', and G. D. Tolstolutskaya, ZhETF Pis. Red. 11, 562 (1970) [JETP Lett. 11, 390 (1970)]; G. N. Polyakova, V. F. Erko, A. V. Zats, and Ya. M. Fogel', ZhETF Pis. Red. 12, 303 (1970) [JETP Lett. 12, 204 (1970)].

92. M. Lipeles, J. Chem. Phys. 51, 1252 (1969).

93. T. T. Kassal and E. S. Fishburne, J. Chem. Phys. 54, 1363 (1971).

94. T. F. Moran and D. C. Fullerton, Chem. Phys. Letters 2, 625 (1968).

95. D. G. Truhlar, J. Chem. Phys. 54, 2635 (1971).

96. C. E. Moore, Natl. Bur. Std. (U. S.) Circ. 467, Vol. I (1949), Vol. II (1952), Vol. III (1958).

97. H. D. Hagstrum, Phys. Rev. 104, 309 (1956).

98. J. J. Kaufman and W. S. Koski, J. Chem. Phys. 50, 1942 (1969).

99. C. F. Giese, Advan. Chem. Ser. 58, 20 (1966).

100. G. Herzberg, *The Spectra and Structures of Simple Free Radicals*, (Cornell University Press, Ithaca, New York, 1971).

101. G. Herzberg, *Molecular Spectra and Molecular Structure, III, Electronic Spectra and Electronic Structure of Polyatomic Molecules*, (D. Van Nostrand, Princeton, New Jersey, 1967).

102. W. A. Lester, Jr., Ed., *Proceedings of the Conference on Potential Energy Surfaces in Chemistry*, (IBM Research Laboratory, San Jose, California, 1971).

103. H. Margenau, Rev. Mod. Phys. 11, 1 (1939).

104. J. O. Hirschfelder, C. F. Curtiss, and R. B. Bird, *Molecular Theory of Gases and Liquids*, (Wiley, New York, 1954).

105. H. Margenau and N. Kestner, *Theory of Intermolecular Forces*, (Pergamon Press, London, 1969).

106. J. O. Hirschfelder and W. J. Meath, Advan. Chem. Phys. 12, 3 (1967).

107. A. D. Buckingham, Advan. Chem. Phys. 12, 107 (1967).

108. W. A. Lester, Jr., J. Chem. Phys. 53, 1511 (1970); J. Chem. Phys. to be published.

109. D. E. Stogryn and A. P. Stogryn, Mol. Phys. 11, 371 (1966).

110. A. Dalgarno, Adv. Phys. 11, 281 (1962).

111. J. L. Franklin, J. G. Dillard, H. M. Rosenstock, J. T. Herron, K. Draxl, and F. H. Field, Natl. Std. Ref. Data System NSR-NBS26, (1969).

112. J. A. Pople, D. L. Beveridge, and P. A. Dobosh, J. Chem. Phys. 47, 2026 (1967); J. A. Pople, D. L. Beveridge, and N. S. Ostland, Intern. J. Quant. Chem. 1S, 293 (1967); M. S. Gordon and J. A. Pople, J. Chem. Phys. 49, 4643 (1968).

113. J. A. Pople and D. L. Beveridge, *Approximate Molecular Orbital Theory*, (McGraw-Hill, New York, 1970).

114. J. Del Bene and H. H. Jaffé, J. Chem. Phys. 48, 1807, 4056 (1968).

115. H. W. Kroto and D. P. Santry, J. Chem. Phys. 47, 792, 2736 (1967).

116. A. D. Walsh, J. Chem. Soc. 2288 (1953).

117. E. W. McDaniel, *Collision Phenomena in Ionized Gases*, (Wiley, New York, 1964).

VITA

David Fullerton is the first-born of Cleo and Marguerite Fullerton. He was born April 8, 1942 in Colorado Springs, Colorado. In 1960 he graduated from Fountain High School, Fountain, Colorado and entered Colorado State University.

In 1964 David received the Bachelor of Science degree in Chemistry and in 1966 was awarded the Master of Science degree in Physical Chemistry. Both degrees were from Colorado State University.

In the fall of 1966 he came to Georgia Tech in pursuit of his doctorate. Shortly after arriving in Atlanta he met Juana Mae Cauble at a bridge party. A few months later they were married. To date they have added no progeny to this overpopulated planet.

Mr. Fullerton is a member of the American Chemical Society, the American Association for the Advancement of Science, and Sigma Xi. In 1971 he received an award for the best graduate paper presented at the spring meeting of the Georgia Academy of Science.